University
of Ljubljana
Veterinary
Faculty

Maja Mandić

FUNCTIONAL INTERPLAY BETWEEN β_2-ADRENERGIC AND INSULIN RECEPTOR

Doctoral dissertation

Ljubljana, 2015

University of Ljubljana
Veterinary Faculty

576.32/.36:577.1/.2:57.088.5(043.3)

Maja Mandić, dr. vet. med.

FUNCTIONAL INTERPLAY BETWEEN β_2-ADRENERGIC AND INSULIN RECEPTOR

Doctoral dissertation

FUNKCIONALNA SOODVISNOST MED β_2-ADRENERGIČNIM IN INZULINSKIM RECEPTORJEM

Doktorska disertacija

Ljubljana, 2015

Maja Mandić

Functional interplay between β_2-adrenergic and insulin receptor

The study was done at the Institute for Anatomy, Histology and Embryology at the Veterinary faculty, University of Ljubljana.

Public presentation was held on: _____

Mentor: prof. dr. Milka Vrecl

Comentor: dr. Jane Nøhr

I declare, that the doctoral dissertation is the result of my own research work.

Maja Mandić

_____

Members of the commission board for the evaluation of the doctoral dissertation:

President: prof. dr. Robert Frangež

Member: doc. dr. Mojca Benčina

Member: prof. dr. Matjaž Zorko

ABSTRACT

Functional interplay between β_2-adrenergic and insulin receptor

Keywords: molecular biology; receptors, adrenergic, beta-2; receptor, insulin; metabolism; cell surface receptors; protein multimerization; signal transduction; bioluminescence resonance energy transfer – methods; cyclic AMP

We investigated possible direct interaction and functional interplay between β_2-adrenergic receptor (β_2AR), which represents seven transmembrane receptors (7TMRs) and insulin receptor (IR), which represents receptor tyrosine kinases (RTKs). We showed that β_2AR and IR colocalizied as well as that IR coexpression reduced both β_2AR surface expression and accelerated its internalization. Bioluminescence resonance energy transfer 2 ($BRET^2$) data suggested constitutive β_2AR and IR homo- and heteromerization. Calculated acceptor/donor (AD_{50}) values as a measure of the relative affinity for homo- and heteromer formation differed among the heteromers that could not be explained by a simple dimer model. Heterologous competition assays data suggested higher-order heteromer formation, while bioinformatic data suggested homodimers as basic units engaged in heteromerization. Computational peptide scanning of β_2AR and IR identified intracellular domains at the end of the 7th transmembrane (7TM) domain and carboxy (C)-terminal tail of β_2AR and a cytoplasmic part of the IR β chain as prospective interaction domains. In addition, using $BRET^2$ we were able to confirm that the cytoplasmic part of the IR β chain is actually a requisite for the interaction with the β_2AR. Using heteromer investigation technology (HIT) and cyclic adenosine monophosphate (cAMP) assay we gained additional results about functional interaction between IR and β_2AR which are: i) constitutive and isoproterenol induced β-arrestin 2 (βarr2) recruitment to the β_2AR:IR heteromer, ii) constitutive interaction between IR and βarr2 C-domain and iii) significantly lower potency of isoproterenol in cAMP assay in cells coexpressing IR and β_2AR concomitantly treated with insulin, compared to cells treated with isoproterenol only.

IZVLEČEK

Funkcionalna soodvisnost med β_2-adrenergičnim in inzulinskim receptorjem

Ključne besede: molekularna biologija; receptor, adrenergični, beta-2; inzulinski receptor; metabolizem; receptorji celične površine; multimerizacija proteinov; prenos signalov; resonančni prenos energije z bioluminiscenco – metode; ciklični AMP

Doktorska naloga obravnava možnost neposredne interakcije in funkcionalne soodvisnosti med β_2-adrenergičnim receptorjem (β_2AR), predstavnikom receptorjev s sedmimi transmembranskimi območji (7TMR) in inzulinskim receptorjem (IR), predstavnikom receptorjev s tirozin-kinazno aktivnostjo (RTK). Pokazali smo kolokalizacijo β_2AR in IR ter da soizražanje IR zmanjša površinsko izražanje in zviša hitrost internalizacije β_2AR. S testi BRET^2 (resonančni prenos energije z bioluminiscenco) smo pokazali tvorbo konstitutivnih homo- in heteromerov. Razmerje akceptor/donor, ki da 50 % maksimalne vrednosti signala BRET^2 (A/C_{50}), je merilo za relativno afiniteto tvorbe homo- in heteromera, je bilo različno med heteromeri, kar ni mogoče pojasniti s preprostim modelom za dimere. Rezultati heterolognega testa izpodrivanja BRET in računalniške analize, ki predvidevajo oblikovanje heteromerov iz homodimerov so pokazali na oblikovanje heteromerov višjega reda. Z metodami bioinformatike smo identificirali področji na koncu sedmega transmembranskega področja (7TM) in karboksilnega (C)-terminalnega repka β_2AR ter v citoplazemskem delu verige β IR kot morebitni interakcijski domeni. Pomen citoplazemskega dela verige β IR za heteromerizacijo z β_2AR smo potrdili s testi BRET^2. S pristopom HIT (tehnologija ugotavljanja heteromerov) in testom kopičenja znotrajceličnega cikličnega adenozin monofosfata (cAMP) smo pridobili dodatne dokaze za funkcionalno interakcijo med β_2AR in IR, in sicer za: i) konstitutivno in z izoproterenolom spodbujeno interakcijo med β-arestin 2 (βar2) in heteromerom β_2AR:IR, ii) konstitutivno interakcijo med IR in C-območjem βar2 in iii) značilno nižjo potenco izoproterenola v testu cAMP v celicah, ki so izražale β_2AR in IR in bile sočasno izpostavljene inzulinu, v primerjavi z celicami ki so bile izpostavljene samo izoproterenolu.

INDEX

ABSTRACT 4
IZVLEČEK 5
INDEX OF FIGURES 10
INDEX OF TABLES 12
ABBREVATIONS 14
1 INTRODUCTION 18
2 LITERATURE REVIEW 21
2.1 SEVEN TRANSMEMBRANE RECEPTORS (7TMRs) 21
2.1.1 Classification of 7TMRs 21
2.1.2 Structure of 7TMRs 22
2.1.3 Mechanisms of 7TMRs signaling 23
2.1.4 β_2-adrenergic receptor (β_2AR) 26
2.1.4.1 Crystal structure of the β_2AR 26
2.1.4.2 Insights into the β_2AR signaling and trafficking 27
2.1.4.3 Homooligomerization of the β_2AR 28
2.1.4.4 Heteromerization of the β_2AR 29
2.2 RECEPTOR TYROSINE KINASES (RTKs) 31
2.2.1 Overall architecture and domain organization 31
2.2.2 Mechanisms of receptor activation and oligomerization 32
2.2.3 Insulin receptor (IR) 33
2.2.3.1 Structure of the IR 33
2.2.3.2 IR signaling and endocytosis 35

2.3 THE ARRESTIN FAMILY OF PROTEINS 37

2.3.1 β-arrestin and β_2AR signaling 38

2.3.2 β-arrestin and IR signaling 40

2.4 SHC FAMILY OF ADAPTER PROTEINS 42

2.4.1 Shc and IR signaling 43

2.4.2 Shc and β_2AR signaling 43

2.5 7TMRs:RTKs CROSSTALK 44

2.5.1 INTERACTION BETWEEN β_2AR AND IR 46

2.6 METHODS FOR INVESTIGATION OF 7TMR:RTK HETEROMERS 48

2.6.1 BRET methodology in investigation of 7TMRs, RTKs and 7TMR:RTK heteromers 49

2.6.2 Informational spectrum method (ISM) 52

3 MATERIALS AND METHODS 54

3.1 CELL CULTURE AND TRANSFECTION 54

3.1.1 Cell culture 54

3.1.2 Transient transfection 54

3.2 STANDARD MOLECULAR BIOLOGY METHODS 55

3.2.1 Fusion constructs 55

3.2.2 Plasmid DNA preparation 56

3.2.3 Plasmid DNA isolation and spectrophotometric quantification 57

3.2.4 Restriction enzyme analysis of DNA 57

3.2.5 Agarose gel electrophoresis 58

3.3 METHODS TO EVALUATE RECEPTOR EXPRESSION AND INTERNALIZATION 59

3.3.1 Luminescence and fluorescence measurements 59

3.3.2 Enzyme-linked immunosorbent assay (ELISA) 59

3.3.3 Receptor binding assay 60

3.3.4 Receptor internalization assay 61

3.3.5 Confocal microscopy 62

3.4 METHODS FOR DETECTION AND ANALYSIS OF PROTEIN-PROTEIN INTERACTIONS 63

3.4.1 Bioluminescence resonance energy transfer (BRET) 63

3.4.1.1 $BRET^2$ dilution, saturation and competition assays 65

3.4.1.2 $BRET^2$ assay data evaluation 66

3.4.1.3 $BRET^2$ assay for monitoring the recruitment of β-arrestins to β_2AR or IR 68

3.4.2 Seven transmembrane receptor: Receptor tyrosine kinases-heteromer identification technology (7TMR:RTK-HIT) 68

3.4.2.1 Seven transmembrane receptor: Receptor tyrosine kinases-heteromer identification technology (7TMR:RTK-HIT) assay with β-arrestin 2 (βarr2) 69

3.4.2.2 Seven transmembrane receptor: Receptor tyrosine kinases-heteromer identification technology (7TMR:RTK-HIT) assay with Shc 70

3.4.3 Informational spectrum method (ISM) 71

3.4.3.1 Computational peptide scanning 72

3.4.3.2 Datasets 72

3.5 cAMP ASSAY 73

3.6. STATISTICAL ANALYSIS 74

4 RESULTS 75

4.1 CHARACTERISTICS OF THE FUSION CONSTRUCTS 75

4.1.1 Pharmacological characterization of β_2AR fusion constructs 75

4.1.2 Cellular localization of receptor constructs visualized by confocal microscopy 78

4.1.3 Colocalization of β_2ARs visualized by confocal microscopy 79

4.2 THE EFFECT OF IR COEXPRESSION ON β_2AR SURFACE EXPRESSION AND INTERNALIZATION 80

4.3 VISUALIZATION OF β_2AR AND IR CELLULAR LOCALIZATION BY CONFOCAL MICROSCOPY 83

4.4 INTERACTION BETWEEN β_2AR AND IR—BRET^2 EVIDENCE 84

4.4.1 Correlation between total luminescence and fluorescence and the corresponding number of β_2AR binding sites 85

4.4.2 BRET^2 dilution assays 85

4.4.3 BRET^2 saturation assays 87

4.4.4 BRET^2 competition assays 92

4.5 INTERACTION BETWEEN β_2AR AND IR CHARACTERIZED BY INFORMATIONAL SPECTRUM METHOD (ISM) 95

4.5.1 Identification of the key protein domains responsible for the interaction between β_2AR and IR 97

4.5.2 Affinity of interaction between protomers 98

4.6 INVESTIGATION OF THE β_2AR:IR HETEROMER IN TERMS OF β-ARRESTIN 2 (βARR2) RECRUITMENT 99

4.6.1 BRET^2 assay with GFP^2-βarr2 1–185 mutant 104

4.7 THE IMPORTANCE OF IR RESIDUES 1269–1314 IN FORMATION OF THE β_2AR:IR HETEROMER 107

4.8 INVESTIGATION OF THE β_2AR:IR HETEROMER IN TERMS OF SHC RECRUIMENT 108

4.9 THE EFFECT OF IR COEXPRESSION ON β_2AR cAMP PRODUCTION 109

5 DISCUSSION 112

5.1 FUSION CONSTRUCTS CHARACTERIZATION BY RADIOLIGAND BINDING ASSAY AND CONFOCAL MICOSCROPY 112

5.2 COLOCALIZATION OF β_2AR VISUALIZED BY CONFOCAL MICROSCOPY .. 113

5.3 THE EFFECT OF IR ON β_2AR BINDING PROPERTIES, SURFACE EXPRESSION AND INTERNALIZATION 113

5.4 INTERACTION BETWEEN β_2AR AND IR CHARACTERIZED BY BRET^2 AND INFORMATIONAL SPECTRUM METHOD (ISM) 114

5.5 INVESTIGATION OF THE β_2AR:IR HETEROMER IN TERMS OF βARR2 AND SHC RECRUITMENT 117

5.6 EFFECT OF IR COEXPRESSION ON β_2AR cAMP PRODUCTION 119

6 CONCLUSIONS 122

7 SUMMARY 123

8 POVZETEK 125

9 ACKNOWLEDGEMENTS 128

10 LITERATURE 130

11 APPENDIX 145

INDEX OF FIGURES

Figure 1: Schematic representation of 7TMR 23

Figure 2: Schematic representation of 7TMRs signaling 25

Figure 3: Crystallographic structure of the β_2AR 27

Figure 4: Schematic representation of RTK subfamilies [87] 32

Figure 5: Insulin regulation of glucose metabolism 33

Figure 6: Schematic diagram of the IR homodimer 35

Figure 7: β-arrestin dependent internalization of 7TMRs 39

Figure 8: Model of β-arrestin mediated recruitment and targeting of c-Src 40

Figure 9: Structural information of β-arrestins, indicating binding domains for signaling molecules 41

Figure 10: β-arrestin-dependent insulin signaling 42

Figure 11: Schematic representation of $BRET^2$ assay 65

Figure 12: Schematic representation of 7TMR:RTK-HIT in live cells 69

Figure 13: Binding properties of β_2AR fusion constructs expressed in HEK-293 cells 75

Figure 14: The effect of IR coexpression on binding properties of β_2AR in HEK-293 cells 77

Figure 15: Visualization of HA-β_2AR-RLuc8, β_2AR-GFP^2 and IR-GFP^2 cellular localization by confocal microscopy 79

Figure 16: Visualization of β_2ARs colocalization by confocal microscopy 80

Figure 17: The effect of IR coexpression on β_2AR cell surface expression in HEK-293 cells 81

Figure 18: The effect of IR coexpression on β_2AR internalization in HEK-293 cells 82

Figure 19: Effect of IR coexpression on the time-course of β_2AR internalization 83

Figure 20: Visualization of β_2AR and IR cellular localization by confocal microscopy 84

Figure 21: Correlation between total luminescence and fluorescence and the corresponding number of β_2AR binding sites 85

Figure 22: $BRET^2$ dilution curves of β_2AR and IR homomers 86

Figure 23: Theoretical BRET dilution curves [181] 87

Figure 24: $BRET^2$ saturation curves of β_2AR and IR homo- and heteromers 88

Figure 25: Relationship between receptor-RLuc8 and receptor-GFP^2 constructs expression..... 89

Figure 26: Random collisions between the RLuc8-tagged receptors and membrane-inserted GFP^2-tagged construct (GFP^2-17aa)..... 90

Figure 27: Comparison of theoretical BRET saturation curves with different affinities for trimer formation..... 92

Figure 28: Homologous and heterologous $BRET^2$ competition assay 94

Figure 29: Numerical simulation of heterologous BRET competition assay for trimers..... 95

Figure 30: Informational spectrum (IS) of (A) β_2AR; (B) IR and (C) CS of the β_2AR and IR..... 96

Figure 31: Cross-spectrum (CS) of (A) wild type β_2AR and IR, (B) scrambled β_2AR and wild type IR and (C) scrambled IR and wild type β_2AR 96

Figure 32: Mapping of the domains with maximal contribution to the frequency component F(0.216) in the informational spectrum of of (A) β_2AR and (B) IR..... 97

Figure 33: CIS of β_2AR:IR tetramers with the characteristic peak at F(0.216) 98

Figure 34: β_2AR:IR-HIT assay with β-arrestin 2 102

Figure 35: $BRET^2$ assay with βarr2 1-185 mutant 106

Figure 36: $BRET^2$ saturation curves of IR 1–1271 mutant homo- and heteromers 107

Figure 37: IR 1–1271:β_2AR HIT assay with βarr2..... 108

Figure 38: IR-RLuc8:β_2AR-HIT assay using Shc 109

INDEX OF TABLES

Table 1: Binding properties of β_2AR fusion constructs in HEK-293 cells..... 76

Table 2: The effect of IR coexpression on binding properties of β_2AR fusion constructs in HEK-293 cells 78

Table 3: $BRET^2$ saturation assay fitting results 91

Table 4: The affinity of interaction between the β_2AR and IR homo- and heteromers characterized by the signal-to-noise ratio (S/N) at the characteristic frequency (F) in the CIS 99

Table 5: Constitutive $BRET^2$ signal ($BRET^2_{const}$) generated by non-activated receptor interaction with βarr2 in the absence or presence of untagged receptor 100

Table 6: Maximal $BRET^2$ signal ($BRET^2_{max}$) generated by agonist-activated receptor interaction with the βarr2 in the absence or presence of untagged receptor 103

Table 7: Pharmacological characterization of the receptor interaction with βarr2 103

Table 8: cAMP maximal response in agonist stimulated β_2AR-, IR- or β_2AR and IR-expressing cells 110

Table 9: EC_{50} values for agonists in cAMP assay 111

ABBREVATIONS

5-HT4R	serotonin 4 receptor
7TMH	seven transmembrane α-helices
7TMRs	seven transmembrane receptors
A/C	acceptor/donor
A2aR	adenosine A2a receptor
AC	adenylyl cyclase
AMPA	α-amino-3-hydroxy-5-methyl-4-isoxazolepropionic acid
AP2	adaptor protein 2
ARRDCs	arrestin domain-containing proteins
ARTs	arrestin-related trafficking adaptors
AT_1R	angiotensin type 1 receptor
Bk_2R	bradykinin type 2 receptor
BRET	bioluminescence resonance energy transfer
$BRET_{const}$	BRET constitutive
$BRET_{max}$	BRET maximal
cAMP	cyclic adenosine monophosphate
CB1R	cannibinoid 1 receptor
CCR_2	chemokine receptor type 2
cDNA	complementary DNA
cGMP	cyclic guanosine monophosphate
CHO	Chinese hamster ovary
CHW	Chinese hamster fibroblasts
CIS	consensus information spectrum
cpm	counts per minute
CS	cross spectrum
C-tail	carboxy-tail
$CXCR_4$	chemokine receptor type 4
DAG	diacylglycerol
DMEM	Dulbecco's modified Eagle's medium
DNA/RNA	deoxyribonucleic/ribonucleic acid
DOR	δ-opioid receptor
DPBS	Dulbecco's phosphate buffered saline
DRD_1	D_1 dopamine receptor
DSCR3	Down syndrome critical region gene 3
E. coli	*Escherichia coli*
EC	extracellular
EC_{50}	half maximal effective concentration
ECL1-3	three extracellular loops

EDTA	ethylenediaminetetraacetic acid
EGFR	epidermal growth factor receptor
EP1R	prostaglandin E receptor 1
ERK ½	extracellular signal-regulated kinase 1 and 2
FCS	foetal calf serum
FGFR	fibroblast growth factor receptor
FOXO 1	forkhead box O1
FRET	fluorescence resonance energy transfer
G proteins	guanine-nucleotide binding proteins
GAB1	Grb2 associated binding protein 1
GDP	guanosine diphosphate
GEF	guanine nucleotide exchange factor
GFP	green fluorescent protein
GIP	gastric inhibitory polypeptide
GLUT	glucose transporter
GPCRs	G protein-coupled receptors
GRAFS	glutamate, rhodopsin, adhesion, frizzled/taste2, secretin
Grb2	growth factor receptor-bound protein 2
GRK	G protein-coupled receptor kinase
Gs	stimulatory G protein
GSK3	glycogen synthase kinase 3
GTP	guanosine triphosphate
GTPase	guanosine triphosphatase
Gα	G protein α-subunit
$G\alpha_i$	G protein inhibitory Gα-subunit
Gβγ	G protein βγ-subunit
h	hour
H8	helix 8
HEK	human embryonic kidney
HER3	heregulin receptor 3
HIT	heteromer investigation technology
HSL	hormone sensitive lipase
HTRF	homogenous time-resolved fluorescence
IC	intracellular
IC_{50}	half maximal inhibitory concentration
ICL	intracellular loop
ID	insert domain
IGF ½	insulin-like growth factor ½
IGFR	insulin-like growth factor receptor
IP3	inositol triphosphate
IR	insulin receptor
IRRR	insulin receptor related receptor

IRS	insulin receptor substrate
ISM	informational spectrum method
JM	juxtamembrane
JNK3	Jun N-terminal kinase 3
KOR	K-opioid receptor
LB	Luria-Bertani
LPAR1	lysophosphatidic acid receptor 1
MAPKs	mitogen-activated protein kinases
mBU	milliBRET units
Mdm2	mouse double minute 2 homolog
MEK	mitogen-activated protein kinase kinase
min	minutes
MOPr	μ-opioid receptor
mTOR	mechanistic target of rapamycin
N-terminus	amino-terminus
NTRK1/TrkA	neurotrophic tyrosine kinase receptor 1/tropomyosin-related kinase receptor A
PAC1R	pituitary adenylate cyclase-activating peptide type 1
PC	rat adrenal phaeochromocytoma
PDGFRβ	platelet-derived growth factor receptor β
PDK1	protein kinase 3-phosphoinositide-dependent protein kinase 1
PI3K	phosphoinositide 3-kinase
PKA	protein kinase A
PKB	protein kinase B
PLC	phospholipase C
PTB	phosphotyrosine binding
PTB	phosphotyrosine-binding
PtdIns(4,5)P_2	phosphatidylinositol (4,5) bisphosphate
PTPase	protein tyrosine phosphatases
RET	resonance energy transfer
RLuc	*Renilla luciferase*
RT	room temperature
RTKs	receptor tyrosine kinases
S/N	signal-to-noise ratio
$S1PR_1$	sphingosine 1-phosphate receptor 1
Ser/Thr	serine/threonine
SH2	Src homology 2
SOC	super optimal with catabolite repression
SOS	son of sevenless
SSTR5	somatostatin receptor 5
TBE	tris-borate EDTA
TH	transmembrane helix
TK	tyrosine kinase

TM	transmembrane
Tyr	tyrosine
Tyr(P)	phosphotyrosine
VEGFR2	vascular endothelial growth factor receptor 2
VPS	vacuolar protein sort
YFP	yellow fluorescent protein
α_1dAR	A_1d-adrenergic receptor
β_2AR	β_2-adrenergic receptor
β_3AR	β_3-adrenergic receptor
βarr1	β-arrestin 1
βarr2	β-arrestin 2

1 INTRODUCTION

The functional interplay between different classes of receptors represents a means of fine-tuning the control of cellular functions that could be fundamental for understanding pathologic conditions and responses to therapeutic agents that interact with cell surface receptors. Seven transmembrane receptors (7TMRs) constitute the largest class of cell surface-localized receptors that mediate important physiological processes such as perception of light, pain, taste and smell, immune system function, neurotransmission, digestion, and cardiovascular regulation [1, 2]. Receptor tyrosine kinases (RTKs) are the second largest family of membrane receptors involved in cellular signaling pathways that regulate metabolic processes and key cell functions such as cellular proliferation, differentiation, and apoptosis [3]. Originally, 7TMRs and RTKs, together with their respective downstream effectors, were thought to represent distinct and linear signaling units. However, studies have provided evidence for functional crosstalk between these different types of receptors. Indeed, signal integration and diversification arises from a complex network involving crosstalk between separate signaling units. The crosstalk between these different classes of receptors may occur at the 7TMR/RTK level or via various intracellular effector/adaptor molecules, since these receptor families share many signaling molecules, such as β-arrestin 2 (βarr2) [4, 5].

Glucose metabolism is under the cooperative regulation of both insulin receptor (IR) and β_2-adrenergic receptor (β_2AR), which represent RTKs and 7TMRs, respectively. At the molecular level, the ability of insulin to counter regulate β_2ARs can be exerted through insulin-stimulated phosphorylation of β_2AR and its subsequent internalization. An early *in vitro* study demonstrated that, in the presence of insulin, IR catalyzes the phosphorylation of β_2AR predominantly at residues located in the cytoplasmic tail of β_2AR, i.e. tyrosine residues Tyr350/Tyr354, and Tyr364 [6]. This finding was consistent with the hypothesis that IR directly interacts with and phosphorylates β_2AR. In addition, insulin-induced activation of mitogen-activated protein kinases (MAPKs**)** extracellular signal-regulated kinase 1 and 2 (ERK 1/2), is potentiated by β_2AR via a mechanism that requires the integrity of Tyr350 [7]. Thus, the functional crosstalk between β_2AR and IR may be to fine tune the signals from multiple receptor signaling pathways. β_2AR and IR are also endogenously coexpressed in other cell types-i.e., pancreatic beta cells, adipocytes, liver cells, skeletal muscle cells, retinal

cells, and astrocytes) [8-12]. Therefore, the formation of heteromeric complexes consisting of these two receptors may be plausible.

Members of β-arrestin protein subfamily are thought to participate in agonist-mediated desensitization of 7TMR and cause specific dampening of cellular responses to stimuli such as hormones, neurotransmitters, or sensory signals [13], as well as having signaling roles in their own right [14, 15]. The ability of β-arrestins to associate with and activate the c-Src was the first observation which identified a role for β-arrestin in the β_2AR-mediated activation of MAPK (ERK1/2), besides their role in the 7TMRs desensitization/trafficking [16]. Recent study also showed that βarr2 controls whole body insulin action by forming a complex with IR, c-Src and Akt and provided *in vivo* evidence that decreased βarr2 levels in muscle and liver contribute to the development of insulin resistance and type 2 diabetes mellitus [17].

The aim of our work was to investigate the formation of functional β_2AR:IR heteromers and characteristics of those interactions, including the distinct pharmacological phenotype. As receptor heteromers have the potential to attain a unique pharmacological profile, their existence adds another level of complexity to cell signaling systems. Our results could provide the opportunity for designing β_2AR:IR heteromer-specific/-biased drugs with improved selectivity and reduced side effects, compared to the existing drugs. Further on, our findings regarding the constitutive and ligand-promoted βarr2 recruitment to the β_2AR:IR heteromer, and direct, constitutive interaction between IR and βarr2 could implicate into new preventive and therapeutic strategies against insulin resistance and type 2 diabetes.

Our hypotheses are:

1. β_2AR forms constitutive heteromers with IR.

2. Receptor affinity for heteromer formation (β_2AR:IR) is higher compared to receptor homomer formation.

3. βarr2 interacts with IR:β_2AR heteromer in a constitutive and ligand-dependent manner.

4. Interaction between IR and βarr2 is constitutive.

5. β_2AR:IR heteromer has distinct pharmacological phenotype.

2 LITERATURE REVIEW

2.1 SEVEN TRANSMEMBRANE RECEPTORS (7TMRs)

7TMRs, also known as G protein coupled receptors (GPCRs) represent the largest superfamily of integral membrane proteins encoded in the human genome. 7TMRs recruit heterotrimeric intracellular guanine-nucleotide binding proteins (G proteins) as an important step in their signaling cascade [18]. Studies have revealed that 7TMR signaling is more complex and diverse than originally anticipated, as well as that it includes signaling through G protein -dependent and -independent pathways [19-21]. Therefore, it has been proposed that the term GPCR be abandoned in favor of 7TMR [22]. 7TMRs respond to multiple stimuli and activate a variety of intracellular signaling pathways. As a result, this family of receptors exerts a wide range of physiological functions, e.g. neurotransmission, hormone response, inflammation and mediate communications with the outside environment (taste, odor and vision) [1]. Consequently, the 7TMRs are currently the richest source of targets for the pharmaceutical industry.

During the past three decades there has been an impressive progress in the field of 7TMR research. Notable milestones include the cloning of the first 7TMR genes, as well as sequencing of the human genome revealing the size of the 7TMR superfamily and the number of orphan 7TMRs. Furthermore, crystallography of 7TMRs has experienced immense growth; the agonist-bound active-state structures of adrenergic, rhodopsin, adenosine and many other receptor systems have been described, including the structure of the β_2AR-G protein complex [23].

2.1.1 Classification of 7TMRs

Although numerous classification schemes have been proposed, the superfamily is classically divided into three main families based on sequence homology and pharmacology; family A (rhodopsin-like), family B (secretin-like), family C (glutamate receptor-like) and others (adhesion, frizzled, taste type-2, unclassified) [24]. More recently, an alternative classification system called GRAFS (Glutamate, Rhodopsin, Adhesion, Frizzled/Taste2, Secretin) has been

proposed [25, 26]. By this system, the 7TMR superfamily is divided into five main families based on sequence similarity within the 7TM segments.

2.1.2 Structure of 7TMRs

7TMRs are integral membrane proteins comprised of an extracellular amino-terminus (N-terminus) followed by seven transmembrane α-helices (7TMH) connected by three extracellular loops (ECL1-3) and three intracellular loops (ICL1-3) of variable length, and finally an intracellular carboxy-tail (C-tail) (Fig. 1). The 7TMH are arranged to form a tight, ring-shaped central core that is highly hydrophobic in nature. This helical bundle contains a number of kinks, mostly induced by proline residues that roughly divide the receptor into extracellular (EC) and intracellular (IC) regions. Many small organic agonists bind within the TM segments, while peptide hormones and proteins often bind to the N-terminus and ECLs joining the TM domains. The N-terminus contains asparagine residues and motifs for N-glycosylation which influences intracellular trafficking of the receptors to the plasma membrane. The first and second ECLs contain highly conserved cysteine residues that form disulfide bonds (Fig. 1) and stabilize the receptor structure [22, 27-29]. IC domains include serine/threonine residues which provide sites for G protein-coupled receptor kinase (GRK)-mediated phosphorylation and receptor desensitization by arrestin family of proteins. The second and the third ICL are involved in the interaction with the G protein. C-terminus comprises cytoplasmic helix 8 (H8) and C-tail that may serve as a site for palmitoylation creating a fourth ICL (Fig. 1) by the palmitoylated cysteine inserted in the plasma membrane [22, 27-29].

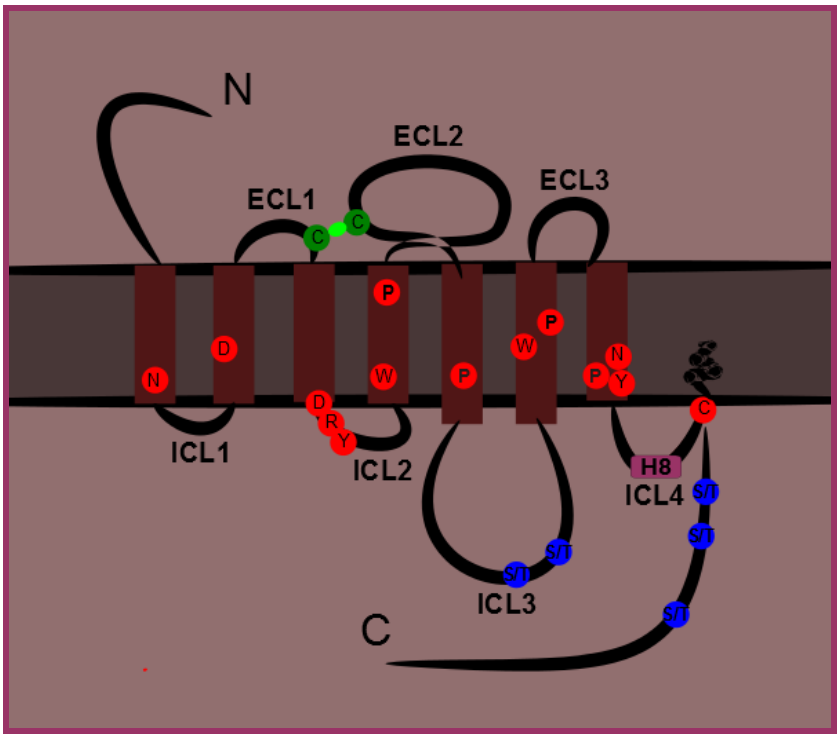

Figure 1: Schematic representation of 7TMR

Shown is a two-dimensional typical heptahelical topology: the three ECLs, the N-tail outside the cell, the four ICLs and the C-terminal tail inside the cell. Sites of phosphorylation are present intracellularly (blue S/T=serine/threonine circles). There is a disulfide bond (green bond between two cysteines (C) in the green circles) linking the top of TM3 with ECL2. There is a site of palmitoylation within the C-tail (C in the red circle anchored), helping to establish H8 adjacent to the inside of the plasma membrane. Also shown are the typical signature sequences of the class A 7TMR family (residues represented in red circles). Figure created by author based on a figure from [30].

2.1.3 Mechanisms of 7TMRs signaling

7TMR function is mediated and modulated through two ubiquitous and generic mechanisms: G protein activity and β-arrestin function. Classic agonists bind the receptor, activate the receptor and induce a conformational change that allows the receptor to function as a guanine nucleotide exchange factor (GEF) exchanging the guanosine 5'-triphosphate (GTP) in place of guanosine 5'-diphosphate (GDP) on G protein α-subunit (Gα). In their inactive form, Gα subunit is bound to GDP and tightly associated with the Gβγ-subunit (Gβγ). Exchange of GDP for GTP leads to the functional dissociation of the Gα subunit from the Gβγ dimer and the receptor. Both Gα-GTP and Gβγ can then trigger different signaling cascades (or second messenger pathways) and effector proteins, while the receptor is able to activate the next G

protein. The Gα subunit and the Gβγ dimer regulate distinct downstream effectors, such as adenylyl cyclase (AC), phosphodiesterases, phospholipase C (PLC), ion channels, etc. (Fig. 2). These effectors in turn regulate the intracellular concentrations of secondary messengers, such as cAMP (cyclic adenosine monophosphate), cGMP (cyclic guanosine monophosphate), DAG (diacylglycerol), IP3 (inositol triphosphate), arachidonic acid, sodium, potassium or calcium cations, which ultimately lead to a physiological response, usually via downstream regulation of gene transcription. The cycle is completed by the hydrolysis of GTP to GDP by intrinsic guanosine triphosphatase (GTPase) activity of Gα subunit, which leads to reassociation of Gα-GDP and Gβγ subunits with termination of signaling [31, 32].

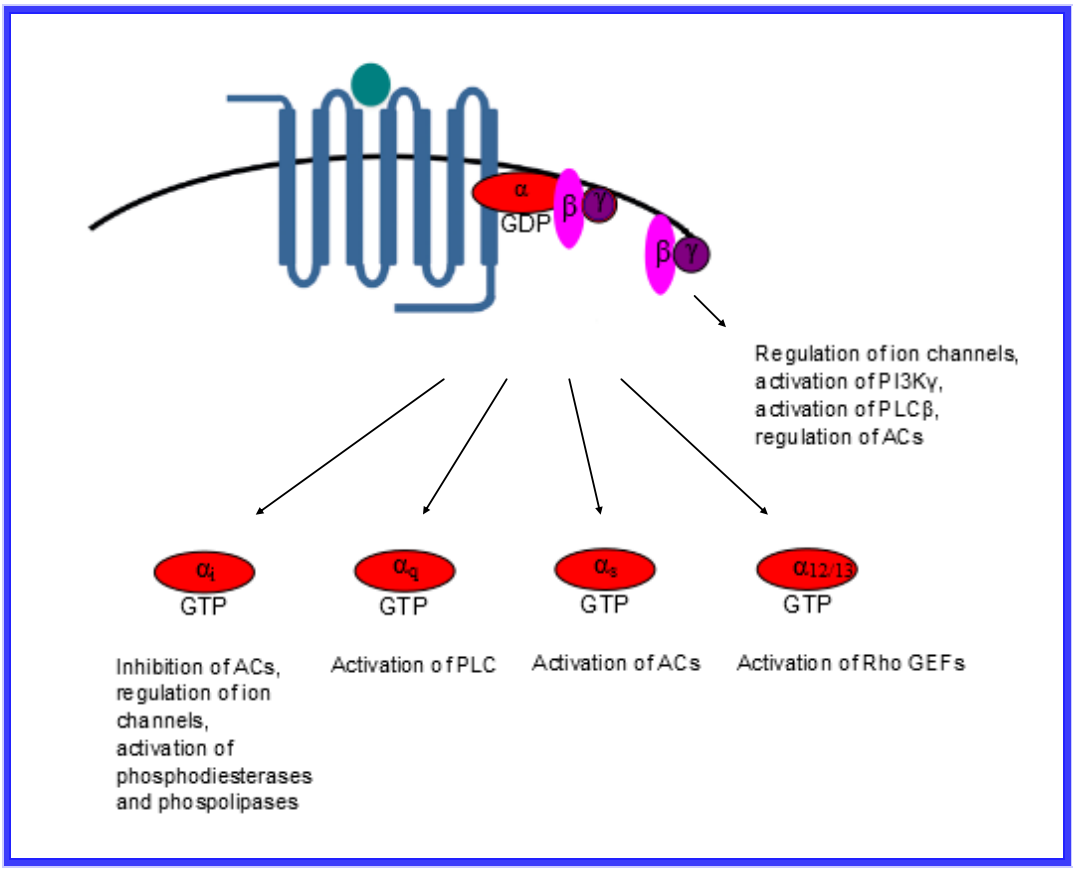

Figure 2: Schematic representation of 7TMRs signaling

Upon ligand binding and receptor activation, G protein dissociates on Gα-GTP and Gβγ-subunits which affect different cellular effectors. ACs=adenylyl cyclases, PLC= phospholipase C, GEFs= guanine nucleotide exchange factors, PI3Kγ= phosphatidylinositol-4,5-bisphosphate 3-kinase γ. Figure created by author based on a figure from [33].

Activated receptors also stimulate and are substrates for GRKs. After phosphorylation by GRKs, receptors bind β-arrestins which sterically interdict further G protein signaling. This limits the signal duration of G protein, resulting in receptor desensitization. β-arrestins also scaffold receptors to membrane-trafficking machinery, thus causing the receptor internalization from the cell surface and sequestration from G proteins. Furthermore, β-arrestins scaffold numerous signaling molecules stimulated by receptor agonism. Thus, as β-arrestins turn off G protein signals, they can simultaneously initiate a second, parallel set of signals [20, 34]. Besides, distinct G protein and β-arrestin pathways can be pharmacologically modulated independently with biased ligands [35, 36].

2.1.4 β_2-adrenergic receptor (β_2AR)

In the past decades, β_2AR has led the way as a model system in the 7TMRs research and besides rhodopsin, presents the most investigated 7TMR. Adrenergic receptors (ARs) belong to the family A of 7TMRs and include nine different receptor subtypes, i.e. three β (β_1, β_2, β_3), three α_1 (α_{1a}, α_{1b} and α_{1d}) and three α_2 receptors (α_{2A}, α_{2B} and α_{2C}) [37]. Adrenergic receptors mediates multiple metabolic and neuroendocrine effects of catecholamines, epinephrine and norepinephrine (also known as adrenaline and noradrenaline). β_2AR is expressed in various organs in the body (mainly in the lungs, heart, gastrointestinal tract, liver, adipose tissue, uterus and skeletal muscle) where binding of a catecholamine to the receptor will generally stimulate the sympathetic nervous system, blood pressure, myocardial contractile rate and force, airway reactivity, as well as effect a variety of metabolic and central nervous system functions [37-39]. As a consequence, β_2AR inverse agonists and antagonists are widely used to treat hypertension and heart disease, while β_2AR agonists are important anti-asthma medicines [40].

2.1.4.1 Crystal structure of the β_2AR

β_2AR possesses the classical structural characteristics of the family A 7TMRs [41]; 3D crystallographic structure has been determined by making a fusion protein with lysozyme to increase the hydrophilic surface area of the protein for crystal contacts (Fig. 3) [42-44]. In comparison with rhodopsin, β_2AR has weaker interactions between the cytoplasmic ends of TM3 and TM6, involving the conserved E/DRY sequences. These differences may be responsible for the relatively high basal activity and structural instability of the β_2AR [42].

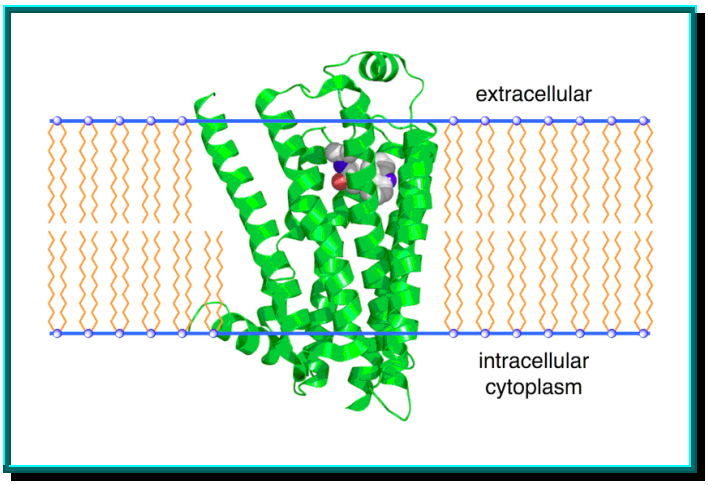

Figure 3: Crystallographic structure of the β_2AR

β_2AR is depicted as a green cartoon and the bound partial inverse agonist carazolol ligand as spheres (carbon atom = grey, oxygen = red, nitrogen = blue). The phospholipid bilayer is depicted as blue spheres (phosphate head groups) and yellow lines (lipid sidechains). Adapted from [44].

2.1.4.2 Insights into the β_2AR signaling and trafficking

Interactions of β_2AR and Gs (stimulatory G protein) formed the foundation of the ternary complex model of 7TMR activation [45, 46]. In the ternary complex consisting of agonist, receptor and Gs protein, the β_2AR has a roughly 100-fold higher affinity for agonists than does β_2AR alone [47] and the specificity of the G protein for guanine nucleotides changes in favor of GTP over GDP. β_2ARs couple primarily to $G\alpha_s$ and stimulate AC (Fig. 2) increasing the production of cAMP. The cAMP directly modulates the gating of hyperpolarization-activated, cyclic nucleotide-gated channels and protein kinase A (PKA). PKA in turn phosphorylates many proteins involved in excitation-contraction coupling including L-type Ca^{2+} channels, phospholamban, and/or troponin I [48]. In a feedback mechanism, PKA phosphorylates the receptor and this phosphorylation results in the switching of the coupling from the $G\alpha_s$ to the $G\alpha_i$ (inhibitory Gα-subunit) [49].

β_2AR undergoes phosphorylation, down-regulation, and sequestration in response to stimulation by agonist [50-52]. Proteins of central importance for β_2AR endocytosis are GRKs and β-arrestins. β_2AR signaling is rapidly attenuated through receptor phosphorylation

by GRKs and subsequent binding of β-arrestins. Agonist-dependent internalization requires β-arrestin binding to agonist-activated phosphorylated β_2AR where β-arrestins serve as cellular trafficking molecules by specifically targeting β_2AR to clathrin-coated vesicles. Ultimately, the receptor undergoes internalization [20, 53, 54]. Following internalization, receptors may be either recycled to the cell surface or targeted for lysosomal degradation [55]. Internalization of β_2AR in the absence of agonist implies that β_2ARs enter cells constitutively by clathrin-independent endocytosis and colocalize with markers of this endosomal pathway on recycling tubular endosomes, indicating that these receptors can subsequently recycle back to the plasma membrane [56].

Understanding of the importance of membrane lipid microenvironment in 7TMRs signaling and trafficking is rapidly evolving. Caveolae, a specific type of lipid microdomain, represent a preferred microenvironment for β_2AR for certain events such as signaling [57]. However, a receptor's maintenance within a specific microenvironment may be subject to dynamic regulation. Further evidence supporting the importance of β_2AR membrane microdomain restriction is that the confinement of β_2AR to caveolae has been reported to be of critical importance for regulation of the intrinsic contraction rate in neonatal cardiac myocyte [58].

2.1.4.3 Homooligomerization of the β_2AR

The appreciation that 7TMRs can exist as dimers or higher-order oligomers has advanced rapidly [59], and β_2AR was the first member of the AR subfamily for which homooligomerization was demonstrated, by using coimmunoprecipitation of epitope tagged receptors [60]. Bioluminescence resonance energy transfer (BRET) technology was then used for the quantitative characterization of oligomeric complexes [61]. The concept that dimerization is a requisite for function may be possible as well. It was demonstrated that mutating residues in TM6 predicted to be important for β_2AR dimerization, reduced the surface trafficking of the receptor, suggesting that dimerization is an early event in receptor biosynthesis [62]. How ligands affect the regulation of the oligomeric status of 7TMRs is still a matter of debate. Some studies indicate that agonist binding could increase the number of

β_2AR dimers formed [60], which is also supported by BRET data [61]. On the contrary, results from Fung et al. [63] suggest otherwise; in their study, agonists and antagonists had little effect on the relative orientation of β_2AR protomers in oligomeric complexes. However, binding of inverse agonists led to significant increases in fluorescence resonance energy transfer (FRET) efficiencies, suggesting that this class of ligand promotes tighter packing of protomers and/or the formation of more complex oligomers by reducing conformational fluctuations in individual β_2AR protomers.

2.1.4.4 Heteromerization of the β_2AR

β_2AR can physically and functionally interact with various receptors, mostly resulting in altered receptor surface expression, signaling profiles or intracellular trafficking. Within the AR subfamily, β_2AR can form heterooligomers with β_1AR [64], β_3AR [65] and α_1d-adrenergic receptor (α_1dAR) [66, 67]. β_1AR and β_2AR are coexpressed in a large number of tissues and cell types [60, 61] and Lavoie et al. [64] found that coexpression of the two receptor subtypes in HEK-293 cells led to their heterodimerization and inhibited both agonist promoted β_2AR internalization and ERK1/2 MAPK stimulation. Further on, heterodimerization with β_2AR promotes surface expression and functional activity of α_1dAR [66, 67]. This suggests that heterodimerization may represent a regulatory crosstalk process arising through the creation of a receptor form that has distinct functional properties.

Several studies have suggested that heterodimerization could affect agonist-promoted β_2AR endocytosis, a well-characterized process classically involved in signal attenuation. In the case of δ-opioid receptor (DOR):β_2AR heteromer, stimulation of only one of the protomers was sufficient to promote cointernalization of both receptors [68]. Moreover, these cells exhibit a substantial decrease in the isoproterenol induced phosphorylation of MAP kinases. By contrast, receptors that do not undergo efficient agonist-promoted endocytosis can act as dominant-negatives for endocytosis-prone receptors after heterodimerization. In that manner, κ-opioid receptor (KOR) inhibited β_2AR endocytosis [68]. The cells cotransfected with β_2AR and somatostatin receptor 5 (SSTR5) exhibit β_2AR or SSTR5 internalization upon

receptor specific activation, however, synergistic activation of both receptors triggers strong colocalization at the cell surface and may account for enhanced FRET efficiency [69].

The potential physiological importance of heterodimerization is supported by studies in cells that endogenously coexpress the studied receptors. In freshly isolated mouse cardiomyocytes, the blockade of either the angiotensin II type 1 receptor (AT_1R) or the β_2AR with selective antagonists inhibits the signaling of both receptors simultaneously [70], a phenomenon linked to the ability of the two receptors to heterodimerize.

In a study by Haack et al. [71] bradykinin type 2 receptor (Bk2R) transactivates β_2AR in a heterodimer formation composed of these two receptors. McGraw et al. [72] showed that the prostaglandin E receptor 1 (EP1R) heterodimerizes (or forms higher-order oligomers) with β_2AR, and the signaling of this complex was manifested by an altered β_2AR conformation and decreased functional interaction with $G\alpha_s$. β_2AR can also interact with olfactory receptor [73] serotonin 4 receptor (5-HT4R) [74], opsin and gastric inhibitory polypeptide (GIP) receptor [75], C-X-C chemokine receptor type 4 (CXCR4) [76], cannabinoid 1 receptor (CB1R) [77, 78], D1 dopamine receptor (D1R) and the μ-opioid receptor (MOPr) [78]. A recent study has expanded this list to include the oxytocin receptor [79].

7TMR and RTK can be a part of a large multiprotein complex which can be assembled in response to agonist stimulation and cotrafficked into endosomes together, as has been demonstrated for the β_2AR and the epidermal growth factor receptor (EGFR) [80]. Formation of this complex appears to mediate transactivation of the EGFR, resulting in EGFR dimerization, tyrosine autophosphorylation, EGFR internalization, and ERK1/2 activation. Thus, crosstalk between β_2AR and EGFR may serve as a cell-specific mechanism to regulate the diversity of β_2AR signaling. Similarly, large signaling arrays have been described for the macromolecular complex including the β_2AR, $G\alpha_s$, PKA, AC and the AMPA (α-amino-3-hydroxy-5-methyl-4-isoxazolepropionic acid)-type glutamate receptor subunit GluR1 [81].

2.2 RECEPTOR TYROSINE KINASES (RTKs)

RTKs represent the second largest receptor superfamily fundamentally important for regulation of cell differentiation, growth, cell cycle control and metabolism. RTKs constitute receptors for growth factors, cytokines, and hormones. In addition to mediating physiological cellular processes, they play a crucial role in the development and progression of many types of cancer. Numerous diseases result from genetic changes or abnormalities that alter the activity, cellular distribution, or regulation of the RTKs signaling pathways. For instance, diabetes mellitus, inflammation, severe bone disorders, arteriosclerosis and angiogenesis can be caused by disturbance in RTK function [82, 83].

2.2.1 Overall architecture and domain organization

Heterogeneities within extracellular ligand binding region present the basis for RTKs classification, which includes twenty different families (Fig. 4). RTKs share structural homology starting from the EC region, a TM helix, a so-called juxtamembrane (JM) domain, followed by a C-region with the catalytic tyrosine kinase (TK) function and a C-terminal tail (Fig. 4). Ligand binding occurs in the EC region, TK domain mediates the biological response, transmits the signal intracellularly and the TM domain connects the EC and IC regions and spans the membrane a single time. RTKs contain one or more regulatory regions consisting of a C-terminal tail or a kinase insert and many autophosphorylation sites are located within these regulatory regions [84-86].

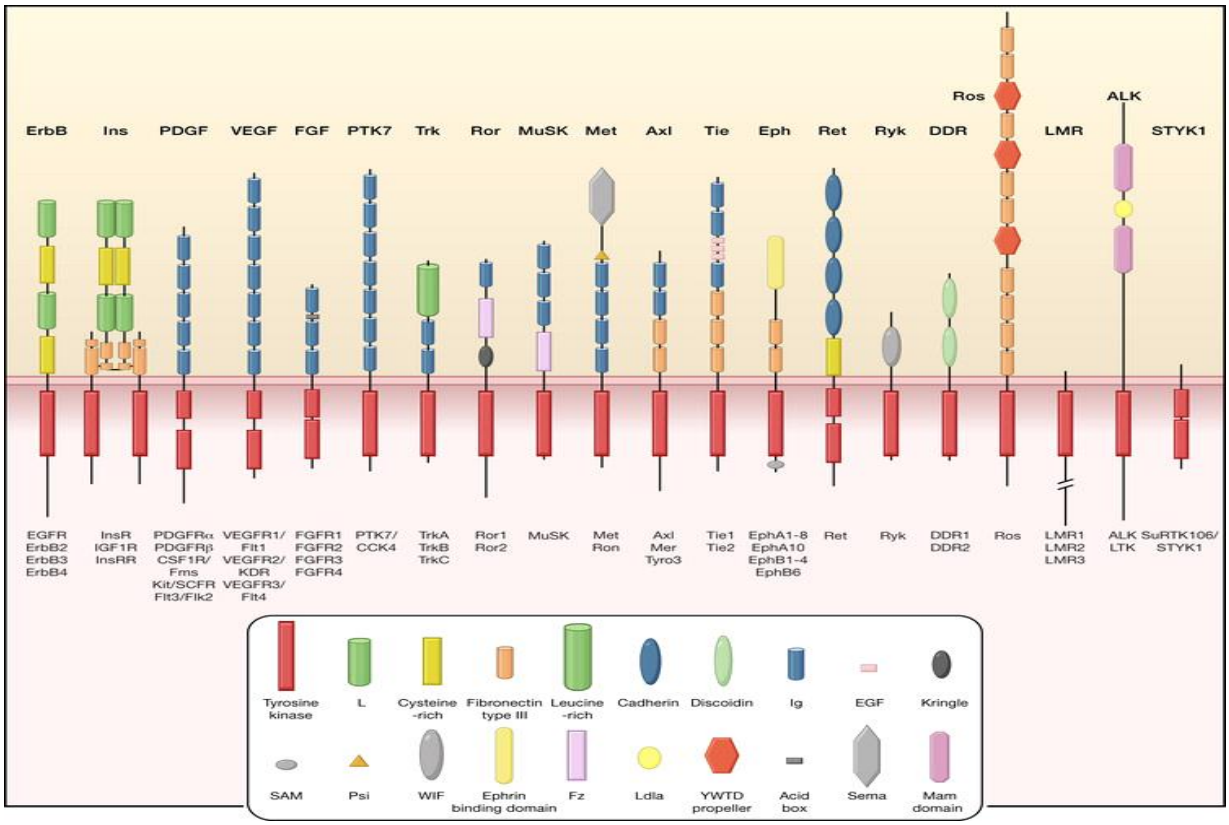

Figure 4: Schematic representation of RTK subfamilies [87]

2.2.2 Mechanisms of receptor activation and oligomerization

The fundamental response of RTKs is mediated by their TK activity. Mutations that eliminate the TK activity also abolish the biological function of the receptor [84]. Ligand binding activates the receptor by inducing structural changes and receptor dimerization, although members of the IR family are predimerized by disulfide bonds and present constitutive dimers [83]. In the ligand-bound receptor, self-association of the EC region is thought to guide the IC domains into a dimeric conformation that activates TK regions. One receptor in the dimer/oligomer phosphorylates one or more tyrosines in a neighboring RTK, and the phosphorylated receptor serves as a site for assembly (and activation) of IC signaling proteins [83, 87].

After ligand binding and dimerization, the receptors cluster into coated pits and are internalized. One possibility is that the internalization is required for receptor signaling. This model implies that certain critical substrates are not available at the cell surface but become

accessible once the activated receptor is internalized. Another model is that the activated receptors have access to all the necessary substrates at the cell surface and that internalization serves to attenuate the signal by down-regulating cell surface receptors [84].

2.2.3 Insulin receptor (IR)

IR is a transmembrane receptor that belongs to the IR family of RTKs, together with insulin-like growth factor receptor (IGFR) and insulin receptor related receptor (IRRR) IR's main physiological role is regulation of glucose metabolism and its endogenous ligands include insulin, insulin-like growth factor 1 and 2 (IGF 1/2) [88]. Insulin is a hormone secreted by pancreatic β cells which triggers the uptake of glucose, fatty acids and amino acids into liver, adipose tissue and muscle, stimulating the storage of these nutrients in the form of glycogen, lipids and proteins (Fig. 5) [89].

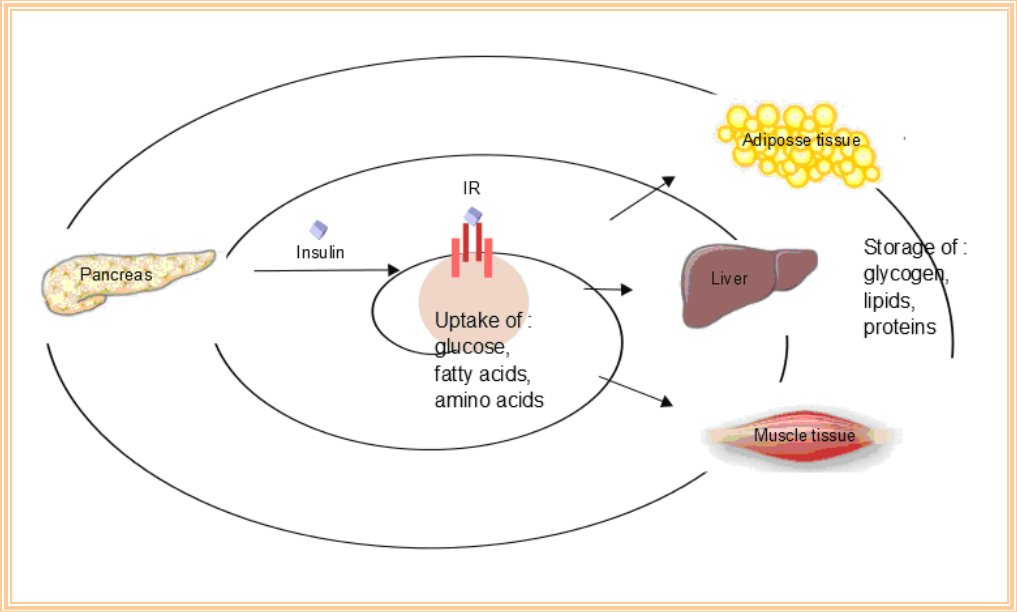

Figure 5: Insulin regulation of glucose metabolism
Figure created by author based on a data from [89].

2.2.3.1 Structure of the IR

IR is encoded on human chromosome 19 and two alternative splice variants derived from the *INSR* gene are translated to form one of two monomeric isomers; IR-A in which exon 11 is excluded, and IR-B in which exon 11 is included. Exon 11 encodes a 12 amino acid segment

localized at the C-tail of the α-subunit which is predicted to influence receptor-ligand interaction [90, 91]. Members of the IR family form disulfide-linked dimers of two polypeptide chains; two extracellular α subunits and two transmembrane β subunits forming α2β2 heterotetramer (Fig. 6). Each IR monomer is structurally organized into 8 distinct domains consisting of; a leucine-rich repeat domain (residues 1–157), a cysteine-rich domain (residues 158–310), an additional leucine rich repeat domain (residues 311–470), domains; FnIII-1 (residues 471–595), FnIII-2 (residues 596–808) and FnIII-3 (residues 809–906). Additionally, an insert domain (ID, residues 638–756) resides within FnIII-2, containing the α/β furin cleavage site, from which proteolysis results in both IDα and IDβ domains. Within the β-chain, downstream of the FnIII-3 region lies a transmembrane helix (TH) and IC JM domain, just upstream of the IC TK catalytic region, responsible for subsequent IC signaling pathways (Fig. 6) [92].

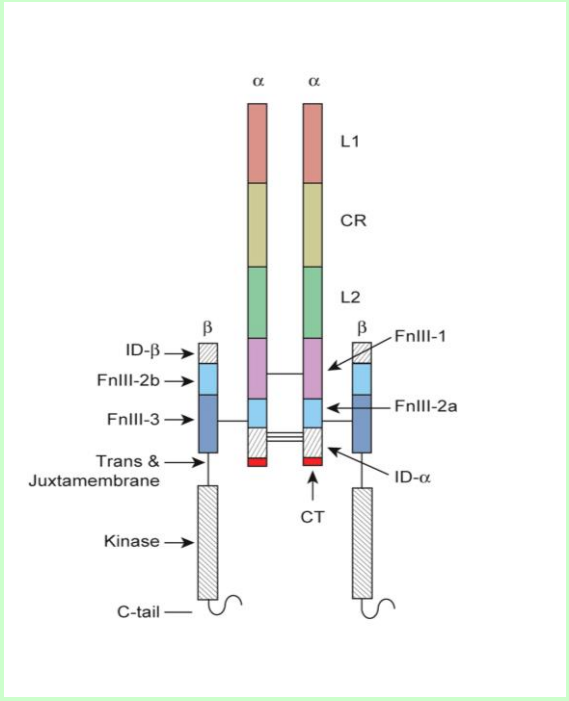

Figure 6: Schematic diagram of the IR homodimer

The leucine-rich repeat domains are denoted as L1 and L2, the cysteine-rich domain as CR, the three fibronectin type III domains as FnIII-1, FnIII-2a/ FnIII-2b and FnIII-3 and the insert region of FnIII-2 as ID. Inter-chain α-α disulphide bonds occur in two places (C524-C524 and at the triplet of cysteine residues at 682, 683 and 685 in ID). The C-terminal 16 residues of the α-chain (the so-called CT-peptide) are also shown. There is only a single α-β disulphide (C647-C860) in each IR monomer. Adapted from [93].

2.2.3.2 IR signaling and endocytosis

Binding of insulin to the IR's α-subunit induces a conformational change that results in a transphosphorylation of a number of tyrosine residues present in the β-subunit, by the ligand-stimulated intrinsic TK of the other β-subunit [94]. Phosphorylated tyrosine residues are recognized by phosphotyrosine-binding (PTB) domains of adaptor proteins such as the insulin receptor substrate (IRS) [95, 96]. As a result, key tyrosine residues on IRS proteins are phosphorylated by the receptor and some are recognized by the Src homology 2 (SH2) domain of the phosphoinositide 3-kinase (PI3K) p85 regulatory subunit [97]. The catalytic subunit of PI3K, p110, phosphorylates phosphatidylinositol (4,5) bisphosphate (PtdIns(4,5)P_2) leading to the formation of Ptd(3,4,5)P_3. A key downstream effector of Ptd(3,4,5)P_3 is Akt (also known as protein kinase B (PKB)), which is recruited to the plasma membrane. Activation of Akt also requires the protein kinase 3-phosphoinositide-dependent protein

kinase-1 (PDK1), which in combination with an as yet unidentified kinase leads to the phosphorylation of Akt. Once active, Akt enters the cytoplasm where it leads to the phosphorylation and inactivation of glycogen synthase kinase 3 (GSK3). A major substrate of GSK3 is glycogen synthase, an enzyme that catalyzes the final step in glycogen synthesis. Phosphorylation of glycogen synthase by GSK3 inhibits glycogen synthesis. Therefore the inactivation of GSK3 by Akt promotes glucose storage as glycogen [95, 96].

Activated Akt phosphorylates downstream kinases and transcription factors such as GSK3, forkhead box O1 (Foxo1), glucose transporter (Glut), hormone sensitive lipase (HSL) and mechanistic target of rapamycin (mTOR), thus being responsible for most metabolic insulin actions of insulin to maintain glucose and lipid, as well as protein homeostasis [95, 96].

As it is the case with other growth factors, insulin activates the MAPK pathway. This pathway involves the tyrosine phosphorylation of IRS proteins and/or Shc, which in turn interact with the adapter protein GRB2, recruiting the SOS (son of sevenless) exchange protein to the plasma membrane for activation of Ras. The activation of Ras also requires stimulation of the tyrosine phosphatase SHP2 through its interaction with receptor substrates such as GAB1 (GRB2 associated binding protein-1) or IRS1/2. Once activated, Ras operates as a molecular switch, stimulating a serine kinase cascade through the stepwise activation of Raf, MEK (mitogen-activated protein kinase kinase, also known as MAPKK) and ERK [98]. Activated ERK can translocate into the nucleus, where it catalyzes the phosphorylation of transcription factors such as p62TCF, initiating a transcriptional programme that leads to cellular proliferation or differentiation [99]. Protein tyrosine phosphatases (PTPase) catalyze the dephosphorylation of insulin receptor and its substrates, leading to attenuation of insulin action.

Like many other cell surface receptors, the IR undergoes a complex endocytotic itinerary. The insulin regulated internalization of IRs has been shown to depend on IR autophosphorylation [100, 101], but to be independent of the downstream phosphorylation or

activation of IRS or PI3K in Chinese hamster ovary (CHO) cells [101]. Most work has concentrated on endocytosis of the IR through the clathrin-coated pit-mediated pathway [102, 103], but reports have also suggested other pathways for IR internalization [104, 105]. After endocytosis, the ligand (insulin) and its receptor are dissociated. Most of the insulin is degraded, whereas the receptors are largely recycled to the cell surface [106].

Endocytosis of hormone receptors has also been suggested to be a part of the signaling process, thus providing access to IC proteins and structures for the active receptor, which can contribute to the pleiotropy in a hormonal response [107]. Evidence in support of this for the IR has accrued [108-111], but there are also reports to the contrary [112, 113], while conclusive evidence for a direct role of endocytosis of the IR in insulin signaling is lacking.

2.3 THE ARRESTIN FAMILY OF PROTEINS

The arrestin family, initially identified in the mid-1980s as cytosolic proteins, is comprised of: visual arrestins (arrestin 1 and arrestin 4) and non-visual arrestins (β-arrestin 1 (βarr1) and βarr2), also designated as arrestin 2 and arrestin 3, respectively). Recently, other proteins distantly related to arrestins on the basis of their sequence (about 10% identity) have been modeled (arrestin domain-containing proteins (ARRDCs), arrestin-related trafficking adaptors (ARTs), DSCR3 (Down syndrome critical region gene 3)) [114, 115] or crystallized (vacuolar protein sort (VPS 26)) [116, 117]. Altogether, they now constitute the arrestin clan (CL0135) [118]. Visual arrestins, as the name indicates are limited exclusively to the retinal rods and cones. Non-visual arrestins, however, are ubiquitously distributed in most mammalian tissues and cell types. Regardless of their dissimilar localization, they are closely related (70% sequence identity) [119]. The amino acid sequences between the βarr1 and βarr2 are 78% identical and highly conserved across species, whereas most of the coding variances occur in the C-terminus (Fig. 8) [119, 120].

The following domains within the arrestin structure have been proposed to be involved in 7TMR binding: (i) a C-terminal acidic region that serves a regulatory role in controlling

arrestin binding selectivity toward the phosphorylated and activated form of a receptor; (ii) a basic N-terminal domain that directly participates in receptor interaction and appears to serve a regulatory role via intramolecular interaction with the C-terminal acidic region; and (iii) two centrally localized receptor binding loops (i.e. finger and lariat/gate loops) that are directly involved in determining receptor binding specificity and selectivity [20, 34, 121].

2.3.1 β-arrestin and β_2AR signaling

Upon activation, β_2AR is phosphorylated by GRK and subsequently recruits β-arrestin [122]. Class A receptors which include β_2AR bind βarr2 with higher affinity than βarr1 [123]. β-arrestin binding uncouples the receptor from the G protein, thus terminating or attenuating G protein-mediated signaling (desensitization). In addition to its role in β_2AR desensitization, β-arrestin recruits and binds the endocytic machinery components, namely adaptor protein-2 (AP-2) [124] and clathrin [54], thereby facilitating receptor removal from the plasma membrane (Fig. 7). Receptor mutations that impair agonist-induced 7TMR phosphorylation limit β-arrestin recruitment and lead to poor receptor internalization, as demonstrated for a β_2AR in which all of the GRK phosphorylation sites had been altered [125]. Expression of dominant-negative mutant β-arrestin proteins (βarr1 V53D or βarr2 V54D) inhibit β_2AR internalization as well [126]. β-arrestin (319–418), a construct that binds well to clathrin but completely lacks 7TMR binding activity, effectively inhibits agonist-induced β_2AR internalization [127]. In addition, βarr2 mutants deficient in their ability to interact with the components of the clathrin-coated vesicles (βarr2 R393E,R395E and βarr2 373 stop) significantly reduce β_2AR internalization as well [128].

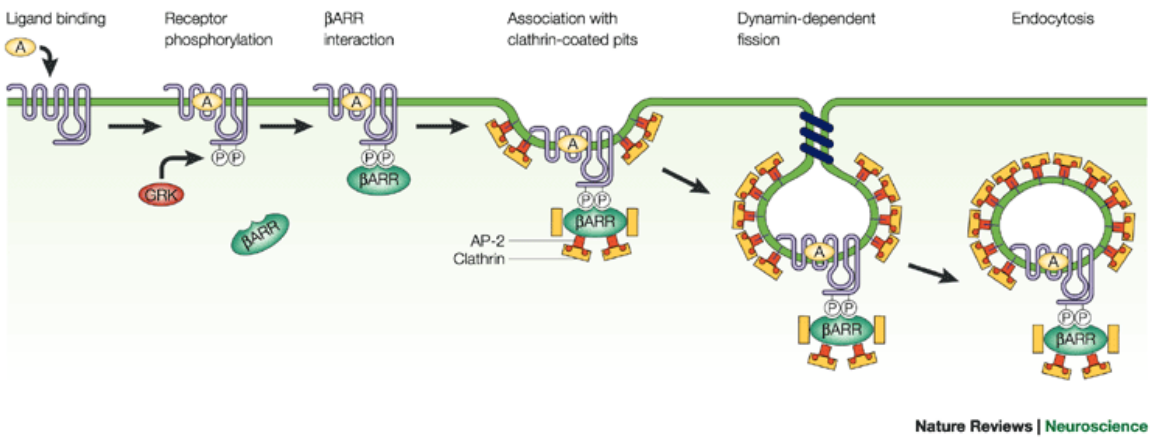

Figure 7: β-arrestin dependent internalization of 7TMRs

After agonist (A) binding to 7TMR, GRK phosphorylate residues in the third intracellular loop and C-tail of 7TMRs, leading to the recruitment of β-arrestins. The β-arrestins recruit clathrin and the AP-2 complex, which target 7TMRs for clathrin-mediated endocytosis [129].

β-arrestins also serve as multi-functional adaptors and signal transducers, linking the 7TMRs to a growing list of signaling molecules, including MAPK, tyrosine kinase c-Src, and serine/threonine (Ser/Thr) kinase Akt [19]. The Ras-dependent activation of MAPK pathways by many receptors coupled to G proteins requires the activation of Src family tyrosine kinases. βarr1 can recruit c-Src, a nonreceptor tyrosine kinase family member to the β_2AR and this newly composed complex can trigger endocytosis leading to the activation of ERK (Fig. 8) [16]. Whereas classical agonists such as isoproterenol stimulate both G protein-mediated and β-arrestin-mediated signaling mechanisms, "biased ligands" can selectively activate G protein or β-arrestin-mediated signaling (carvedilol) and thus elicit distinct biological effects [36, 130-132].

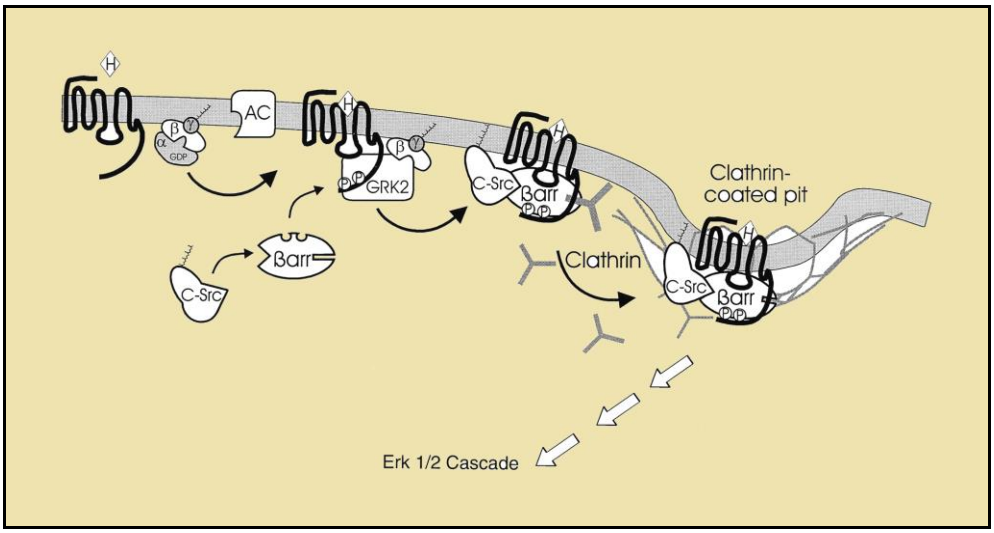

Figure 8: Model of β-arrestin mediated recruitment and targeting of c-Src

βarr1 binds to both GRK-phosphorylated receptor and c-Src, resulting in the recruitment of Src kinase to the membrane. Subsequent interaction of βarr1 with clathrin targets the complex comprising receptor, β-arrestin and Src to clathrin-coated pits. Both β-arrestin mediated Src kinase recruitment and receptor targeting to clathrin-coated pits are required for β_2AR mediated activation of the Erk pathway. Adapted from [16].

2.3.2 β-arrestin and IR signaling

As it is well known, chronic insulin treatment leads to subsequent desensitization of insulin signaling at several steps, such as deactivation of PI3K, dephosphorylation of Akt as well as ubiquitination and degradation of IRS-1 [133]. β-arrestins are important regulators in ubiquitin system and βarr1 can scaffold ubiquitin ligase Mdm2 (Mouse double minute 2 homolog) (binding domain depicted in Fig. 9), thus competitively inhibiting Mdm2-mediated IRS-1 degradation resulting in augmented insulin sensitivity [121].

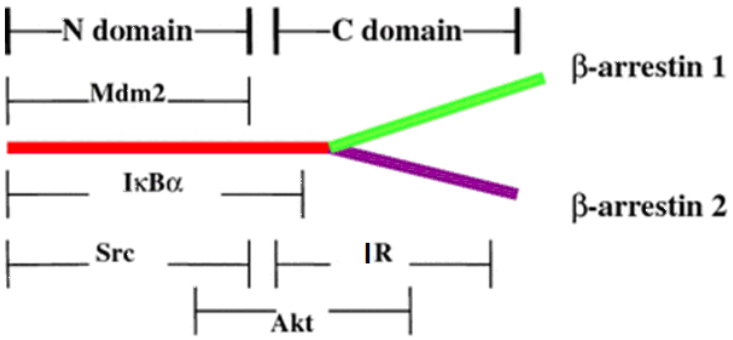

Figure 9: Structural information of β-arrestins, indicating binding domains for signaling molecules

The binding regions for Mdm2 (1–186), Src (1–185), IR (186–409), IκBα (1–240) and Akt are shown. Adapted from [121].

In a β-arrestin-dependent insulin signaling, βarr2 can scaffold IR, Akt and Src forming a new βarr2 signaling complex (binding domains depicted in Fig. 9), which provokes activation of Akt (Fig. 10). β-arrestins can also serve as the signal transducers to guide signals from the cell membrane to MAPK pathway by forming β-arrestin-dependent signaling complexes. They recruit various MAPK such as ERK1/2 and Jun N-terminal kinase 3 (JNK3) to upstream kinases like MAPK kinase and MEK in agonist-dependent manner, thus leading to the activation of ERK1/2 and JNK3 [121].

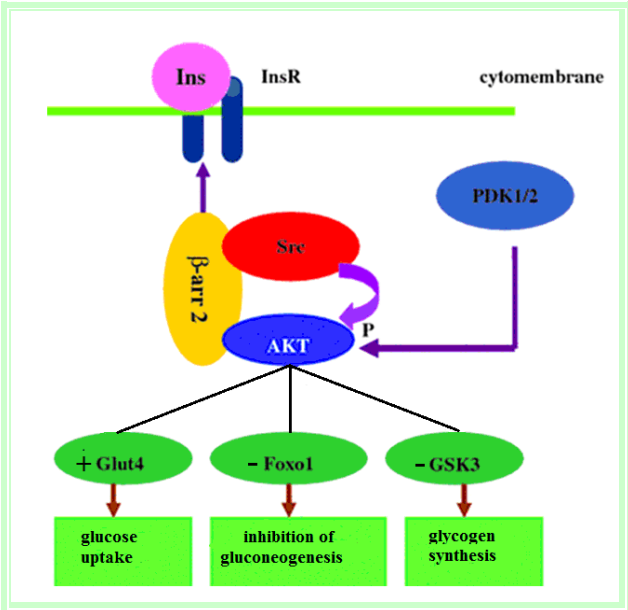

Figure 10: β-arrestin-dependent insulin signaling

Upon insulin stimulation, βarr2 scaffolds Akt and Src to insulin receptor, thus forming a βarr2 signal complex which regulates downstream critical node such as GSK3, Foxo1, and mediates glycogen synthesis, inhibition of gluconeogenesis, and glucose uptake. Adapted from [121].

A study by Luan and his colleagues [17] provided evidence to support the indications that βarr2 deficiency contributes to insulin resistance. In their study, they showed that βarr2 expression in muscle and liver but not adipose tissue, both sites of insulin resistance, is severely downregulated in insulin-resistant animal models. They also found that the similar downregulation exists in liver from a small cohort of patients with type 2 diabetes.

2.4 SHC FAMILY OF ADAPTER PROTEINS

Shc is an adapter protein important for signaling events of numerous types of receptors and there are three Shc gene products in mammals referred to as ShcA, ShcB and ShcC. While ShcB and ShcC expression appears limited to neuronal cells, ShcA protein is ubiquitously expressed. ShcA possessses three isoforms of about 46, 52 and 66 kDa (all generated from the same message either through RNA splicing or alternative translational initiation) [134, 135]. All Shc isoforms comprise N-terminal PTB domain a C-terminal SH2 region and a central proline-rich collagen homology 1 domain which contains critical tyrosine phosphorylation sites. The tyrosine phosphorylation of Shc occurs upon engagement of different cell surface

receptors such as growth fact or receptors; antigen receptors; cytokine receptors; 7TMRs and hormone receptors. Shc has a pivotal role in activation of the Ras/MAPK pathway, and is affiliated with other signaling events such as c-Myc gene activation and cell survival [134].

2.4.1 Shc and IR signaling

Upon insulin activation, IR interacts with Shc in order to activate p21ras and MAP kinase cascade. The NPXY motif around IR's 960-Tyr residue binds to the N-terminal PTB domain of Shc and phosphorylates the 52-kDa, and, to a lesser extent, the 46-kDa Shc isoforms. Although Tyr-239/240 and Tyr-317 residues are the possible phosphorylation sites, IR predominantly phosphorylates the Shc Tyr-317 residue. Phosphorylated Shc binds to Grb2, which forms a complex with Sos GEF for p21ras. Both tyrosine-phosphorylated Shc and IRS can bind to Grb2, but Shc-Grb2-Sos is the predominant coupling pathway from the activated IR to p21 ras. Insulin only transiently activates p21 ras and in the case of longer insulin treatment p21ras is deactivated by dissociation of Sos from the Shc-Grb2-Sos complex while Shc is still complexed with Grb2. Shc is also known to compete with IRS as the substrate of the IR where Shc overexpression leads to decreased IRS mediated glycogen synthesis [136].

2.4.2 Shc and β_2AR signaling

7TMRs stimulate mitogenesis in part via MAPK cascades. β_2AR employs unknown effectors of G$\beta\gamma$ subunits and stimulates tyrosine phosphorylation of plasma membrane associated proteins to create tyrosine phosphoprotein scaffolds. Receptor activation coincides with an increase in tyrosine phosphorylation of the adaptor protein Shc, and phosphorylated Shc interacts with Grb2. In turn, Grb2 binds to Ras GEF and Sos. Thereafter, Grb2-mSos complex is directed to the plasma membrane. Recruitment of mSos triggers Ras GDP/GTP exchange leading to recruitment of Raf into complex with activated Ras. Subsequent signal transduction involves sequential phosphorylation and activation of the MEK and MAPK [137].

2.5 7TMRs:RTKs CROSSTALK

Functional interplay between different classes of receptors has emerged as a notable factor of cellular response in health and disease. The discovery that 7TMRs can merge and condition RTKs mediated signaling and *vice versa* presents a new important field of receptor signaling. Activation of 7TMRs sometimes results in a phenomenon known as transactivation of RTKs, which leads to the recruitment of scaffold proteins, such as Shc, Grb2, and Sos in addition to MAPK activation. In other cases, RTKs use different components of 7TMRs mediated signaling, such as β-arrestins, GRKs, and regulators of G protein signaling to integrate signaling pathways [5, 138, 139].

EGFR is an extensively studied example of transactivation through RTKs [140] in which the activation of 7TMRs promotes production of EGF via metalloproteinase-catalyzed shedding of a transmembrane precursor and, in some cases, induction or tyrosine phosphorylation in the C-tail of the RTK [141]. Wang et al. [142] suggested that D2R activation induces the formation of a macromolecular signaling complex which includes D2R and EGFR in neuroblastoma cells, and that D2R activation of ERKs was dependent on transactivation of EGFR. Flajolet et al. [143] found a direct physical interaction between the adenosine A2a receptor (A2aR) and the fibroblast growth factor receptor (FGFR). Concomitant activation of these two classes of receptors, but not individual activation of either one alone, caused a robust activation of the MAPK/ERK pathway, differentiation and neurite extension of PC (rat adrenal phaeochromocytoma) -12 cells, spine morphogenesis in primary neuronal cultures, and cortico-striatal plasticity induced by a previously unknown A2aR/FGFR-dependent mechanism.

The first indication that RTKs might use G proteins to transmit signals to effectors was the finding that pertussis toxin (which uncouples $G\alpha_i$ from its respective 7TMR) abolished the insulin-induced inhibition of AC in isolated liver membranes and hepatocytes [144]. Moreover, insulin inhibited the pertussis toxin-catalyzed [^{32}P] ADP ribosylation of $G\alpha_i$ in isolated liver membranes, suggesting that the IR might induce changes in the conformational state of $G\alpha_i$ [145]. Luttrell et al. [146] then demonstrated that insulin

promoted pertussis toxin-sensitive GTPγS binding in liver membranes containing $G\alpha_i$. Subsequently, they also reported that pertussis toxin administration or overexpression of the C-terminal tail of GRK2 inhibited the IGF-1R- and insulin-stimulated activation of the ERK-1/2 pathway in fibroblasts [147]. At this point, one could have considered $G\alpha_i$ to function downstream of IR and IGF-1R [5].

Waters et al. [148] found that endogenous platelet-derived growth factor receptor β (PDGFRβ) and the sphingosine 1-phosphate receptor 1 ($S1PR_1$) form a functional complex in airway smooth muscle cells [148] and mouse embryonic fibroblasts [149]. The same heteromeric complex could also be formed by overexpression of these two receptors in HEK (human embryonic kidney) -293 cells [150]. Neither PDGF nor S1P induced changes in the association of these receptors in the complex and S1P did not induce tyrosine phosphorylation of PDGFRβ [148, 150]. However, overexpression of $S1PR_1$ enhanced the PDGF-stimulated activation of the ERK-1/2 pathway in HEK-293 cells expressing PDGFRβ [150]. They also demonstrated that c-Src participates in regulation of PDGFRβ-$S1PR_1$ complex endocytosis in response to PDGF [151]. A role for the constitutively active form of $S1PR_1$ in increasing PDGFRβ signaling was demonstrated by results showing that similar enhancement was achieved by the overexpression of $S1PR_1$ mutants [152], which are deficient in their ability to bind S1P [153].

There are now several other examples of RTK:7TMR signaling platforms in which the constitutively active 7TMR enhances RTK signaling. For instance, IGF-1 uses the $G\alpha_i$-coupled CXCR4 in the absence of chemokine ligand 12 (CXCL12, the natural ligand of CXCR4) to promote migration of breast cancer cells, which is noteworthy because these cells are highly metastatic. This involves the regulation of $G\alpha_i$ and Gβγ subunits by IGF-1 [154]. In another study constitutively active pituitary adenylate cyclase-activating peptide type 1 receptor (PAC1R) forms a complex with IGF-1R, and this is involved in IGF-1-induced survival of neurons. IGF-1 stimulates the c-Src-catalysed tyrosine phosphorylation of PAC1, which results in stimulation of Akt and AC [155]. In follicular thyroid carcinoma cells, the vascular endothelial growth factor receptor-2 (VEGFR-2) forms a complex with $S1PR_1$. The complex evokes bidirectional signaling since the S1P-induced ERK1/2 phosphorylation is

sensitive to VEGFR-2 kinase inhibition and VEGF-A-induced ERK1/2 phosphorylation is sensitive to pertussis toxin treatment as well as $S1P_1$ small interfering RNA expression [156]. The tropomyosin-related kinase A receptor/neurotrophic tyrosine kinase receptor type 1 (NTRK1/TrkA), which binds nerve growth factor (NGF), forms a complex with lysophosphatidic acid receptor-1 (LPAR1). In this case, constitutively active LPAR1 provides $G\beta\gamma$ subunits that are used by the TrkA receptor to enhance activation of ERK-1/2 in response to NGF [157, 158].

It is increasingly evident that 7TMRs and RTKs form an integrated signaling network, and that the transactivation of RTKs by ligand-stimulated 7TMRs is a general process allowing for pleiotropic signaling [159-161]. The majority of these interactions still need to be validated in native tissues and a clear function needs to be attributed to these complexes. Such a higher molecular organization brings new alternatives in term of physiological functions for each of these two receptor families but it also increases the possibilities regarding therapeutic targeting. Biochemical and/or pharmacological properties reported for 7TMR:RTK heteroreceptor complexes are often distinct from those of the corresponding protomers. Thus, heteromerization represents an important mechanism for modulating and integrating the physiological functions of 7TMRs and RTKs. This can take place at different stages of the receptor's life: biosynthesis, ligand binding, G protein activation, desensitization, internalization and degradation [162].

2.5.1 INTERACTION BETWEEN β_2AR AND IR

Glucose metabolism is under the cooperative regulation of both IR and β_2AR. The anabolic action of insulin promotes glycogen synthesis, glucose uptake in skeletal muscle and lipid storage [95]. By contrast, catecholamines act in opposition to insulin, stimulating glycogen breakdown, gluconeogenesis, and lipolysis [163]. The ability of insulin to counterregulate catecholamine action at the tissue level is crucial for the "tight" regulation of serum glucose levels [164] and interaction between IR and β_2AR could be a required action in this process.

At the molecular level, the ability of insulin to counterregulate β_2ARs can be exerted through insulin-stimulated phosphorylation of β_2AR and its subsequent internalization [165-167]. Work from Karoor et al. [166] demonstrated that insulin promoted phosphorylation of Tyr350/354 and Tyr364 in the C-terminal tail of β_2AR as well as that phosphorylation of Tyr350/354 attenuates β_2AR activation of cAMP production in CHO cells. Valiquette et al [167] also showed that insulin promoted tyrosine phosphorylation of the β_2AR, although their work suggested that the phosphorylation occurred on Tyr141 and resulted in an enhanced ability to activate cAMP production in Chinese hamster fibroblasts (CHW). The reason for the striking differences between these studies is not readily apparent but may reflect the different cell types that were used. Indeed, a more detailed *in vitro* analysis suggests that the IR can directly phosphorylate the β_2AR at multiple sites, including Tyr132/141, Tyr350/354, and Tyr363 [6].

These studies raise the intriguing possibility that β_2AR function may be dynamically regulated by RTKs in a cell dependent manner. Another interesting aspect of β_2AR's tyrosine phosphorylation is the possibility of generating SH2 domains. Indeed, Karoor et al. [166] have shown that the adaptor protein Grb2 can bind to Tyr350 after insulin-promoted phosphorylation of β_2AR. Phosphorylation of Tyr350 also appears to create a potential site for Src binding to β_2AR [168], implicating Tyr350 in agonist-induced desensitization of β_2AR.

Additional evidence for crosstalk between RTK and β_2AR is provided by data which demonstrate that insulin activation of the ERK1/2 is potentiated by the β_2AR via a mechanism that requires the integrity of Tyr350 [7]. Although the β_2AR potentiates insulin activation of ERK, it appears to attenuate insulin promoted phosphorylation of IRS 1 and 2 [169].

β_2AR and IR are endogenously expressed in the same cell types (e.g. pancreatic β cells, adipocytes, liver cells, skeletal muscle cells, retinal cells, and astrocytes) [8-12]. Therefore, the formation of heteromeric complexes consisting of these two receptors may be plausible. Jiang et al. [170] suggested that a functional link may exist between maintenance of β_2AR function and maintenance of IR's antiapoptotic pathways, whereas Fu et al. [171]

characterized a complex consisting of IR and β_2AR in mouse hearts where activation of the IR with insulin induced PKA and GRK2 mediated phosphorylation of β_2AR, promoting β_2AR coupling to $G\alpha_i$. After insulin pretreatment, the activated β_2AR-$G\alpha_i$ signaling effectively attenuates cAMP/PKA activity following β-adrenergic stimulation in cardiomyocytes, and consequently inhibits PKA phosphorylation of phospholamban and contractile responses in myocytes *in vitro* and in isolated perfused hearts. These data indicate that IR:β_2AR crosstalk offers a molecular basis for the pathophysiology of metabolic and cardiovascular dysfunction in insulin resistant states.

2.6 METHODS FOR INVESTIGATION OF 7TMR:RTK HETEROMERS

Some authors employ the commonly used coimmunoprecipitation for the detection of 7TMR:RTK heteromers [80, 148, 171], which has several drawbacks, mainly relating to the lysis and solubilization steps. First, it requires the solubilization of the cells; therefore, it obviously cannot be used to study interactions in living cells. Second, the highly hydrophobic nature of the 7TM domains makes solubilization using detergents a difficult task while 7TMRs can form aggregates during this step. In addition, the observed interactions may be due to the *in vivo* formation of larger molecular complexes, therefore in many cases coimmunoprecipitation is not appropriate to draw a conclusion about direct interactions between receptor molecules [172].

Epifluorescence microscopy and confocal microscopy are some of the most commonly used imaging techniques. Using immunofluorescence Water et al. [148] visualized cointernalization of PDGFβR and $S1PR_1$ in endocytic vesicles in response to S1P and/or PDGF. By taking advantage of fluorescent labeled antibodies or proteins, the spatial regulation of signaling pathways can be explored. A major drawback of epifluorescence microscopy is the unwanted "glow" from structures above and below the plane of focus, due to blanket illumination of the sample. This is less of a problem in very flat cells, but in rounder cells, such as HEK-293 cells, this can be avoided by the use of confocal microscopes. Confocal microscopy differs in that the microscope optics is set up to focus on a single plane through the cell and to exclude light from other planes. The sample is scanned by a laser light

source in the X and Y directions. The Z depth can be set by the user. This results in an optical sectioning of the sample and allows superior image quality and resolution [173]. The resolution limit of confocal microscope is generally ~250 nm [174], whereas protein-protein interactions take place at distances up to 10 nm. Therefore, we will employ additional methods to specify and confirm protein-protein interactions in which we are interested.

Although coimmunoprecipitation may serve as a starting point to analyze receptor heteromerization in native tissues, considering the methodical difficulties, additional methods should be used to verify the detected interaction. The development of techniques based on resonance energy transfer (RET), and their application to the investigation of interactions between 7TMRs, revolutionized the field of receptor oligomerization. RET is the non-radiative transfer of energy from a donor molecule to an acceptor molecule as a result of electromagnetic dipole-dipole coupling. In the case of FRET, the energy donor is a fluorescent molecule, excited by exposure to light of a characteristic wavelength, transferring the emitted energy to a fluorescent acceptor molecule. Microscopy is often used to detect FRET, while BRET is usually measured in plate readers. These methods are able to sensitively detect protein-protein interactions in live cells, and in real-time, allowing monitoring of the kinetic and dynamic properties of receptor complexes [175].

2.6.1 BRET methodology in investigation of 7TMRs, RTKs and 7TMR:RTK heteromers

Bioluminescence is a natural phenomenon found in marine animals such as the sea pansy *Renilla reniformis* and the jellyfish *Aequorea victoria* where the oxidation of the intrinsically produced substrate coelenterazine to coelenteramide initializes the bioluminescence [176, 177]. This phenomenon has become extremely important for modern biological science, including the BRET method, an advanced, non-destructive, cell-based assay technology that is well suited for proteomics applications, including receptor research and the mapping of signal transduction pathways [178].

Cell surface receptors present special problems for stoichiometric analysis because, being located within lipid bilayers, they are often very hydrophobic, which means that once isolated they can exhibit a strong tendency to aggregate. A very welcome development, has therefore been the development of *in situ* methods for probing receptor organization, the most important of which are presently based on RET [179]. The strict dependence of the phenomenon on the molecular proximity between energy donors and acceptors makes it a system of choice to monitor protein-protein interactions in living cells [61].

BRET technique allows the sensitive monitoring of interactions between two labels at nanometer scale. BRET sensors have been developed for essentially all steps in 7TMR mediated activation/signaling. These steps involve either conformational changes within proteins (such as the agonist dependent activation of receptors) or protein-protein interactions (such as the receptor/G protein and or receptor/β-arrestin interaction). Both of these can be investigated with RET technologies, provided that the labels are inserted at suitable sites in the relevant proteins [180, 181].

In the first BRET study in 7TMRs research, Angers et al. [61] investigated β_2AR dimerization and association of β_2AR with β-arrestin in mammalian cells. They demonstrated that BRET-based assays could be applied for the study of both constitutive and hormone promoted selective protein-protein interactions. Similar studies followed for the thyrotropin-releasing hormone receptor [182], where receptor-specific differences were subsequently shown for βarr1 versus βarr2 [183]. BRET based assays for the 7TMR/β-arrestin interactions have been published for many receptors (e.g., chemokine [184], opioid [185], dopamine [186], prostanoid [187], V2-vasopressin [188], adrenergic and neurokinin receptors [128]).

BRET method has become a gold standard in receptor complexes investigation studies. Studies investigating oligomerization or other protein-protein interactions of multiple types of 7TMRs have been published, e.g., melatonin receptors [189], CXCR1, 2, and 4 and CCR2 and 5 [190], α/β-adrenergic receptors [191, 192], cholecystokinin receptors [193], yeast α-factor receptors [194], opsin receptors [75], protease-activated receptor 1 [195], and secretin

receptors [196]. BRET has also been used to study the ability of muscarinic acetylcholine receptors, M3 and M5, to form homo- and heterodimers in living cells in a manner independent of receptor activation [197].

BRET method is also highly sensitive for quantifying ligand-independent (constitutive), agonist-induced or antagonist-inhibited RTK activity levels [198]. The first BRET study to quantify constitutive, agonist-induced and antagonist-induced RTK activity was performed by Boute et al. [199], using hormones, growth factors, as well as monoclonal antibodies [199]. Issad et al. [200, 201] followed with their studies on IR activation states. Blanquart et al. [202] utilized BRET to characterize ligand-induced conformational changes that occur within hybrids of IRA/IRB, the two isoforms of IR either containing or not containing exon 11. BRET was also employed in investigation of IR interactions with different intracellular binding partners including protein tyrosine phosphatase-1B [203], Grb14 [204, 205], IRS1, IRS4 and Shc [199, 201, 206].

Siddiqui et al. [207] have provided an overview of functional BRET studies associated with the RTK superfamily involving: neurotrophic receptors (e.g. Trk and p75 neurotrophin receptor); insulinotropic receptors (e.g. IR and IGFR) and growth factor receptors (e.g. ErbB receptors including the EGFR, the FGFR, the VEGFR and the c-kit and PDGFR).

It seems that only the interactions between different receptor classes have not yet been thoroughly investigated. BRET technology could present a powerful method to study the structure of heteroreceptor complexes closely associated with the study of receptor-receptor interactions in such complexes. Borroto-Escuela et al. [208, 209] detected interaction between the 7TMR 5-HT1A and RTK FGFR1 including the recruitment of βarr2 employing BRET methodology. In spite of the increasing understanding of the 7TMR transactivation by RTK ligands and their existence as heteroreceptor complexes, only few examples have until now been validated using the $BRET^2$ methodology [208, 209]. We believe that a well-controlled and carefully analyzed BRET assay has a great potential to identify and/or study 7TMR:RTK heteroreceptor complexes.

Milligan and Smith [210] highlighted the need for developing cell-based screening approaches that incorporate the concept of 7TMR heteromerization. They asserted that 7TMR heteromers should be considered as "individual molecular species" and therefore represent drug targets distinct from those observed when screening a single 7TMR in isolation. Importantly, a 7TMR heteromer complex is also likely to include a range of other proteins that contribute to 7TMR function, including structure, localization, trafficking, scaffolding, signaling, desensitization (largely involving phosphorylation), internalization, resensitization/recycling, and/or degradation. Therefore, two 7TMRs within such a complex can influence each other's function without physically touching and, consequently, still fall under the recently agreed definition of a receptor heteromer as a macromolecular complex composed of at least two (functional) receptor units with biochemical properties that are demonstrably different from those of its individual components [211].

In that manner, See et al. [212] developed the 7TMR-heteromer investigation technology (7TMR-HIT), a modified BRET approach that enables monitoring of constitutive or dynamic interactions between receptors that are, crucially, both ligand-dependent in terms of reporter output. Using 7TMR-HIT they profiled the CCR2-CCR5 and CCR2-CXCR4 chemokine receptor heteromers in terms of their ability to recruit the βarr2 specifically to the heteromer complex. As follows, Ayoub et al. [213] reported an adaptation of 7TMR-HIT and demonstrated the utility of this approach for investigating RTK heteromerization by examining the functional interaction between the EGFR and heregulin receptor 3 (HER3) in live HEK-293FT cells using recruitment of Grb2 to the activated receptors. The development of new cell-based assays to assess the heteromerization of the 7TMRs:RTKs, as well as to profile their pharmacology and signaling in real-time and live cells, is of great interest in pharmacological studies, together with drug discovery programs.

2.6.2 Informational spectrum method (ISM)

In order to advance in our understanding of 7TMR:RTK heteroreceptor complexes as well as their potential role as therapeutic targets, we need to continuously look for methods and

technologies that can be used to demonstrate and evaluate such heteroreceptor complexes and their receptor-receptor interactions. The field of bioinformatics has emerged as a significant tool in the management of biological information. ISM represents a methodology based on signal processing which analyses characteristic spectral motifs in DNA/RNA (deoxyribonucleic/ ribonucleic acid) and protein sequences enabling the prediction of protein-protein interactions. In these approaches, protein residues are first converted into numerical sequences (signals) using one out of over 600 available amino acids parameters that are responsible for the biological functionality. These numerical sequences (signals) are then processed by means of discrete Fourier transform to present the biological characteristics of the proteins in the form of an informational spectra [214-216]. The ISM was, this far, successfully applied in the structure-function analysis of different protein sequences [217], prediction of new protein interactors [218] and identification of protein domains responsible for long-range interactions [215, 216].

3 MATERIALS AND METHODS

The techniques described include standard molecular biology methods and specific methods used to: i) express the constructs in eukaryotic cells, ii) measure receptor expression on the cell surface, iii) characterize receptor binding properties, iv) quantify the receptor/ligand internalization process, v) visualize cellular localization/colocalization of receptors and intracellular trafficking of ligand activated receptors, and vi) investigate and characterize protein-protein interactions.

3.1 CELL CULTURE AND TRANSFECTION

3.1.1 Cell culture

HEK-293 cells were obtained from the European Collection of Animal Cell Cultures, Salisbury, UK. The cells were routinely maintained and passaged in Dulbecco's modified Eagle's Medium (DMEM) supplemented with 10% (v/v) heat inactivated foetal calf serum (FCS), 2 mM Glutamax-I, penicillin (100 U/mL) and streptomycin (100 µg/mL) at 37°C in a humidified atmosphere of 5% (v/v) CO_2. For passaging, medium was removed; cells were washed with sterile Dulbecco's Phosphate Buffered Saline (DPBS), without calcium chloride and magnesium chloride and then detached from the bottom of the plate by incubation in Trypsin-EDTA solution (0.05% Trypsin, 0.02% EDTA) for 5 min at 37°C. Molecular biology reagents, cell culture media and reagents were purchased from Sigma-Aldrich (Taufkirchen, Germany) and Gibco®, Life Technologies (Breda, The Netherlands) unless otherwise specified.

3.1.2 Transient transfection

Transfection is the process of deliberately introducing nucleic acids into the cells. The transfection methods are broadly classified into three groups: biological, chemical, and physical. Chemical transfection methods are the most widely used methods in contemporary research and the underlying principle of chemical methods is similar. Positively charged chemicals make nucleic acid/chemical complexes with negatively charged nucleic acids, and these positively charged nucleic acid/chemical complexes are attracted to the negatively

charged cell membrane. The exact mechanism of how nucleic acid/chemical complexes pass through the cell membrane is unknown, but it is believed that endocytosis and phagocytosis are involved in the process. Transfected DNA must be delivered to the nucleus to be expressed. Again, the translocation mechanism to the nucleus is not known [219].

HEK-293 cells were 70–90% confluent at the time of transfection. On the day of transfection, Lipofectamine™ 2000 reagent (Gibco®, Life Technologies) was resuspended in 500 μL of serum–free media (Opti-MEM®; Gibco®, Life Technologies) in a 1.5 mL cryovial tube (TPP,Trasadingen Switzerland) and incubated for 5 min at room temperature. In another 1.5 mL cryovial tubeplasmid DNA was resuspended in 500 μL of Opti-MEM®; plasmid DNA (μg) to Lipofectamine™ 2000 (μL) ratio of 1: 3 was used in all transfections. Upon incubation, 500 μL of Opti-MEM® containing plasmid DNA was combined with Opti-MEM® containing Lipofectamine™ 2000 and the transfection mix was incubated for 20 min at room temperature (RT). In the meantime, complete media was removed and replaced with Opti-MEM®. Following incubation, the transfection mix was pipetted dropwise into the dishes and flasks containing 2 ml and 5 mL of Opti-MEM®, respectively; and incubated for 4 h at 37°C. In due time, Opti-MEM® was replaced with complete DMEM and cells were incubated for another 48 h at 37°C.

3.2 STANDARD MOLECULAR BIOLOGY METHODS

3.2.1 Fusion constructs

Human HA-tagged β_2AR (HA-β_2AR) cDNA (complementary DNA) in vector pcDNA3.1 was purchased from Missouri S&T cDNA Resource Center (University of Missouri-Rolla, USA). HA-β_2AR C-terminally tagged with the RLuc8 (HA-β_2AR-RLuc8), WT human IR isoform A that lacks exon 11, C-terminally GFP^2-tagged IR (IR-GFP^2) and N-terminally GFP^2-tagged Shc (GFP^2-Shc) were generated and verified at Novo Nordisk A/S (Måløv, Denmark). C-terminally RLuc8-tagged IR (IR-RLuc8), C-terminally GFP^2-tagged β_2AR (β_2AR-GFP^2) and the membrane-inserted GFP^2-tagged construct (GFP^2-17aa) were the same as described previously [128, 206, 220]. Human β-arrestin 2 N-terminally tagged with GFP^2 (GFP^2-βarr2)

was purchased from PerkinElmer BioSignal, Inc. (Montreal, Canada) and cloned into the vector pcDNA3.1(+) using the NheI/XbaI restriction sites. GFP^2-βarr2 1-185 (E186- stop; GAA-TAA) and IR 1–1271-RLuc8 were generated by site-directed mutagenesis and verified by sequencing at Genscript USA Inc. (New Jersey, USA). All generated cDNA clones were inserted in the expression vector pcDNA3.1(+).

3.2.2 Plasmid DNA preparation

Introduction of plasmid DNA into the cells by transformation has been of central importance for the rapid advancement of plasmid biology and for the development of DNA cloning methods [221]. Several methods have been described in the literature to incorporate plasmid DNA into the cells. These methods include chemical treatment [222, 223], electroporation [224, 225], use of biolistic gun [226], polyethylene glycol [227], ultrasound [228], microwave [228], and hydrogel [221]. The chemical methods have attained much attention in most of the laboratories due to their accessibility and cost effectiveness. Uptake of free DNA by *Escherichia coli (E. coli)* cells, which have become competent by treatment of chemicals providing Ca^{2+} ions followed by a heat shock pulse was first reported by Mandel and Higa [229]. Subsequently, several modifications of this method have become available [230-232].

Chemically competent *E. coli* TOP10F' cells (Invitrogen™, Life Technologies) were used for transformation. First, TOP10F' cells were thawed on ice and ~0.5 μg of plasmid DNA was added to the 25 μL of bacterial cells (in a 1.5 mL Eppendorf tube). Next, the transformation mixture was incubated on ice for 30 min, followed by a 30 sec heat shock at 42°C (water bath) to promote plasmid uptake into the cells. Thereafter, the mixture was chilled on ice for 2 min to reduce the damage to *E.coli* cells and 250 μL of SOC medium (Super Optimal broth with Catabolite repression) (Sigma-Aldrich) was added and incubated for 1 h at 37°C in a shaking incubator. Transformation mixture (25 μL) was spread on Luria-Bertani (LB) agar plates containing 100 μg/mL ampicillin and grown overnight at 37°C. Only cells that contain the plasmid are able to grow/divide and form colonies. One colony was picked and spread on new LB agar plate containing 100 μg/mL ampicillin and grown overnight at 37°C to confirm antibiotic resistance and to refine selection. Next, one colony

was selected and transferred to 10 mL of LB medium (in a 50 mL Falcon tube (TPP)) containing 100 µg/mL ampicillin and grown for 7 h at 37°C in a shaking incubator. 1 mL of bacterial culture was then transferred to a new 250 mL LB medium containing 100 µg/mL ampicillin in a 2 L Erlenmeyer flask and grown overnight at 37°C in a shaking incubator. Subsequently, the medium with grown transformed bacteria was centrifuged at 6000 rpm for 15 min at 4°C and cell pellet was used for plasmid DNA isolation.

3.2.3 Plasmid DNA isolation and spectrophotometric quantification

The plasmid DNA from bacterial cultures was isolated using Qiagen Plasmid Purification Kit (Qiagen, Venlo, Limburg, The Netherlands) according to the manufacturer's protocol. The protocol is based on a modified alkaline lysis procedure and the principle of this method is based on selective alkaline denaturation of high molecular weight chromosomal DNA while covalently closed circular DNA remains double stranded [233]. Next, the plasmid DNA was bound to an anion-exchange resin under appropriate low salt and pH conditions. Plasmid DNA is eluted by this principle by a high salt buffer, concentrated, and desalted by isopropanol precipitation [234].

The concentration of a 1:100 dilution of a plasmid DNA preparation was determined with Lambda 12 spectrophotometer (PerkinElmer, Boston, MA, USA) by measuring the optical density at both 260 and 280 nm for DNA and protein concentration, respectively. A 260 reading is equivalent for double-stranded DNA. The ratio of absorbance at 260 nm and 280 nm is used to assess the purity of DNA. A 260/280 ratio of ~1.8 indicates good DNA sample purity.

3.2.4 Restriction enzyme analysis of DNA

Restriction enzymes are able to scan along a length of DNA looking for a particular sequence of bases that they recognize. This recognition site or sequence is generally from 4 to 6 base pairs in length. Once it is located, the enzyme will attach to the DNA molecule and cut each strand of the double helix. The restriction enzyme will continue to do the same along the full

length of the DNA molecule which will then break into fragments. The size of these fragments is measured in base pairs or kilobase pairs [235, 236].

Restriction mixture was made with 1µg of plasmid DNA, 2 µL of 10x buffer (Promega, Madison, WI, USA), 1 µL of 2 selected adequate enzymes (Promega) and H_2O was added to the total volume of 20 µL. The mixture was incubated for 3 h at 37°C in a water bath and the resulting fragments resolved by agarose gel electrophoresis.

3.2.5 Agarose gel electrophoresis

Agarose powder was mixed with electrophoresis buffer 0.5% TBE (tris-borate EDTA (Sigma-Aldrich)) to the 0.8% concentration, and subsequently heated in a microwave oven until completely melted. At this point 0.1 µL/mL of ethidium bromide was added to the gel to facilitate visualization of DNA after electrophoresis. After cooling the solution to about 60°C, it was poured into a casting tray containing a sample comb and allowed to solidify at room temperature. After the gel has solidified, the comb was carefully removed as to not rip the bottom of the wells. The gel, still in its plastic tray, was inserted horizontally into the electrophoresis chamber and covered with 0.5% TBE buffer. Samples containing DNA mixed with 2 µL of loading buffer (0.2% bromophenol blue dye, 0.2% xylene cyanol dye and 30% glycerol in a Tris-EDTA buffer) were then pipeted into the sample wells. DNA marker, containing linear DNA (1 kilobase pairs (kb) plus DNA ladder (Boehringer, Mannheim, Germany)), as a reference, was run alongside samples to ascertain the size of DNA fragments. The gel was run in 0.5x TBE buffer at 100 V for approximately ½ h, until the bromophenol blue dye reached the second half of the gel in the electrophoresis chamber. DNA bands were visualized under ultra violet (UV) light with UV Transilluminator 4000 (Stratagene, Heidelberg, Germany). Images were taken using Gene Genius Bio Imaging System with software Gene Snap (Syngene, Cambridge, UK).

3.3 METHODS TO EVALUATE RECEPTOR EXPRESSION AND INTERNALIZATION

3.3.1 Luminescence and fluorescence measurements

Expression levels of RLuc8- and GFP^2-tagged receptor constructs were monitored by total luminescence and fluorescence measurements as previously described [75, 128]. At 48 h after transfections, HEK-293 cells were trypsinized, washed once in DPBS and resuspended in DPBS supplemented with Ca^{2+}/Mg^{2+}, 1 g/L glucose and 36 mg/L sodium pyruvate. For luminescence measurements, 180 μL of resuspended cells containing ~2×10^5 cells was distributed in white 96-well microplates (Optiplate; Packard BioScience, Meriden, CT, USA). After addition of coelenterazine 400a (Biotrend Chemikalien GmbH, Köln, Germany) to a final concentration of 5 μM, total luminescence was measured by using the TriStar LB 942 microplate reader (Berthold Technologies, Bad Wildbad, Germany). For fluorescence measurements 180 μL of resuspended cells containing ~2×10^5 cells from the same transfections was plated in black 96-well FIA-plates (Greiner Bio-One, Frickenhausen, Germany). Total fluorescence was measured using the TriStar LB 942 microplate reader, with an excitation filter at 380 nm and an emission filter at 515 nm. Background values obtained with mock transfected HEK-293 cells were subtracted in both measurements and the means of triplicates wells/sample were then calculated. Data were analyzed and presented using GraphPad Prism 5.0. (La Jolla, CA, USA).

3.3.2 Enzyme-linked immunosorbent assay (ELISA)

ELISA assays for measurements of surface expressed HA-β_2AR and quantification of receptor internalization was performed as described previously [237-239]. HEK-293 cells were transiently transfected with either HA-β_2AR-RLuc8 or with HA-β_2AR-RLuc8 and IR-GFP^2 and 1 μg of each receptor construct was used. All transfections were performed in T-75 flasks and the total amount of cDNA used (4 μg) was kept uniform by adding empty pcDNA3.1 vector. After transfections, cells were trypsinized, diluted and seeded out at a density ~1×10^5 cells per well in poly-D-Lysine coated 24-well plate. An aliquot of cells (~5×10^5) from each transfection was also transferred into a 60 mm dish for total luminescence/fluorescence measurements as described previously. After 48 h, cells were first subjected to 2 h starvation period, and then treated with appropriate ligand in HEPES-

modified DMEM with 0.1% BSA for 30 min at 37°C before fixing with 4% paraformaldehyde for 20 min at 4°C. Cells were then washed 3 times in DPBS and blocked (DPBS containing 1% BSA) for 60 min at room temperature. Cells were kept at room temperature for all subsequent steps. First, cells were incubated for 2 h with anti-hemagglutinin (HA) high affinity rat monoclonal antibody (Roche, Basel, Switzerland) antibody in 1:600 dilutions. After 3 washes, cells were incubated with anti-rat horseradish peroxidase-conjugated antibody (Sigma-Aldrich) at 1:1000 dilution. After extensive washing, the reaction was developed in dark using the 3, 3', 5, 5'-tetra-methylbenzidine liquid substrate system (200 µL per well). The enzymatic reaction was terminated after 15 min by adding 100 µL of 0.2 N H_2SO_4 per well. The absorbance was measured at 450 nm in a microplate reader Rosys Anthos 2010 (Anthos Labtec Instruments, Wals, Austria). Mock transfected HEK-293 cells were assayed concurrently to determine background. Determinations were made in triplicates. Data were analyzed and presented using GraphPad Prism 5.0.

3.3.3 Receptor binding assay

Radioligand binding assays are used to characterize the binding of a ligand to its target receptor. Three types of assay are described: saturation, displacement, and kinetic assays. Using a competition radioligand binding assay, we can determine the affinity and selectivity of an unlabeled ligand to compete for the binding of a fixed concentration of a radiolabeled ligand to a receptor [240].

To establish a relationship between the luminescence/fluorescence signals generated by the RLuc8- or GFP^2-tagged β_2ARs and the cell-surface receptor number a self-displacement radioligand binding assays were carried out on whole cells as previously described [128]. HEK-293 cells were transiently transfected with increasing amounts of HA-β_2AR-RLuc8 (0.05–4 µg) or β_2AR-GFP^2 (0.025–3 µg). All transfections were performed in T-75 flasks and the total amount of cDNA used (4 µg) was kept uniform by adding empty pcDNA3.1 vector. After transfections, cells were plated into 24-well plates precoated with poly-D-lysine at a density of ~1×10^5 cells per well. An aliquot of cells (~5×10^5) from each transfection was also transferred into a 60 mm dish for total luminescence/fluorescence

measurements as described previously. For the whole cells radioligand binding assay, cells were washed once with assay buffer (HEPES-modified DMEM with 0.1% bovine serum albumin (BSA)) before being incubated with the β_2AR antagonist [^{125}I]-iodopindolol (PerkinElmer, Health Sciences B.V. Groningen, The Netherlands) (30,000 cpm/well) and increasing concentrations of unlabeled pindolol (Sigma-Aldrich) (10^{-12} to 10^{-5} M final concentration) in a assay buffer for 2 h at 4°C. Cells were then washed 3 times with ice-cold DPBS, solubilized with 0.2M NaOH and 1% sodium dodecyl sulfate (SDS) solution, and radioactivity determined with γ counter (LKB Wallac, Turku, Finland). Determinations were performed in triplicates. Binding parameters were determined from self-displacement curves generated by sigmoidal dose-response curve fit (GraphPad Prism 5.0). Receptor density, expressed as receptor number per cell, was calculated as previously described by Ramsay et al. [241].

Whole cell radioligand binding assays were also performed with HEK-293 cells transiently transfected with HA-β_2AR alone or with HA-β_2AR and IR and 1 μg of each receptor was used. All transfections were performed in T-75 flasks and the total amount of cDNA used (4 μg) was kept uniform by adding empty pcDNA3.1 vector. Displacement curves were generated using [^{125}I]-iodopindolol (30,000 cpm/well) and increasing concentrations of pindolol (10^{-12}–10^{-5} M), isoproterenol (10^{-12}–10^{-5} M) or pindolol (10^{-12}–10^{-5} M) and insulin S100 (0.1 μM) (Novo Nordisk A/S) and IC_{50} values were determined using a sigmoidal dose-response curve fit (GraphPad Prism 5.0).

3.3.4 Receptor internalization assay

Internalization assays were performed as described previously [128]. HEK-293 cells were transiently transfected with either the HA-β_2AR alone or HA-β_2AR and IR and 1 μg of each receptor was used. All transfections were performed in T-75 flasks and the total amount of plasmid DNA used (4 μg) was kept uniform by adding empty pcDNA3.1 vector. After transfections, cells were plated into 24-well plates precoated with poly-D-lysine at a density of ~1×10^5 cells per well. After 48 h, cells were first subjected to 2 h starvation period in assay medium (HEPES-modified DMEM with 0.01% BSA) before being incubated with 10 μM

isoproterenol or combination of isoproterenol (10 μM) and insulin S100 (0.1 μM) in a assay medium for time intervals ranging from 5 min to 60 min at 37°C. Cells were then placed on ice, washed 3 times with ice-cold DPBS and incubated for 2 h with [^{125}I]-iodopindolol in the presence or absence of 10 μM pindolol at 4°C. Cells were then washed 3 times with ice-cold DPBS and harvested by solubilization in 0.2 M NaOH and 1% SDS and radioactivity determined with γ counter (LKB Wallac). Specific binding in each fraction was determined as the difference between radiolabeled ligand detected in the presence and absence of a 10 μM pindolol. Receptor sequestration was then defined as the decrease in specific [^{125}I]-iodopindolol binding compared to total binding obtained in untreated cells. The amount of internalized receptors as a function of time was fitted using a one site binding (hyperbola) curve fit (GraphPad Prism 5.0) to estimate the half-time of internalization ($t_{1/2}$). All time points were in triplicates.

3.3.5 Confocal microscopy

The confocal laser scanning microscopy collects images that are almost free of out-of-focus signals, which results in improved spatial resolution and discrimination as compared with conventional microscopy. Moreover, it allows optical sectioning of specimens e.g. whole cells. Quantitative evaluation of microscopic images is hindered by out-of-focus signals because they interfere with specific signals in the image. In confocal microscopy only one single point in microscopic objects is illuminated at any time, and this point is then imaged into the pinhole at the entrance of the photo-detector and subsequently digitized [242].

We have used this technique to determine cellular distribution and colocalization of GFP^2- and HA-tagged receptors in fixed HEK-293 cells. HEK-293 cells were transiently transfected with constructs encoding HA-tagged and/or GFP^2-tagged receptor constructs and 1 μg of each receptor construct was used. All transfections were performed in 60 mm tissue culture dishes and the total amount of plasmid used (3 μg) was kept uniform by adding empty pcDNA3.1 vector. Following transfections, cells were trypsinized and plated on poly-L-lysine-coated glass coverslips in complete DMEM. After 48 h cells were treated as required with either 10 μM isoproterenol, 0.1 μM insulin S100 or combination of both in HEPES-

modified DMEM for 10 min at 37°C. Upon treatment, cells were washed with ice-cold DPBS and fixed with 4% paraformaldehyde for 20 min at 4°C. Following washing with DPBS (3 times) if permeabilized cells were required, to enable the visualization of internalized HA-tagged receptors, cells were permeabilized with DPBS containing 0.01 % Triton X-100 for 20 min. To reduce the nonspecific binding, cells transfected with the HA-tagged receptors were incubated in blocking solution (DPBS containing 1% BSA) for 30 min. Subsequently, cells were incubated with a 1:100 dilution of primary rat anti-HA antibodies in DPBS overnight at 4°C. Following washing with DPBS (3 times) cells were incubated with a 1:50 dilution of secondary rabbit anti-rat TRITC-conjugated antibodies (Sigma-Aldrich) for 60 min at room temperature in dark. Cells were then mounted with an anti-fading ProLong®Gold reagent (Molecular Probes, Leiden, The Netherlands), sealed and examined under an oil immersion objective (Planapo 40×, N.A.=1.25) using a Leica multispectral confocal laser microscope (Leica TCS NT, Heidelberg, Germany). The sequential detection of GFP[2] and TRITC stained receptors was achieved with the use of excitation laser lines at 488 nm (Argon) and 543 nm (Helium-Neon), respectively. The fluorescence from the channels was collected sequentially and images produced with 8-fold frame averaging at a resolution of 1024×1024 pixels. Optical sections (1.0 µm) were taken and representative sections corresponding to the middle of the cells were presented using Adobe Photoshop 6.0 (San Jose, CA, USA).

3.4 METHODS FOR DETECTION AND ANALYSIS OF PROTEIN-PROTEIN INTERACTIONS

3.4.1 Bioluminescence resonance energy transfer (BRET)

BRET is a method that employs non-radiative energy transfer from a luminescent donor, bioluminescent enzyme (a version of *Renilla luciferase*, RLuc) which reacts with the substrate to produce excitation, to a fluorescent acceptor, typically a modified variant of green fluorescent protein (GFP), which re-emits light at longer wavelength (Fig. 11). BRET requires a sufficient overlap between the emission spectrum of a donor molecule and the excitation spectrum of an acceptor molecule. BRET signal indicates that the donor and acceptor moieties are at distance less than 10 nm (Fig. 11). In addition, BRET depends on the relative orientation of protein partners, due to the dipole-dipole nature of the resonance energy transfer mechanism [181]. The strict dependence of the phenomenon on the molecular

proximity between energy donors and acceptors, e.g. donor- and acceptor tagged receptors, makes it a system of choice to monitor protein-protein interactions in live cells [243].

In addition to the original $BRET^1$ technology [244], which is based on RLuc as a donor and yellow fluorescent protein (YFP) as an acceptor, several versions of BRET assays have been developed that use different substrates and/or energy donor/acceptor pairs. In optimized $BRET^2$ version, we have used RLuc8 as the donor and GFP variant two (GFP^2) as the acceptor molecule. $BRET^2$ enables superior separation of donor and acceptor emission peaks, as well as efficient filtration of the excitation light, thereby enabling detection of the weak fluorescence signal. The major disadvantage of $BRET^2$ compared to $BRET^1$ is the 100–300 times lower intensity of emitted light and its very fast decay [245]. This was improved by the development of suitably sensitive instruments and the use of RLuc mutants with improved quantum efficiency and/or stability (e.g., RLuc8, RLuc8.6, and RLuc-M) as donor [246]. The combination of 8 favorable mutations generated a mutant RLuc8 that exhibits a greater than 150-fold stability improvement in murine serum when compared to RLuc (<1 h versus >100 h), along with a 4-fold improvement in light output [247]. Moreover, $BRET^2$ donor/acceptor pair result in a larger Stokes shift of 115 nm, compared to the approximately 50 nm Stokes shift obtained in $BRET^1$ systems. Larger Stokes shift enables better separation of the RLuc and GFP light and therefore a lower background [181, 245, 248].

The described properties make BRET a straightforward biophysical technique suitable for monitoring protein-protein interactions, constitutive and agonist-induced receptor homo- and heteromers, and their modulations (i.e. conformational changes) in live cells [245].

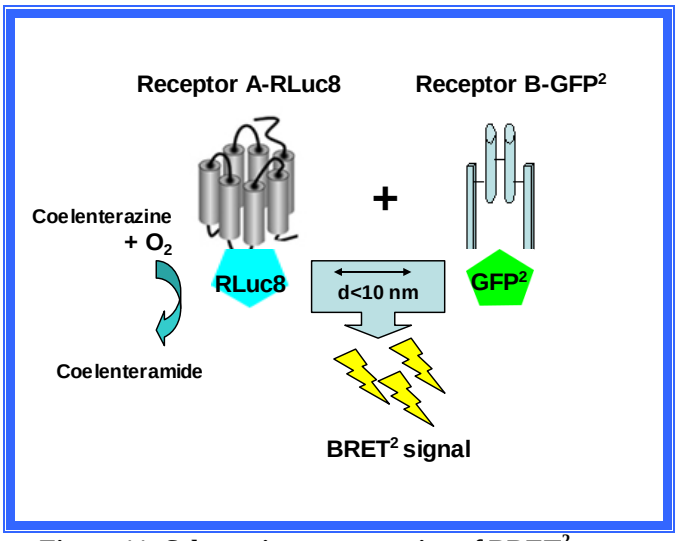

Figure 11: Schematic representation of BRET^2 assay

If the tagged Receptor A and tagged Receptor B- interact and position the energy donor and acceptor within a distance less than 10 nm, upon addition of a substrate, a resonance energy transfer occurs and BRET^2 signal can be detected.

3.4.1.1 BRET^2 dilution, saturation and competition assays

For BRET^2 dilution assays, HEK-293 cells were transiently cotransfected with increasing amounts (0.01–1.5 µg) of the constructs encoding RLuc8-tagged receptors, together with equal increasing amounts of the constructs encoding GFP^2-tagged receptors. For homologous BRET^2 saturation assays, HEK-293 cells were transiently cotransfected with constant amounts of HA-β_2AR-RLuc8 (0.05 µg) or IR-RLuc8 (0.015 µg) together with increasing amounts of the constructs encoding GFP^2-tagged receptors (0.05–2 µg of β_2AR-GFP^2 or 0.01–1.5 µg of IR-GFP^2). For heterologous BRET^2 saturation assays, HEK-293 cells were transiently cotransfected with constant amounts of HA-β_2AR-RLuc8 (0.05 µg) or IR-RLuc8 (0.015 µg) together with increasing amounts of the constructs encoding GFP^2-tagged receptors (0.05–2 µg of IR-GFP^2 or 0.01–1.5 µg of β_2AR-GFP^2). When C-terminally RLuc8 tagged IR 1–1271 mutant (IR 1–1271-RLuc8) was used in saturation assays, the same amounts of plasmid DNA were used as with IR-RLuc8.

For BRET^2 competition assays, HEK-293 cells were transiently cotransfected with constant amounts of the constructs encoding RLuc8- and GFP^2-tagged receptors (0.05 µg of HA-β_2AR-RLuc8 and 0.25 µg β_2AR-GFP^2 or 0.015 µg of IR-RLuc8 and 0.1 µg of IR-GFP^2)

together with increasing amounts of untagged receptors (0.01–1.5 μg). All transfections were performed in 60 mm tissue culture dishes and the total amount of plasmid used (3 μg) was kept uniform by adding empty pcDNA3.1 vector.

Control experiments were performed with membrane-inserted GFP^2-tagged construct (GFP^2-17aa), when HEK-293 cells were transiently cotransfected with a constant amount of IR-RLuc8 (0.015 μg) or HA-β_2AR-RLuc8 (0.25 μg) and increasing amounts GFP^2-17aa encoding construct (0.01–1 μg). $BRET^2$ assays were performed as described previously [75, 128]. After 48 h, HEK-293 cells were trypsinized, washed once in DPBS and resuspended in DPBS supplemented with Ca^{2+}/Mg^{2+}, 1 g/L glucose and 36 mg/L sodium pyruvate. 180 μL of resuspended cells containing ~2×10^5 cells was distributed in 96-well microplates (white Optiplate; Packard BioScience, Meriden, CT, USA). After addition of coelenterazine 400a by injector to a final concentration of 5 μM, readings were collected with TriStar LB 942 microplate reader. Signals at 410 (the peak of RLuc8 luminescence signal) and 515 nm (the peak of light emission from excited GFP^2) were measured sequentially, and 515/410 ratios ($BRET^2$ signal) were calculated. Results were expressed in milliBRET units (mBU); BRET ratio x 1000. Expression levels of RLuc8- and GFP^2-tagged constructs for each experiment were assessed by total luminescence and fluorescence measurement as described in section 3.3.1. Determinations were made in triplicates. Data were analyzed and presented using GraphPad Prism 5.0.

3.4.1.2 $BRET^2$ assay data evaluation

The $BRET^2$ values were fitted using the following equation for dimers: $BRET=BRET_{max}(1/(1+AD_{50}/X))$, where X is the ratio of acceptor (A; Receptor-GFP^2) to donor ((D; Receptor-RLuc8) molecules. $BRET_{max}$ is the maximum $BRET^2$ signal when all of the donor molecules are interacting with acceptor molecules. AD_{50} value corresponds to the acceptor/donor ratio providing 50% of the $BRET_{max}$ and reflects the relative affinity of the acceptor (GFP^2-tagged receptor) for the donor molecules (RLuc8-tagged receptor). Fitting parameters were compared using Welch's t-test.

The BRET model for trimers is based on the Veacht and Steyer (1977) concept [249]. The theoretical saturation curve for trimers with the same association affinity is:

$$BRET = \frac{I_{acceptor}}{I_{donor}} = \frac{2EAAD + 2EADD}{(1-2E)AAD + 2(1-E)ADD + DDD} \quad (1)$$

where A, D and E are acceptor, donor and energy transfer efficiency, respectively. If we have different affinities for the formation of AAD trimer, we introduce enhancement factor X:

$$BRET = \frac{I_{acceptor}}{I_{donor}} = \frac{2EXAAD + 2EADD}{(1-2E)XAAD + 2(1-E)ADD + DDD} \quad (2)$$

The BRET model for trimer competition is based on the Veacht and Steyer (1977) concept [249]. For receptors with equal affinities to form trimers we determine the frequency of each trimer type (A=acceptor, D=donor and W=wild type receptor):

$$(A*D*W)^3 = AAA + 3AAD + 3AAW + 3ADD + 6ADW + 3AWW + 3DDW + 3DWW + DDD + WWW \quad (3)$$

BRET is defined as a ratio of light emission from acceptor divided by that of the donor. E is resonance energy transfer ratio:

$$BRET = \frac{I_{acceptor}}{I_{donor}} = \frac{2EAAD + 2EADD + 2EADW}{(1-2E)AAD + 2(1-E)ADD + 2(1-E)ADW + 2DDW + DWW + DDD} \quad (4)$$

If the energy transfer ratio E is different for ADW trimers the following equation is obtained:

$$BRET = \frac{I_{acceptor}}{I_{donor}} = \frac{2E_1AAD + 2E_1ADD + 2E_2ADW}{(1-2E_1)AAD + 2(1-E_1)ADD + 2(1-E_2)ADW + 2DDW + DWW + DDD} \quad (5)$$

BRET data evaluation was done by Luka Drinovec at Aerosol d.o.o. Ljubljana, Slovenia.

3.4.1.3 $BRET^2$ assay for monitoring the recruitment of β-arrestins to β_2AR or IR

HEK-293 cells were transiently cotransfected with constructs encoding RLuc8-tagged receptors (0.25 μg) together with constructs encoding GFP^2-βarr2 (2.25 μg) or GFP^2-βarr2 1–185 (E186– stop; GAA–TAA) mutant (2.25 μg), which lacks the binding region (amino acids 186–409) for the interaction with the IR [121]. All transfections were performed in T-75 flasks and the total amount of plasmid DNAused (6 μg) was kept uniform by adding empty pcDNA3.1 vector. At 48 h after transfections, HEK-293 cells were trypsinized, washed once in DPBS and resuspended in DPBS supplemented with Ca^{2+}/Mg^{2+}, 1 g/L glucose and 36 mg/L sodium pyruvate. 180 μL of resuspended cells containing ~2×10^5 cells were distributed in 96-well microplates and treated with either 0.1 μM insulin S100, 10 μM isoproterenol or combination of both insulin S100 (0.1 μM) and isoproterenol (10 μM). $BRET^2$ signals were measured as described in section 3.4.1.1. Results were expressed in mBU. Expression levels of RLuc8- and GFP^2-tagged constructs for each experiment were assessed by total luminescence and fluorescence measurement as described in section 3.3.1. Determinations were made in triplicates. Data were analyzed and presented using GraphPad Prism 5.0.

3.4.2 Seven transmembrane receptor: Receptor tyrosine kinases-heteromer identification technology (7TMR:RTK-HIT)

The 7TMR:RTK-HIT is a relatively novel approach to identify and profile heteromers and the ligands that act on them. In contrast to the classical BRET assay, only one receptor subtype is fused to RLuc8 (Receptor A-RLuc8) and the second receptor subtype is untagged with respect to the BRET system (Receptor B). A third protein capable of interacting specifically with one or both receptors in a ligand-dependent manner is fused to a GFP^2 (Protein C-GFP^2). BRET measurements can then be carried out after activation of Receptor B or the heteromer. If a ligand-induced BRET signal is detected, this indicates that activation of Receptor B or the heteromer results in recruitment of Protein C-GFP^2 specifically to the heteromer complex. Binding of Protein C-GFP^2 to Receptor B such that energy transfer between Receptor A-RLuc8 and Protein C-GFP^2 is detected indicates that Receptor A-RLuc8 and Receptor B are in a heteromeric complex (Fig. 12). Binding of Protein C-GFP^2 to Receptor A-RLuc8, following activation of Receptor B, implicates allosteric modulation of Receptor A-RLuc8 by

activated Receptor B as a consequence of heterodimerization. Therefore, both of these alternatives implicate specific receptor-receptor interactions [250]. As a signal is only detected as a result of heteromerization and not homomerization, this assay avoids the "noise" that can be an issue when trying to differentiate signals originating from heteromers or homomers.

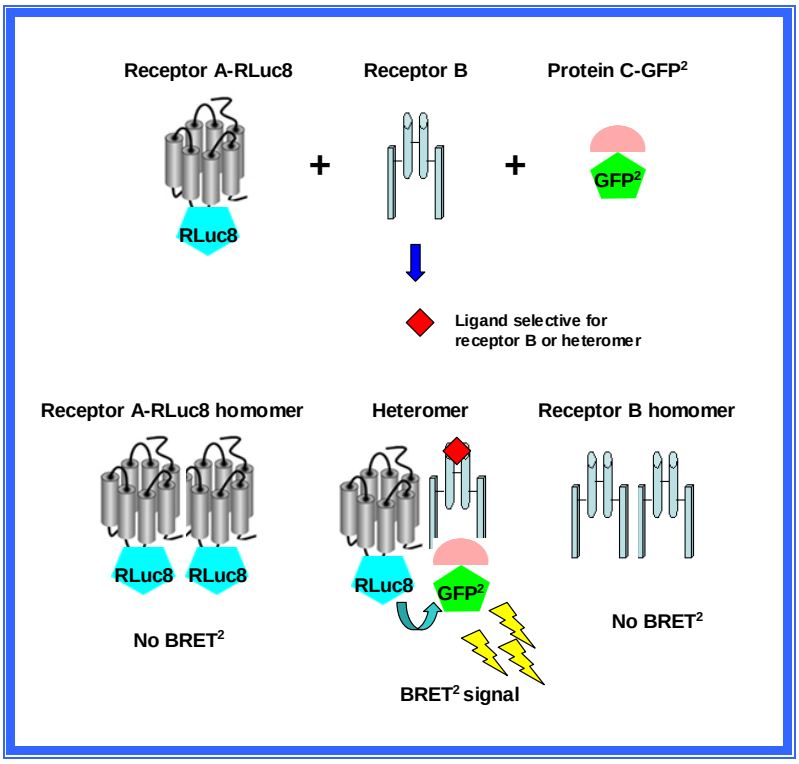

Figure 12: Schematic representation of 7TMR:RTK-HIT in live cells

The 7TMR:RTK-HIT uses cotransfection of a tagged Receptor A, untagged Receptor B, and a tagged Protein C (such as β-arrestin) that interacts with Receptor B or the heteromer after binding of a ligand selective for Receptor B or the heteromer. Figure created by author based on a figure from [251].

3.4.2.1 Seven transmembrane receptor: Receptor tyrosine kinases-heteromer identification technology (7TMR:RTK-HIT) assay with β-arrestin 2 (βarr2)

To investigate β_2AR:IR heteromer using βarr2, HEK-293 cells were transiently cotransfected with HA-β_2AR-RLuc8 (0.5 µg), GFP^2-βarr2 (4.5 µg) and with or without untagged IR (1 µg) as controls; or with IR-RLuc8 (0.5 µg), GFP^2-βarr2 (4.5 µg) together with or without untagged HA-β_2AR (1 µg) as controls. When C- terminally RLuc8 tagged IR 1–1271 mutant

(IR 1–1271-RLuc8) was used, the same amounts of plasmid DNA were used as with IR-RLuc8. All transfections were performed in T-75 flasks and the total amount of plasmid DNA used (6 μg) was kept uniform by adding empty pcDNA3.1 vector. At 48 h after transfections, HEK-293 cells were trypsinized, washed once in DPBS and resuspended in DPBS supplemented with Ca^{2+}/Mg^{2+}, 1 g/L glucose and 36 mg/L sodium pyruvate. 180 μL of resuspended cells containing ~2×10^5 cells was distributed in 96-well microplates and treated with either insulin S100 (10^{-12} to 10^{-5} M), isoproterenol (10^{-12} to 10^{-5} M), pindolol (10^{-12} to 10^{-5} M) and isoproterenol (10 μM) or isoproterenol (10^{-12} to 10^{-5} M) and insulin S100 (0.1 μM). $BRET^2$ signals were measured as described in section 3.4.1.1. Results were expressed in mBU. Expression levels of RLuc8- and GFP^2-tagged constructs for each experiment were assessed by total luminescence and fluorescence measurement as described in section 3.3.1. Determinations were made in triplicates. Data were presented and analyzed using GraphPad Prism 5.0.

3.4.2.2 Seven transmembrane receptor: Receptor tyrosine kinases-heteromer identification technology (7TMR:RTK-HIT) assay with Shc

To investigate the β_2AR:IR heteromer in terms of Shc recruitment, HEK-293 cells were transiently cotransfected with IR-RLuc8 (0.5 μg), GFP^2-Shc (3 μg) with or without untagged HA-β_2AR (2.5 μg) as controls; or with HA-β_2AR-RLuc8 (0.5 μg), GFP^2-Shc (3 μg) with or without untagged IR (0.5 μg) as controls. All transfections were performed in T-75 flasks and the total amount of cDNA used (6 μg) was kept uniform by adding empty pcDNA3.1 vector. At 48 h after transfections, HEK-293 cells were trypsinized, washed once in DPBS and resuspended in DPBS supplemented with Ca^{2+}/Mg^{2+}, 1 g/L glucose and 36 mg/L sodium pyruvate. 180 μL of resuspended cells containing ~2×10^5 cells was distributed in 96-well microplates and treated with either insulin (10^{-12} to 10^{-5} M), isoproterenol (10^{-12} to 10^{-5} M) or combination of both isoproterenol (10^{-12} to 10^{-5} M) and insulin S100 (0.1 μM). $BRET^2$ signals were measured as described in section 3.4.1.1. Results were expressed in mBU. Expression levels of RLuc8- and GFP^2-tagged constructs for each experiment were assessed by total luminescence and fluorescence measurement as described in section 3.3.1. Determinations were made in triplicates. Data were analyzed and presented using GraphPad Prism 5.0.

3.4.3 Informational spectrum method (ISM)

The ISM is based on a model that assigns to each amino acid a defined parameter describing a physico-chemical property involved in the biological activity of the protein and corresponding to electron-ion interaction potential (EIIP). These values determine the electronic properties of amino acids responsible for their intermolecular interactions [217].

The obtained numerical sequence, representing the primary structure of a protein, is then subjected to a discrete Fourier transformation defined as follows:

$$X(n) = \Sigma\, x(m)e^{-j(2/N)nm},\ n = 1, 2, ..., N/2 \qquad (6)$$

where x(m) is the m-th member of a given numerical series, N is the total number of points in this series, and X(n) are discrete Fourier transformation coefficients. These coefficients describe the amplitude, phase and frequency of sinusoids, which comprised the original signal. The absolute value of complex discrete Fourier transformation defines the amplitude spectrum and the phase spectrum. The complete information about the original sequence is contained in both spectral functions. However, in the case of protein analysis, relevant information is presented in energy density spectrum [217] which is defined as follows:

$$S(n) = X(n)X^{*}(n) = |X(n)|^{2},\ n = 1, 2, ..., N/2. \qquad (7)$$

Thus, the initial information defined by the sequence of amino acids now is presented in the form of the informational spectrum (IS), representing the series of frequencies and their amplitudes.

The IS frequencies correspond to the distribution of structural motifs with defined physico-chemical characteristics responsible for the biological function of a protein. When comparing proteins that share the same biological or biochemical function, ISM allows the detection of code/frequency pairs that are specific for their common biological properties or correlate with their specific interaction. This common informational characteristic of sequences is determined by a cross-spectrum (CS) for two proteins or consensus informational spectrum (CIS) for two or more proteins—i.e., the Fourier transformation of the

correlation functions for the spectrum. In this way, any spectral component (frequency) not present in all of the compared ISs is eliminated. Peak frequencies in CIS are common frequency components for the analyzed sequences. A measure of similarity for each peak is the signal-to-noise ratio (S/N), representing the ratio between the signal intensity at one particular IS frequency and the main value of the whole spectrum. If a CIS is calculated for a group of proteins with different primary structures, and strictly defined peak frequencies are found, the analyzed proteins likely participate in a mutual interaction or have a common biological function. The ISM was, thus far, successfully applied in the structure-function analysis of different protein sequences [217], prediction of new protein interactors [218] as well as identification of protein domains responsible for long-range interactions [215, 216].

3.4.3.1 Computational peptide scanning

Computational peptide scanning was used to define linear protein regions contributing the most to the amplitude at the characteristic frequency, and therefore responsible for interaction(s) described by the particular spectral characteristic. To identify the regions with the highest amplitudes at predefined Fourier frequencies, the entire sequences of β_2AR and IR were scanned by the ISM algorithm with overlapping windows of different length, which led to the identification of regions with the highest amplitudes at predefined Fourier frequencies. Bioinformatics analysis was performed with help by Sanja Glišić and Nevena Veljković at the Center for Multidisciplinary Research at the Institute of Nuclear Sciences VINCA, University of Belgrade.

3.4.3.2 Datasets

The sequences used for bioinformatics analysis were retrieved from the Uniprot database with the following accession numbers: human P07550 (human β_2AR) and P06213 (human IR isoform A that lacks exon 11).

3.5 cAMP ASSAY

The cAMP cell-based assay kit (Cisbio Bioassays, Codolet, France) was used to determine cAMP accumulation in living cells according to manufacturer's instruction. The cAMP kit from Cisbio is based on the Homogenous Time-Resolved Fluorescence (HTRF) technology. HTRF takes advantage of a long life fluorescence donor, combined with FRET to an energy acceptor. In this assay, the donor is an anti-cAMP antibody, whereas the acceptor is cAMP labelled with a dye. It is a competition assay between cAMP produced by the cells and the acceptor-labelled cAMP for binding on donor-labelled anti-cAMP antibody. The signal is inversely proportional to the concentration of cAMP produced by the cells, i.e. the more cAMP produced the lower FRET signal.

HEK-293 cells were transiently transfected with constructs encoding either β_2AR or IR or with both receptors where 1 μg of each receptor construct was used and the total amount of plasmid used for transfection was kept uniform by adding empty pcDNA3.1 vector. The day before the assay transient transfected cells were seeded (50.000 cells/well) in 96 well plates (Thermo Scientific Nunclon) in growth medium (DMEM with glutamax, supplemented with 10% FBS). The following day, cells were washed twice in HBSS buffer (HBSS with Ca, Mg and 10mM Hepes) prior to pre-incubation for 30 min at 37°C in 90 μL HBSS buffer supplemented with 0.1% pluronic and 500 μM IBMX (3-isobutyl-1-methylxanthine). Cells were then stimulated for 30 min at 37°C with 10 μL ligand diluted to working concentration in HBSS buffer supplemented with 0.1% pluronic and 500 μM IBMX. Cells were treated with increasing concentration of isoproterenol (10^{-13} to 10^{-6} M final concentration), insulin S100 (10^{-13} to 10^{-6} M final concentration) or combination of isoproterenol (10^{-13} to 10^{-6} M final concentration) and 100 nM insulin S100. After aspiration of the ligands, the cells were lysed immediately in 50 μl lysis buffer (Cisbio). The plates were shaken for 10 min at RT and frozen at -80°C.

After thawing and mixing of the cell lysates 10 μl were transferred to a 384-well Optiplate (PerkinElmer) and the detecting reagents (cryptate-labeled anti-cAMP antibody and d2-labeled cAMP) were diluted in detection buffer (Cisbio) and added. After incubation in the

dark at RT for at least 2 h, TR-FRET signal was read in an Envision 2104 Multilabel Reader (PerkinElmer). Obtained data were transferred to GraphPad Prism and the concentration of cAMP produced was interpolated from a standard curve (prepared according to the protocol from the kit). EC_{50} values (nM ± S.E.M.) generated using sigmoidal-dose response curve fit (GraphPad Prism). cAMP assays were performed by Christina Pedersen at Novo Nordisk A/S, Denmark.

3.6. STATISTICAL ANALYSIS

Statistical analysis was carried using Student’s t-test and Welch's t-test. Observed differences between results were considered statistically significant if a *p* value was less than 0.05.

4 RESULTS

4.1 CHARACTERISTICS OF THE FUSION CONSTRUCTS

4.1.1 Pharmacological characterization of β_2AR fusion constructs

Pharmacological characterization of the human HA-β_2AR fused at the C-terminus with energy donor RLuc8 or the β_2AR fused at the C-terminus with energy acceptor GFP^2 was performed using radioligand binding assays (Fig. 13). The IC_{50} values of pindolol for HA-β_2AR-RLuc8 (1.16 ± 0.11 nM) and β_2AR-GFP^2 (1.88 ± 0.58 nM) were in agreement with those obtained for HA-β_2AR (1.58 ± 0.26 nM) (Table 1) and were also in the previously reported range for β_2AR-RLuc fusion construct [128].

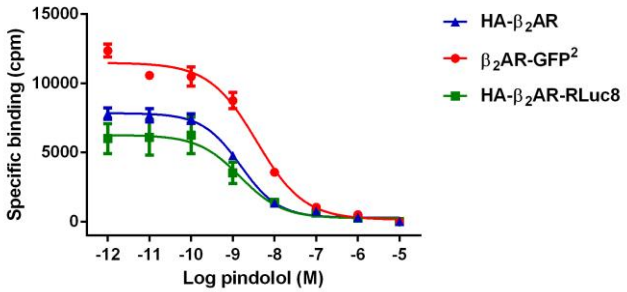

Figure 13: Binding properties of β_2AR fusion constructs expressed in HEK-293 cells

HA-β_2AR, β_2AR-GFP^2 or HA-β_2AR-RLuc8 were transiently expressed in HEK-293 cells, self-competition binding experiments were performed using [^{125}I]-iodopindolol and increasing concentrations of unlabeled pindolol (10^{-12} to 10^{-5} M). Competitive binding curves were generated using a sigmoidal dose-response curve fit (GraphPad Prism 5.0). Data are means ± S.E. of three independent experiments each performed in triplicate.

Table 1: Binding properties of β_2AR fusion constructs in HEK-293 cells

IC_{50} values were derived from competitive binding curves (Fig. 14) generated by sigmoidal dose-response curve fit (GraphPad Prism 5.0). Data are means ± S.E. of three independent experiments each performed in triplicate.

Receptors	**IC_{50} (nM)**
HA-β_2AR	1.58 ± 0.26
HA-β_2AR-RLuc8	1.16 ± 0.11
β_2AR-GFP[2]	1.88 ± 0.58
β_2AR-RLuc	0.94 ± 0.06[a]

[a]Data from Vrecl et al. [128].

Radioligand binding assays were also performed with HEK-293 cells cotransfected with plasmid DNA encoding HA-β_2AR and IR at a 1:1 ratio (Fig. 14). The obtained IC_{50} values for tested β_2AR ligands i.e. pindolol and isoproterenol were comparable in HA-β_2AR- and in HA-β_2AR- and IR-expressing cells (Table 2). Adition of insulin increased the IC_{50} values of pindolol in HA-β_2AR- expressing cells, however, not significantly (Table 2).

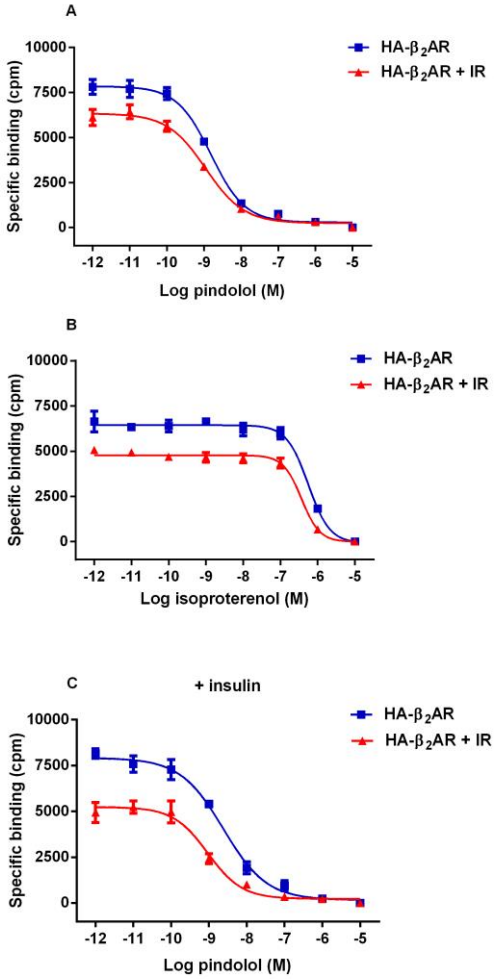

Figure 14: The effect of IR coexpression on binding properties of β_2AR in HEK-293 cells

HEK-293 cells expressing HA-β_2AR alone or HA-β_2AR together with IR at a 1:1 plasmid DNA ratio were incubated with [^{125}I]-iodopindolol and increasing concentrations of the indicated ligands (10^{-12} to 10^{-5} M). When the concomitant effect of pindolol and insulin was tested, insulin was added to a 0.1 μM final concentration (panel C). Competitive binding curves were generated using a sigmoidal dose-response curve fit (GraphPad Prism 5.0). Data are means ± S.E. of three independent experiments each performed in triplicate.

Table 2: The effect of IR coexpression on binding properties of β_2AR fusion constructs in HEK-293 cells

IC_{50} values were derived from competitive binding curves (Fig. 15) generated by sigmodial dose-response curve fit (GraphPad Prism 5.0). Data are means ± S.E. of three independent experiments each performed in triplicate.

	IC_{50} (nM)	
Ligands	**HA-β_2AR**	**HA-β_2AR + IR**
pindolol	1.58 ± 0.26	1.15 ± 0.15
isoproterenol	576.7 ± 134.2	406.5 ± 36.5
insulin	ND	ND
pindolol + insulin	2.73 ± 0.58	1.13 ± 0.23

ND – not detected.

4.1.2 Cellular localization of receptor constructs visualized by confocal microscopy

HEK-293 cells were transiently transfected with HA-β_2AR-RLuc8, β_2AR-GFP[2] or IR-GFP[2]. Receptor distribution was examined in control (untreated) cells and cells treated with isoproterenol (10 μM) or insulin (0.1 μM). In untreated cells, receptors were predominantly located on the cell surface with very little intracellular fluorescence (Fig. 15, upper panels). Addition of agonists promoted receptor redistribution into intracellular vesicles, indicating ligand-promoted receptor internalization (Fig. 15, lower panels).

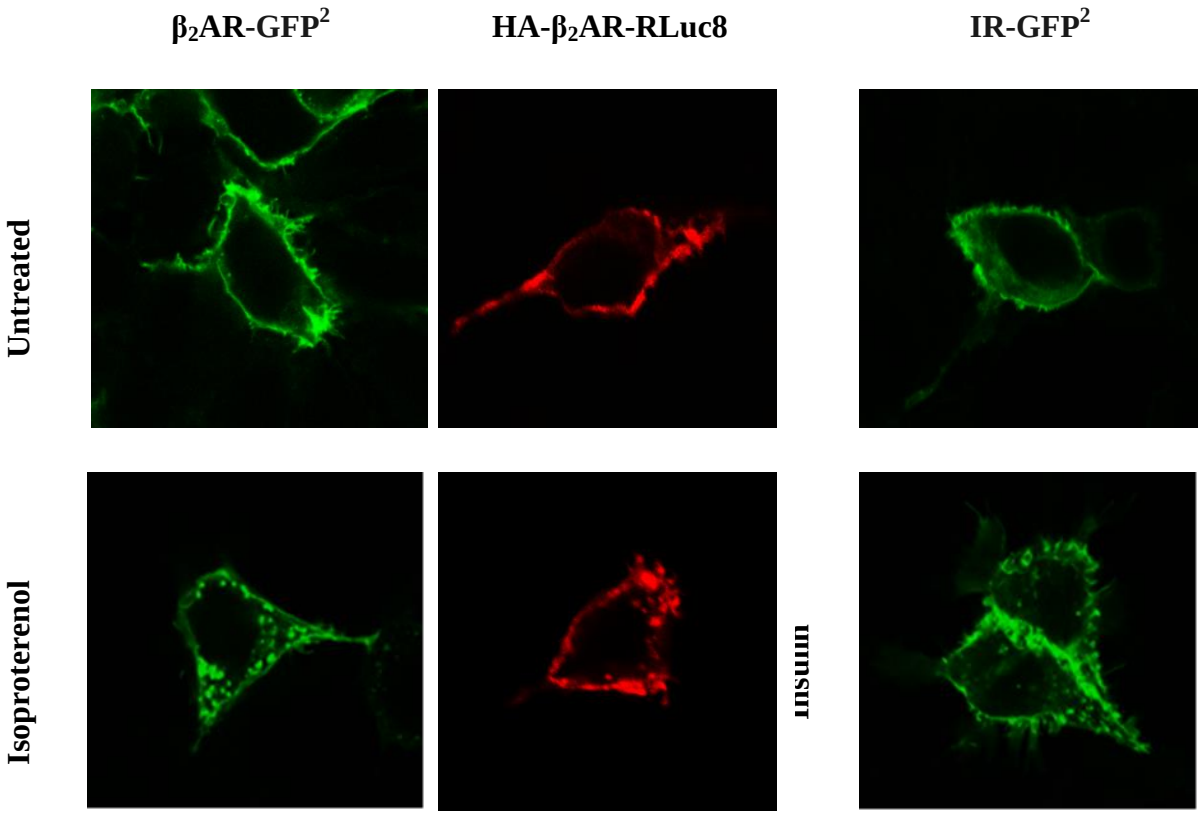

Figure 15: Visualization of HA-β_2AR-RLuc8, β_2AR-GFP^2 and IR-GFP^2 cellular localization by confocal microscopy

HA-β_2AR-RLuc8, β_2AR-GFP^2 and IR-GFP^2 cellular localization is shown in unstimulated (control) cells (upper panels) and cells treated with isoproterenol (10 μM) or insulin (0.1 μM) for 10 min at 37°C (lower panels). The green color indicates β_2AR-GFP^2 or IR-GFP^2 while red indicates HA-β_2AR-RLuc8. Note the receptors plasma membrane localization in untreated cells and internalized receptors in treated cells. Objective 40× and zoom factor 4 apply for all images.

4.1.3 Colocalization of β_2ARs visualized by confocal microscopy

Abundant evidence suggests that β_2AR can self-associate as dimers or higher-order oligomers [61, 63, 192, 252]. To examine whether the β_2AR-GFP^2 and HA-β_2AR-RLuc8 colocalize, HEK-293 cells were transiently transfected with β_2AR-GFP^2 and HA-β_2AR-RLuc8 and left untreated, or treated with isoproterenol (10 μM). Overlap of fluorescence (seen as yellow/orange) was observed on the cell surface due to the close proximity of receptors, suggesting homo-oligomerization in untreated cells. Receptor constructs also displayed some intracellular fluorescence, which is consistent with constitutive internalization of β_2ARs (Fig.

16, upper panels). In treated cells we can see most of the fluorescence intracellulary, as β_2ARs internalized in response to isoproterenol and a fraction of β_2ARs which colocalized intracellulary (Fig. 16, lower panels). In both treated and untreated cells, there is a proportion of receptors that did not colocalize.

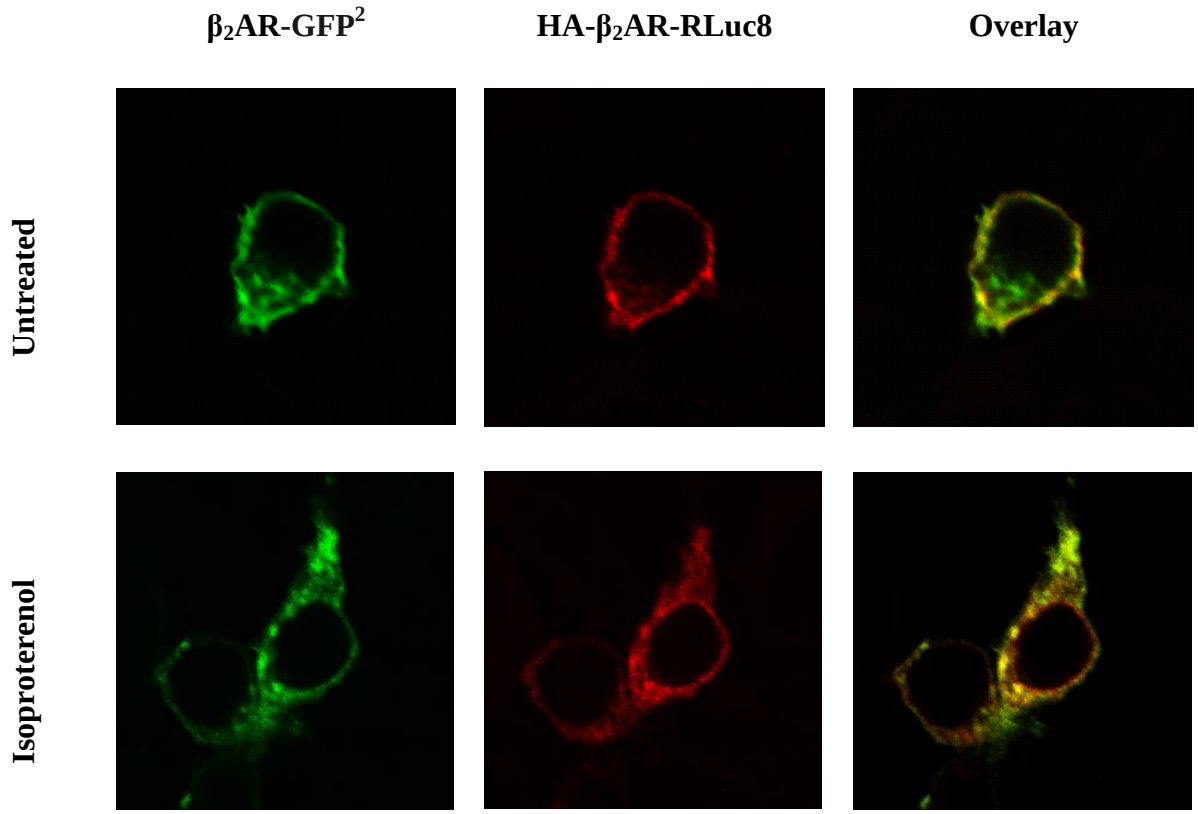

Figure 16: Visualization of β_2ARs colocalization by confocal microscopy

HA-β_2AR-RLuc8 and β_2AR-GFP^2 cellular localization is shown in unstimulated (control) cells (upper panels) and cells treated with isoproterenol (10 μM) for 10 min at 37°C (lower panels). The green color indicates β_2AR-GFP^2, red indicates HA-β_2AR-RLuc8 and yellow/orange is the overlapping region indicating colocalization of HA-β_2AR-RLuc8 and β_2AR-GFP^2. Note that HA-β_2AR-RLuc8 and β_2AR-GFP^2 colocalize in untreated and treated cells. Objective 40× and zoom factor 4 apply for all images.

4.2 THE EFFECT OF IR COEXPRESSION ON β_2AR SURFACE EXPRESSION AND INTERNALIZATION

The effect of IR coexpression on β_2AR surface expression and internalization was evaluated by ELISA and by radioligand binding assays. ELISA measurements demonstrated a significant decrease of approximately 35% in the β_2AR surface expression in intact HEK-293

cells cotransfected with HA-β_2AR-RLuc8 and IR-GFP^2 compared with cells transfected with HA-β_2AR-RLuc8 alone ($p < 0.05$; Fig. 17A). However, total HA-β_2AR-RLuc8 expression was not affected by IR-GFP^2 coexpression, as shown by luminescence measurements, whereas IR-GFP^2 expression was validated by fluorescence measurements (Fig. 17A). Similar observations in β_2AR surface expression were detected using radioligand binding assays (Fig. 17B), where β_2AR surface expression decreased by around 30% (27.89 ± 2.11) in HEK-293 cells cotransfected with IR compared with β_2AR-expressing cells ($p < 0.05$; Fig. 17B).

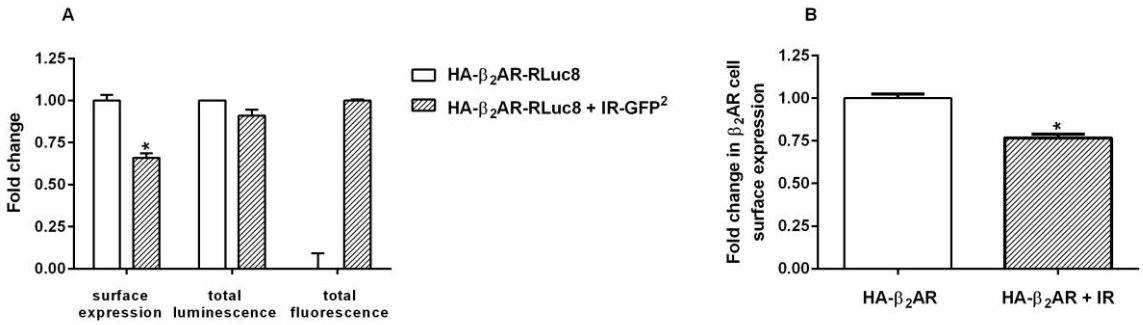

Figure 17: The effect of IR coexpression on β_2AR cell surface expression in HEK-293 cells

A) ELISA was performed on HEK-293 cells transiently transfected with HA-β_2AR-RLuc8 alone or HA-β_2AR-RLuc8, together with the IR-GFP^2 at a 1:1 plasmid DNA ratio, using an antibody directed against the HA epitope. Total luminescence and fluorescence was measured as described in Materials and methods. Fold change is relative to open bars for surface expression and total luminescence, and relative to hatched bars for total fluorescence. *, $p < 0.05$ as compared with HA-β_2AR-RLuc8 transfected cells. **B)** Radioligand binding assay was performed on HEK-293 cells transiently transfected with HA-β_2AR alone or HA-β_2AR together with the IR at a 1:1 cDNA ratio using [^{125}I]-iodopindolol. Data are expressed as the means ± S.E. of three independent experiments performed in triplicate. *, $p < 0.05$ as compared with HA-β_2AR transfected cells.

Additionally, ELISA measurements suggested that IR coexpression moderately increased isoproterenol-induced β_2AR internalization, whereas concomitant treatment with isoproterenol and insulin evoked a somewhat higher internalization rate. Treatment with insulin alone induced only ~10% and ~15% of β_2AR to internalize in β_2AR- and β_2AR and IR- expressing cells (Fig. 18).

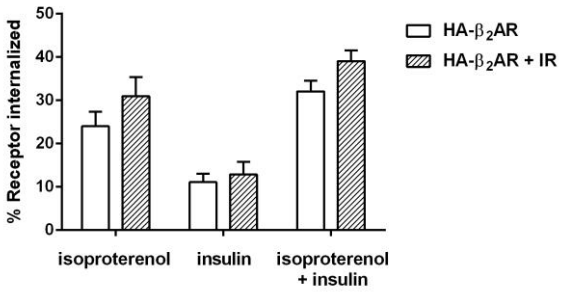

Figure 18: The effect of IR coexpression on β_2AR internalization in HEK-293 cells

HA-β_2AR internalization was quantified using ELISA in cells transiently transfected with HA-β_2AR or HA-β_2AR together with IR at a 1:1 plasmid DNA ratio and incubated at 37°C with either isoproterenol (10 μM), insulin (0.1 μM) or combination of both ligands for 30 min. The amount of internalized receptor was then calculated from the decrease in the level of surface-expressed receptor after ligand treatment compared with untreated, control cells. Data are expressed as the means ± S.E. from three independent experiments performed in triplicate.

To quantify the amount of internalized β_2AR at different time points and the effect of IR coexpression, HEK-293 cells expressing HA-β_2AR or HA-β_2AR and IR were treated with isoproterenol (10 μM) or both isoproterenol (10 μM) and insulin (0.1 μM) for varying periods of time (5 min to 1 h). The number of cell surface binding sites was determined by radioligand binding assay and time-course of agonist-induced receptor internalization is presented in Fig. 20. In the HA-β_2AR-, HA-β_2AR- and IR-expressing cells treated with isoproterenol, the intracellular receptor pool progressively increased from 15.54 ± 3.13% to 37.89 ± 0.54% and from 21.06 ± 3.06% to 40.04 ± 1.74% (Fig. 19A) within 1 hour at 37°C. In the isoproterenol and insulin treated cells, the intracellular receptor pool progressively increased from 13.35 ± 3% to 38.3 ± 1.15%, and 16.26 ± 1.48% to 49.48 ± 1.6% (Fig. 19B) within 1 hour at 37°C.

The rate of isoproterenol-induced β_2AR internalization was significantly increased by coexpression of IR ($p < 0.05$), as the estimated $t_{1/2}$ was 8.6 ± 1.3 and 5.4 ± 0.6 min in β_2AR- and in β_2AR- and IR-expressing cells (Fig. 19A). Comparable results were obtained when either β_2AR- or β_2AR- and IR-expressing cells were concomitantly treated with isoproterenol and insulin (Fig. 19B).

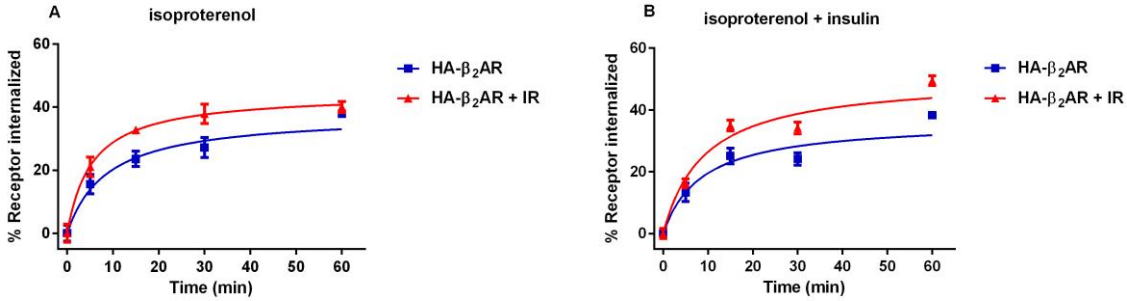

Figure 19: Effect of IR coexpression on the time-course of β_2AR internalization

HEK-293 cells were transiently transfected with either HA-β_2AR or HA-β_2AR together with the IR at a 1:1 plasmid DNA ratio. β_2AR internalization was first induced by isoproterenol (10 μM) or the combination of isoproterenol (10 μM) and insulin (0.1 μM) for the indicated time intervals. Receptor sequestration was then defined as the decrease in specific [^{125}I]-iodopindolol binding compared with the total binding obtained in untreated cells. The amount of internalized receptors as a function of time was fitted using a one-site binding (hyperbola) curve fit (GraphPad Prism 5.0). Data are expressed as the means ± S.E. from three independent experiments performed in triplicate.

4.3 VISUALIZATION OF β_2AR AND IR CELLULAR LOCALIZATION BY CONFOCAL MICROSCOPY

To study cellular localization and agonist-dependent endocytosis of β_2AR and IR by confocal microscopy, HEK-293 cells were transiently cotransfected with HA-β_2AR and IR-GFP^2 and left untreated or treated with both isoproterenol (10 μM) and insulin (0.1 μM). The two receptors demonstrated predominant plasma membrane localization and their colocalization in untreated cells (Fig. 20, upper panels). Concomitant treatment of HA-β_2AR- and IR-GFP^2 expressing cells with isoproterenol and insulin (Fig. 20, lower panels) promoted receptor redistribution to the cytoplasm, indicating receptor internalization. Again, agonist-redistributed HA-β_2AR and IR-GFP^2 showed a similar distribution pattern with a high degree of colocalization. Nevertheless, a proportion of intracellular receptors did not colocalize.

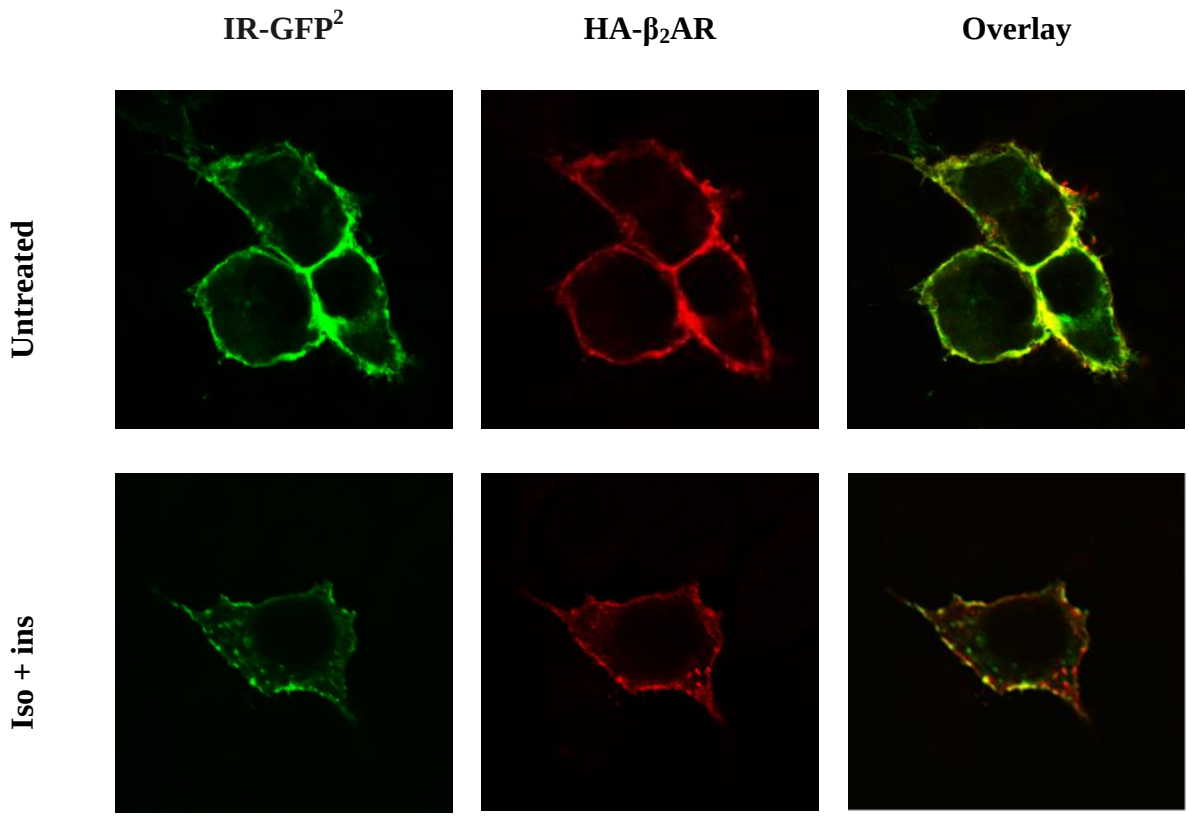

Figure 20: Visualization of β_2AR and IR cellular localization by confocal microscopy

IR-GFP^2 and HA-β_2AR cellular localization is shown in unstimulated (control) cells (upper panels) and cells concomitantly treated with isoproterenol (iso; 10 µM) and insulin (ins; 0.1 µM) for 10 min at 37°C (lower panels). The green color indicates the IR-GFP^2; red, HA-β_2AR; yellow/orange is the overlapping region indicating colocalization of IR-GFP^2 and HA-β_2AR. Note that both receptors have comparable localization in untreated and agonist-stimulated cells and that they exhibit a high degree of colocalization. Objective 40x and zoom factor 4 apply for all images.

4.4 INTERACTION BETWEEN β_2AR AND IR—BRET^2 EVIDENCE

Considering the observed effects of IR coexpression on β_2AR surface expression and internalization, as well as colocalization between both receptors in HEK-293 cells, we next investigated whether the proximity indicative of direct interaction occurs between β_2AR and IR by performing BRET^2 dilution, saturation and competition assays.

4.4.1 Correlation between total luminescence and fluorescence and the corresponding number of β_2AR binding sites

To obtain an absolute value of donor [D] and acceptor [A] molecules—i.e., Receptor-RLuc8 and Receptor-GFP^2—we first generated correlation curves between total luminescence and fluorescence *versus* the number of receptor-binding sites determined by radioligand binding. The correlations between the total luminescence/fluorescence and the number of HA-β_2AR-RLuc8 and β_2AR-GFP^2 binding sites were linear (Fig. 21). The derived correlation factors to convert total luminescence and total fluorescence into receptor number were 0.00031 and 0.0089, respectively.

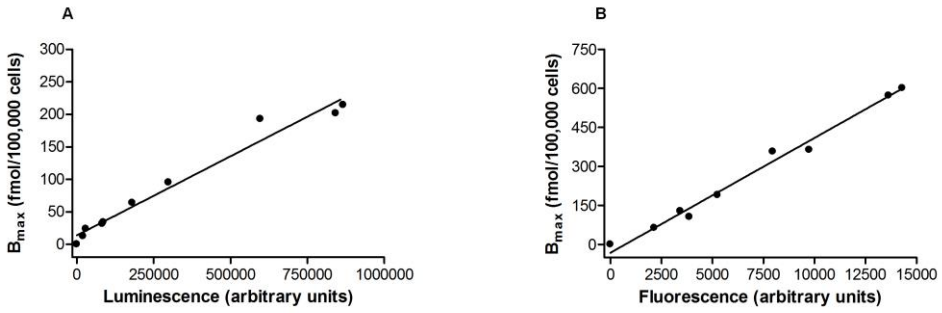

Figure 21: Correlation between total luminescence and fluorescence and the corresponding number of β_2AR binding sites

HEK-293 cells were transfected with increasing amounts of HA-β_2AR-RLuc8 (A) or β_2AR-GFP^2 (B). The receptor density (B_{max}) was determined by radioligand binding assays using [^{125}I]-iodopindolol as a tracer as described in the Material and methods section. Total luminescence was measured after the addition of the RLuc8 substrate coelenterazine 400a. Total fluorescence was measured with an excitation filter at 380 nm and an emission filter at 515 nm. The linear regression curves were generated using GraphPad Prism 5.0. R^2 fit values of 0.9705 and 0.9861 were obtained for β_2AR-RLuc8 (A) and β_2AR-GFP^2 (B), respectively.

4.4.2 BRET^2 dilution assays

A dilution assay is the simplest control experiment to distinguish random collision of receptors as a result of high receptor density, from true oligomerization. BRET^2 dilution assays were performed to set the concentration range for the saturation assays and to distinguish monomers from dimers, as previously described [181]. For BRET^2 dilution assay, cells were transfected with increasing amounts of RLuc8-tagged (HA-β_2AR-RLuc8, IR-

RLuc8) and with the same increasing amounts of GFP^2-tagged (β_2AR-GFP^2, IR-GFP^2) receptor constructs, resulting in a constant [*A*]/[*D*] ratio (Fig. 22). Our results demonstrated a gradual linear increase in the $BRET^2$ signal with increasing receptor concentrations, suggesting that higher receptor frequency contributed to random collisions of receptors resulting in bystander $BRET^2$ (Fig. 22). By simultaneously lowering the concentration of both receptors (dilution), the $BRET^2$ signal decreases toward the real oligomerization signal. This behavior was previously predicted with theoretical BRET dilution curves shown in Fig. 23 [181]. Due to the increasing noise in calculated $BRET^2$ at low luminescence intensities, the lowest amount of the HA-β_2AR-RLuc8 and IR-RLuc8 cDNA used for transfection in saturation assays was determined at 0.05 and 0.015 μg, respectively. Expression levels of receptor constructs were measured by luminescence and fluorescence measurements (data not shown).

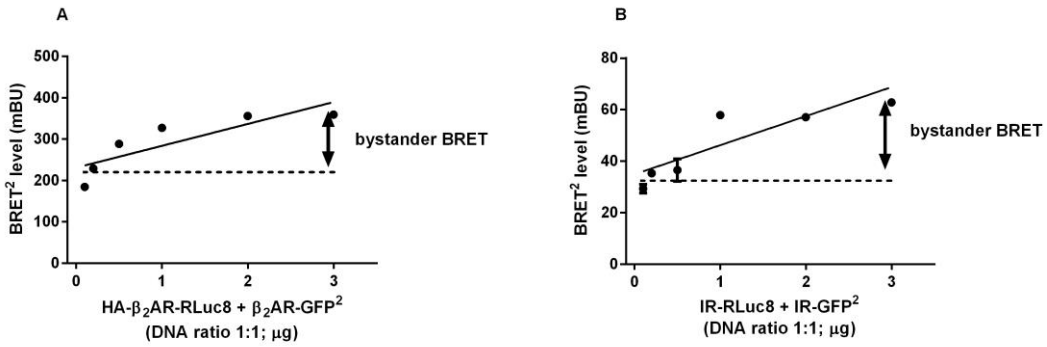

Figure 22: $BRET^2$ dilution curves of β_2AR and IR homomers

HEK-293 cells were transiently cotransfected with increasing amounts of both RLuc8-tagged and GFP^2-tagged receptor constructs. Linear regression curves were generated with GraphPad Prism 5.0. The results are expressed as the means ± S.E. of three independent experiments carried out in triplicate.

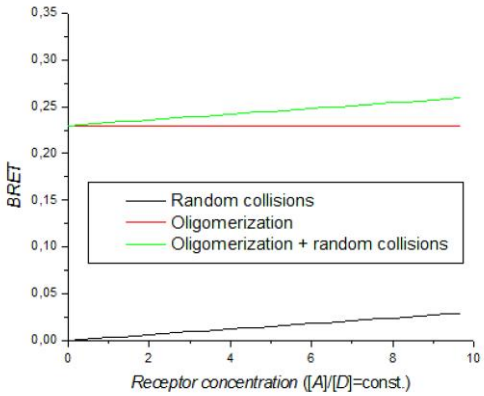

Figure 23: Theoretical BRET dilution curves [181]

4.4.3 BRET^2 saturation assays

BRET^2 saturation assays were performed to investigate homo- and heteromerization of β_2AR and IR. The BRET^2 signal was measured in live HEK-293 cells that were transiently transfected with constant amounts of RLuc8-tagged (HA-β_2AR-RLuc8, IR-RLuc8) and with increasing amounts of GFP^2-tagged (β_2AR-GFP^2, IR-GFP^2) receptor encoding constructs. In dimers and higher oligomers, the probability of BRET interaction increases with increasing acceptor/donor ratio until all of the acceptors have pairs and the maximum BRET^2 level (BRET$^2_{max}$), or until plateau is reached. The A/D$_{50}$ value (also designated as BRET$_{50}$) was also included to compare the affinity for homo-/heteromer formation. BRET^2 saturation experiments data are shown in Fig. 24 and the expression levels of RLuc8- and GFP^2-tagged receptor constructs are shown in Fig. 25**.** For all of the receptor combinations the BRET^2 signal plotted as a function of the A/D ratio increased as a hyperbolic function reaching a saturation level (Fig. 24).

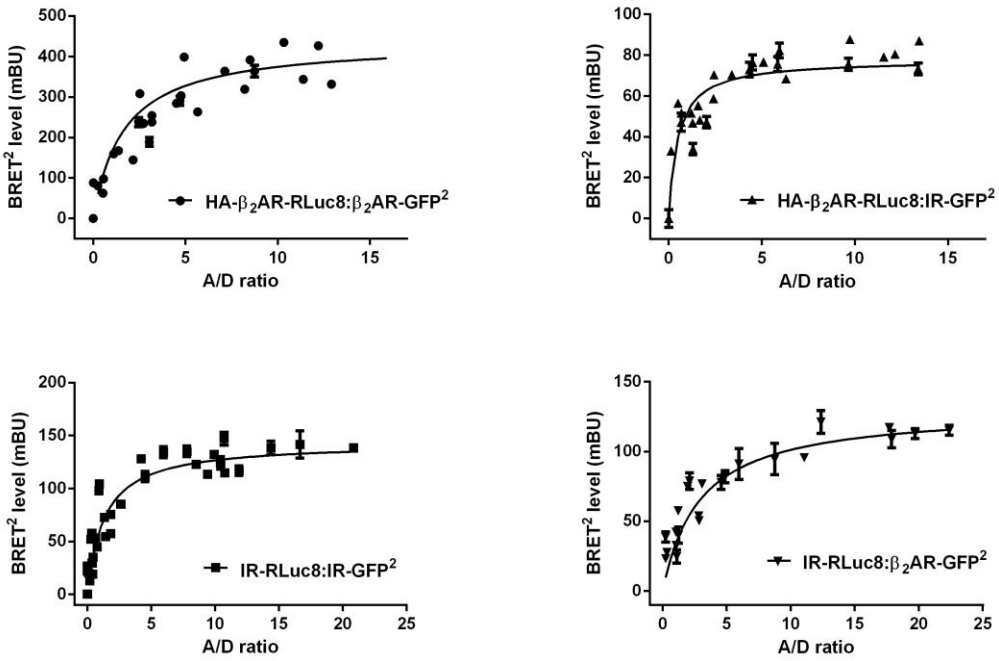

Figure 24: BRET^2 saturation curves of β_2AR and IR homo- and heteromers

HEK-293 cells were transiently cotransfected with constant amounts of RLuc8-tagged and increasing amounts GFP^2-tagged receptor encoding constructs. BRET^2 values were plotted as a function of the ratio between the acceptor and donor fusion proteins (A/D ratio). A dataset is composed of three to five independent saturation experiments that were fitted using a nonlinear regression equation assuming a single binding site using GraphPad Prism 5.0 (Fitting results are found in Table 3).

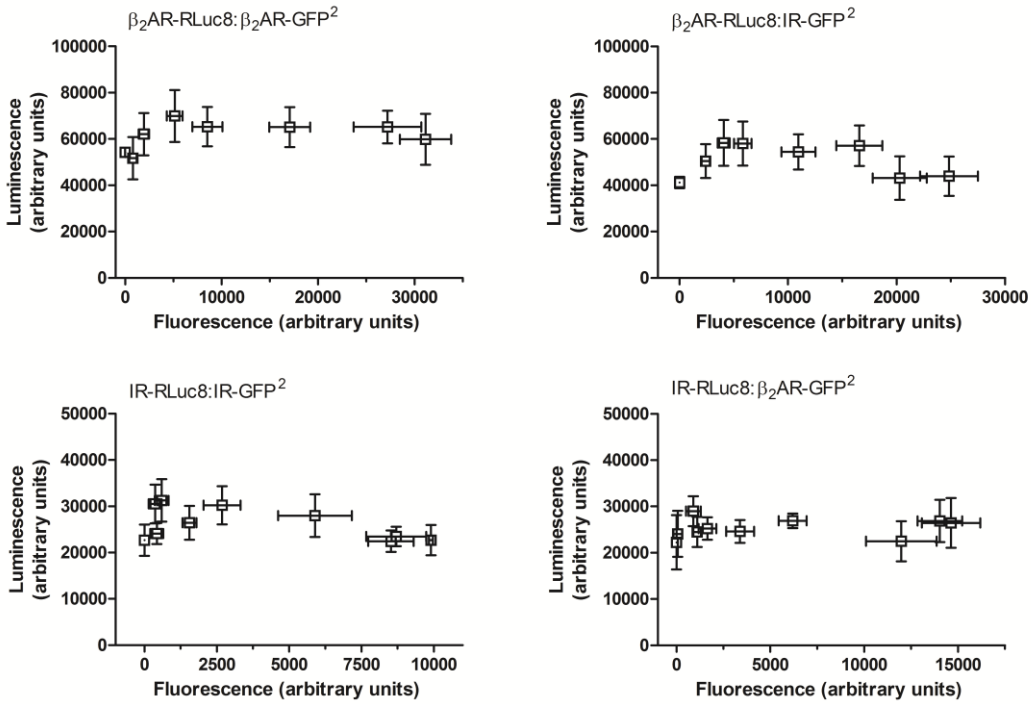

Figure 25: Relationship between receptor-RLuc8 and receptor-GFP^2 constructs expression

Expression levels of RLuc8- and GFP^2-tagged constructs used in BRET^2 saturation assays were monitored by luminescence and fluorescence measurements as described in Materials and methods. Data are expressed as the means $\pm$ S.E. of three to five independent saturation experiments.

Control experiments for the specificity of the interaction were performed by cotransfecting RLuc8-tagged receptors with increasing amounts of GFP^2-17aa. Plasma membrane localization of the GFP^2-17aa construct was previously demonstrated [220]. The BRET^2 signal increased linearly with the increase in fluorescence/luminescence (GFP^2/RLuc8) ratio, most likely reflecting random collisions between the RLuc8-tagged receptors and control unrelated GFP^2-17aa (Fig. 26).

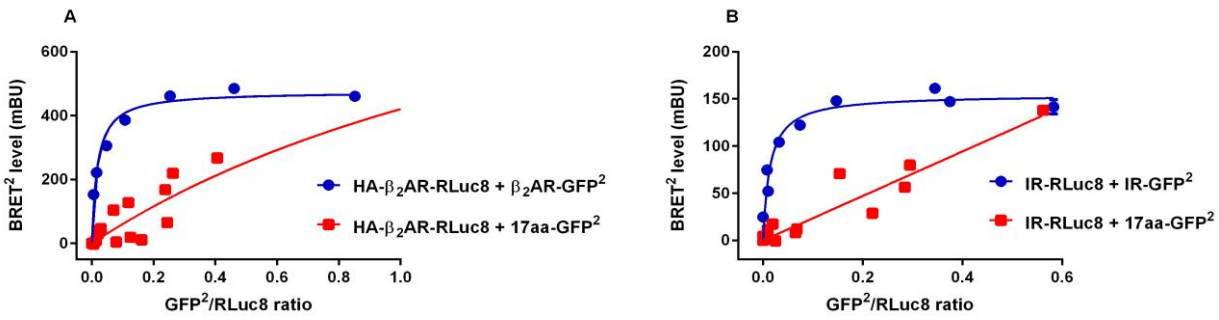

Figure 26: Random collisions between the RLuc8-tagged receptors and membrane-inserted GFP^2-tagged construct (GFP^2-17aa)

HEK-293 cells were transiently cotransfected with a constant amount of RLuc8-tagged receptors and increasing amounts of GFP^2-17aa encoding construct, which resulted in high, but nonspecific linear increase of the $BRET^2$ signal. Data are expressed as the means ± S.E. from three independent experiments performed in triplicate. Representative $BRET^2$ saturation curves of β_2AR and IR homomers are shown for comparison**.**

Saturation assay data were fitted using a dimer model in the approximation of small energy transfer [181] (Table 3). We observed the highest $BRET^2_{max}$—i.e., 437 mBU in the β_2AR homologous saturation assay and considerably lower $BRET^2_{max}$ values for other receptor combinations. It should be stressed that the $BRET_{max}$ value is a function of the distance between BRET pairs and is not a measure of the strength of interaction between the acceptor- and donor-tagged receptors. In homologous saturation assays, the values of AD_{50} for the IR homomer was significantly lower ($p < 0.05$) than that for the β_2AR homomer (Table 3). For the receptor complex consisting of β_2AR-RLuc8:IR-GFP^2, the AD_{50} value was significantly lower ($p < 0.05$) than the AD_{50} value for the IR-RLuc8:β_2AR-GFP^2. For heterodimers, there should be no difference in the relative affinity between AD and DA dimers.

To interpret our data, we developed a simplistic trimer model for interpretation of AD_{50} values in a BRET saturation assay. According to this model, different AD_{50} values are derived from theoretical BRET saturation curves with different affinities for various types of

trimer formation (Fig. 27). This model should be used with caution because it does not take into account the simultaneous formation of dimers, trimers and higher-order oligomers. Stimulation with the agonists insulin or isoproterenol did not promote any detectable change in the $BRET^2$ signal (data not shown), indicating that the receptor dimers/oligomers form constitutively and that addition of agonists does not induce a detectable change in the conformational or oligomerization state of the receptor complexes. However, it needs to be stressed that BRET only provides information concerning a steady-state population of dimer/higher-order oligomers and is not suited to monitor the rapid, "real-time" dynamic type of di-/oligomerization [253].

Table 3: $BRET^2$ saturation assay fitting results

$BRET^2$ data from saturation assays were fitted using the following equation for dimers: $BRET=BRET_{max}(1/(1+AD_{50}/X))$ where X is the ratio of acceptor (A; Receptor-GFP^2) to donor (D; Receptor-RLuc8) molecules. The $BRET^2_{max}$ is the maximal $BRET^2$ obtained for a given pair and AD_{50} value corresponds to the A/D ratio providing 50% of the $BRET^2_{max}$. The best-fit parameters and standard errors were derived from the data presented in Fig. 25. Fitting parameters were compared using Welch's t-test. Statistical analysis shows that AD_{50} and $BRET^2_{max}$ values differ significantly ($p < 0.05$) between all of the tests.

Receptor pair	$BRET^2_{max}$ (mBU)	AD_{50}
HA-β_2AR-RLuc8:β_2AR-GFP^2	437 ± 35	1.7 ± 0.5
IR-RLuc8:IR-GFP^2	143 ± 10	1.3 ± 0.4
HA-β_2AR-RLuc8:IR-GFP^2	78 ± 4	0.5 ± 0.1
IR-RLuc8:β_2AR-GFP^2	131 ± 11	2.9 ± 0.7

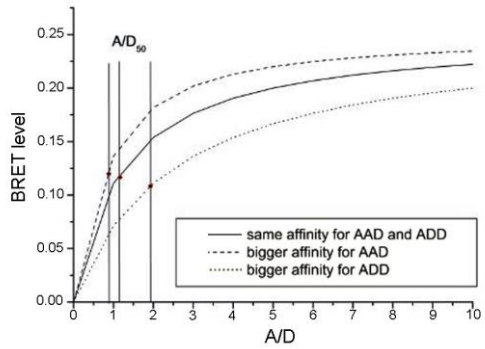

Figure 27: Comparison of theoretical BRET saturation curves with different affinities for trimer formation

Shown are simulated BRET saturation curves for the case with the same affinity for AAD and ADD formation (solid line) and two special cases with different affinities for formation of AAD compared to ADD (hatched and dotted lines). Note that in all three cases the AD_{50} values are different. A: acceptor; D: donor.

4.4.4 BRET^2 competition assays

To further support the findings from the saturation assays, we performed homologous and heterologous BRET^2 competition assays where HEK-293 cells were cotransfected with a constant amount of RLuc8- and GFP^2-tagged receptor, while increasing the amount of untagged receptor (Fig. 28A and B). Competition experiments were carried out at the relatively constant Receptor-GFP^2/Receptor-RLuc8 expression ratio to avoid possible variations in the BRET^2 signal due to fluctuation in the relative expression levels of the energy donor and acceptor (Fig. 28C and D). GFP^2/RLuc8 ratios used in the competition assays were 3- to7-fold higher than estimated BRET$^2_{50}$ values that were 0.017 ± 0.001 and 0.013 ± 0.002 for the β_2AR and IR, respectively (as assessed from the β_2AR and IR BRET^2 saturation curves; Fig.26A and B) and should give close to maximal BRET^2 signal.

It is expected that the BRET^2 signal would decrease if untagged receptors compete with the tagged receptors for the binding in complexes. In the IR homologous competition assay, we observed a typical competition curve for dimers, where introduction of the same amount of untagged receptor produced an approximately 50% reduction in the observed BRET^2 signal. In the β_2AR homologous competition assay, the reduction of the BRET^2 signal was smaller. This observation cannot be explained by a simple dimer or trimer model; it could

be attributed to clustering of the β_2AR where several acceptors can interact with each donor. In heterologous competition assays, we observed a transient increase in the BRET^2 signal with a later hyperbolical decrease (see Fig. 28A and B). Untagged β_2AR caused approximately 1.4-fold increase in the IR BRET^2 signal, while the effect of untagged IR on the β_2AR BRET^2 signal was less obvious; maximal observed increase was less than 1.2-fold. The transient increase in the BRET^2 signal with a subsequent hyperbolical decrease is theoretically predicted for trimers or higher order oligomers, where the donor, acceptor and competitor are all present in the same complex (Fig. 29).

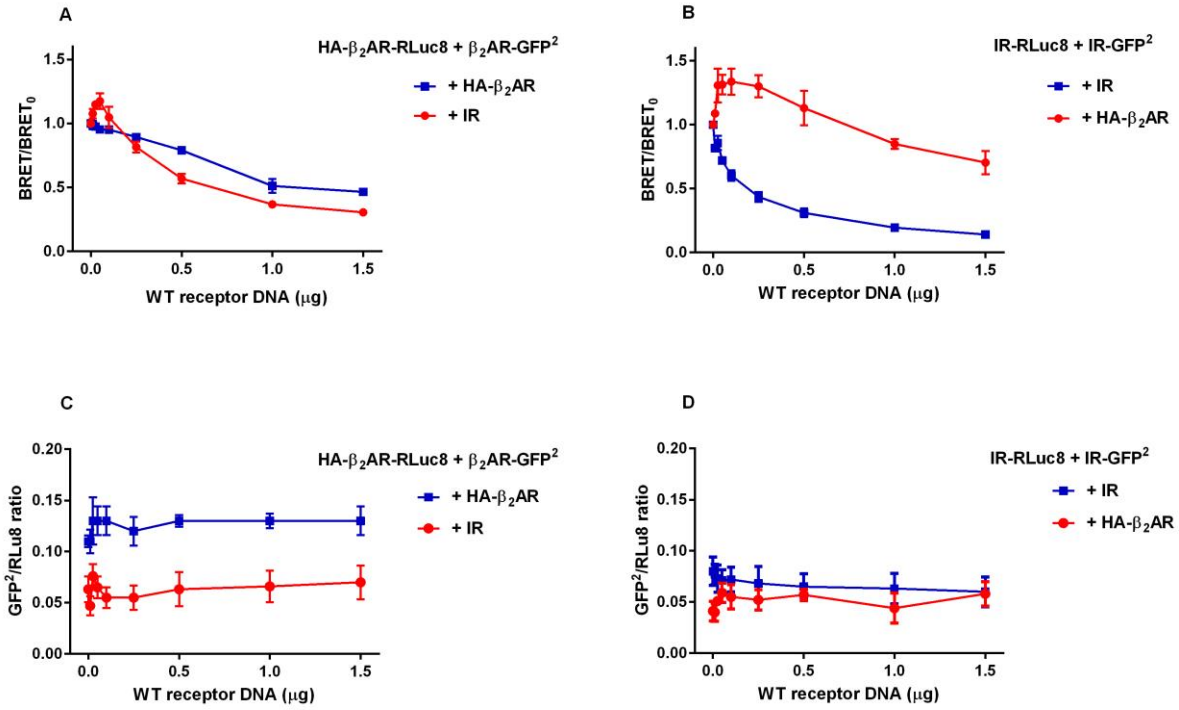

Figure 28: Homologous and heterologous BRET^2 competition assay

(A, B) HEK-293 cells were cotransfected with a constant amount of RLuc8- and GFP^2-tagged receptors and with increasing amounts of untagged receptor. In the homologous competition assay (blue line), BRET^2 signals decreased with increasing amounts of WT receptor confirming the competition effect. In the heterologous BRET^2 assay (red line), where different WT receptors were used to compete with the tagged homomer receptor pair, a transient increase in the BRET^2 signal with a subsequent hyperbolical decrease was observed. BRET$_0$ is the BRET^2 signal obtained in the absence of competitor. Data are expressed as the means ± S.E. from three independent experiments performed in triplicate.

(C, D) Receptor-GFP^2/Receptor-RLuc8 expression ratio (GFP^2/RLuc8 ratio) in each sample was evaluated for total luminescence and total fluorescence. Total luminescence and total fluorescence was measured as described under Material and methods. Note that GFP^2/RLuc8 ratio was roughly constant in the absence or presence of increasing concentrations of competitor (untagged β_2AR or IR). Data are expressed as the means ± S.E. from three independent experiments performed in triplicate.

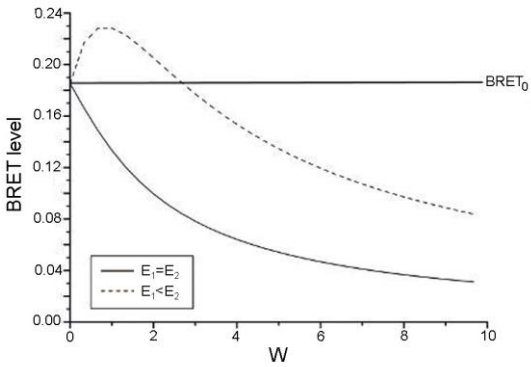

Figure 29: Numerical simulation of heterologous BRET competition assay for trimers

Comparison of simulated BRET competition curves for trimers with the same (E_1=E_2=0.1) and different (E_1=0.1, E_2=0.3) energy transfer ratios for ADD and ADW, where A, D and W are concentrations of acceptor (A=1), donor (D=1) and (W) wild type receptors i.e. competitor. Transient increase in BRET signal is observed in the case of different (E_1=0.1, E_2=0.3) energy transfer ratios (dotted line). $BRET_0$ is the BRET signal obtained in the absence of competitor.

4.5 INTERACTION BETWEEN β_2AR AND IR CHARACTERIZED BY INFORMATIONAL SPECTRUM METHOD (ISM)

To support our experimental evidence with the bioinformatics data, we next applied the ISM, a virtual spectroscopy method to investigate protein-protein interactions and to analyze the structure/function relationship of proteins. ISM was utilized to identify important informational characteristic of the interaction between β_2AR and IR, and identify the structural determinants potentially involved in receptor heteromerization**.** The primary structure of proteins encodes the information represented by the informational spectrum (IS) frequencies that correspond to the protein biological function. Mutually interacting proteins share common information that is represented by peaks in their cross-spectrum (CS) [217]. The informational spectrum of β_2AR is presented in Fig. 30A. It contains two characteristic peaks at the frequency F(0.216) and F(0.355). Fig. 30B represents the IS of the IR. By performing CS analysis of β_2AR and IR, we have identified that these two molecules share common information corresponding to the IS frequency F(0.216) (Fig. 31C).

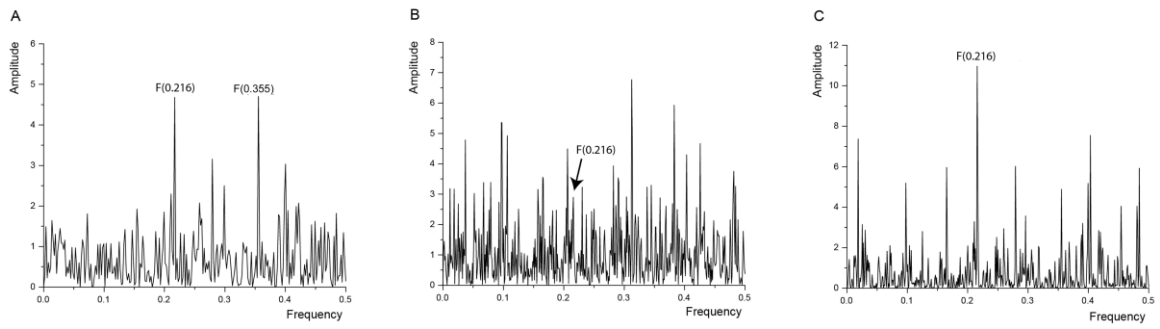

Figure 30: Informational spectrum (IS) of (A) β_2AR; (B) IR and (C) CS of the β_2AR and IR

Note that β_2AR contains two characteristic peaks at the frequency F(0.216) and F(0.355). Cross-spectral analysis (CS) of β_2AR and IR revealed common information corresponding to the IS frequency F(0.216) (panel C).

To further evaluate the importance of the peak at F(0.216), we performed CS analysis of β_2AR and IR with scrambled IR and β_2AR proteins as negative controls. The scrambled proteins with the identical amino acid composition to that of β_2AR and IR were created by random permutation of original proteins. CS analysis between wild type receptors and randomly selected scrambled β_2AR and IR are presented in Fig. 31. The intensity of whole spectrum and the value of amplitudes at the characteristic peak F(0.216) is higher in CS of two wild type proteins compared to CS of original and scrambled proteins confirming the importance of the characteristic peak at the F(0.216) for interaction between β_2AR and IR.

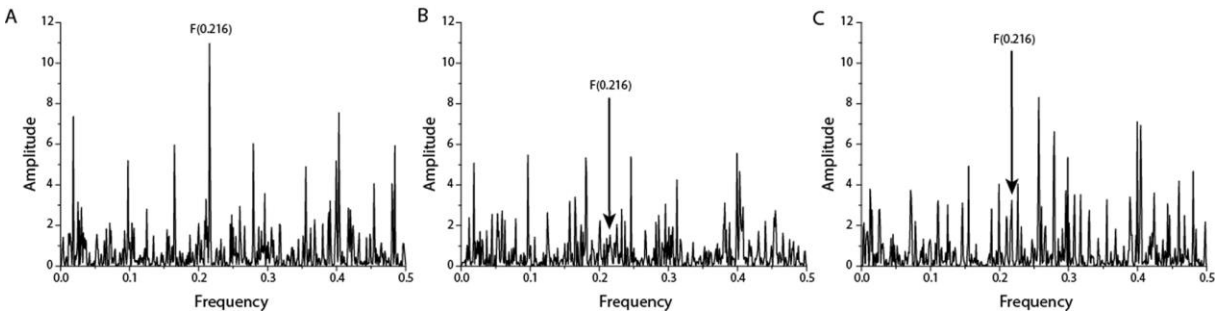

Figure 31: Cross-spectrum (CS) of (A) wild type β_2AR and IR, (B) scrambled β_2AR and wild type IR and (C) scrambled IR and wild type β_2AR

Note that the value of amplitudes at the characteristic peak F(0.216) is higher in CS of two wild type proteins (panel A) compared to the CS of wild type and scrambled proteins (panels B and C).

4.5.1 Identification of the key protein domains responsible for the interaction between β_2AR and IR

Computational peptide scanning of β_2AR and IR was performed to identify the regions of proteins essential for information corresponding to the frequency F(0.216). The computer-assisted peptide scanning survey of the primary structure of β_2AR with overlapping windows of different lengths revealed that the region encompassing residues 325–364 is essential for the information represented by the frequency F(0.216) (Fig. 32A). Identified regions represent residues at the end of the 7th TM domain and C-terminal tail of β_2AR [254]. Further peptide scanning of IR identified the region encompassing residues 1269–1314 as essential for the information represented by the frequency F(0.216) (Fig. 32B). Identified regions represent a cytoplasmic part of IR β chain as prospective interaction domain [255].

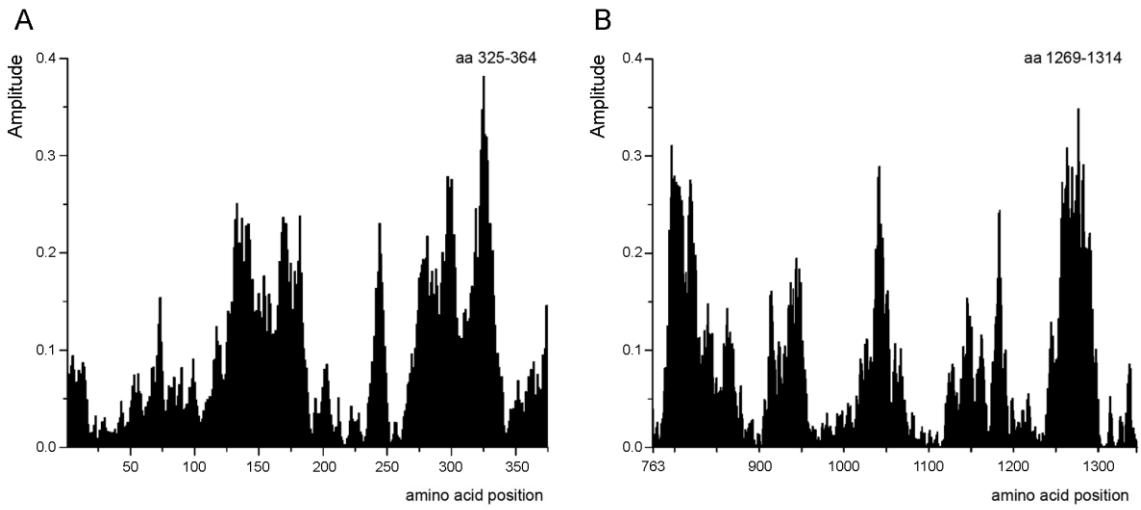

Figure 32: Mapping of the domains with maximal contribution to the frequency component F(0.216) in the informational spectrum of of (A) β_2AR and (B) IR

Domains encompassing residues 325–364 and 1269-1314 are essential for the information represented by the frequency F(0.216) in the β_2AR (A) and IR (B). The position of the first amino acid (aa) in the domain is shown. Panel B; the amino acid position denote the positions in IR β subunit starting from amino acid 763.

4.5.2 Affinity of interaction between protomers

Peak frequencies in consensus information spectrum (CIS) represent the common information encoded by the primary structures of analyzed proteins. Significance of information is determined by the signal-to-noise ratio (S/N), representing the ratio between the signal intensity at one particular IS frequency and main value of the whole spectrum. A higher S/N value at the characteristic frequency (F) in CS/CIS of two or more proteins suggests a higher propensity for their interaction.

The current analysis showed that the interaction affinities between the homomers of β_2AR and IR are similar and that at the level of dimer formation, both β_2AR and IR displayed a higher propensity toward homodimerization than heterodimerization (Table 4). Considering that in the CS of the β_2AR and IR, the two receptors share common information corresponding to the IS frequency F(0.216), it can be assumed that this frequency is equally important for heterodimerization and for higher-order hetero-oligomer formation. The obtained S/N values at F(0.216) in the CS of β_2AR:β_2AR:β_2AR:IR and β_2AR:β_2AR:IR:IR tetramers were comparable, whereas that for the IR trimer displayed a considerably lower affinity for interaction with the β_2AR monomer (Fig. 33 and Table 4).

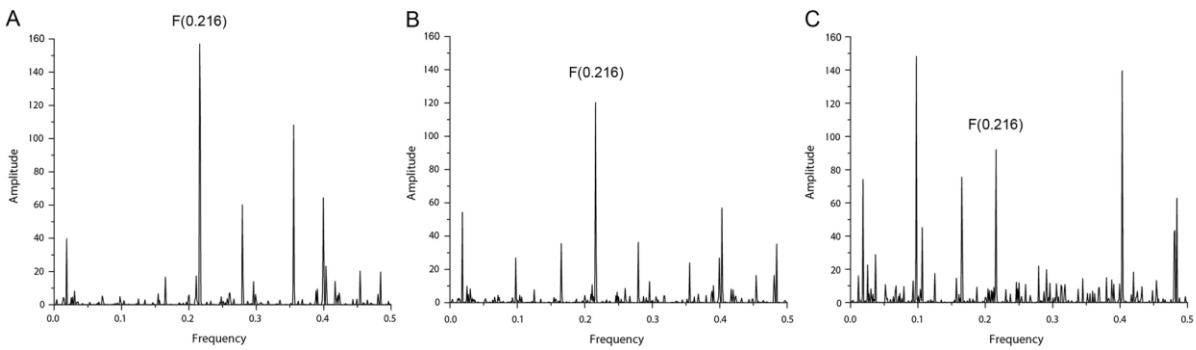

Figure 33: CIS of β_2AR:IR tetramers with the characteristic peak at F(0.216)

(A) β_2AR:β_2AR:β_2AR:IR, (B) β_2AR:β_2AR:IR:IR and (C) β_2AR:IR:IR:IR tetramers. Note that the interaction affinities among the receptors decreased in the order β_2AR:β_2AR:β_2AR:IR $\geq$ β_2AR:β_2AR:IR:IR > β_2AR:IR:IR:IR.

Table 4: The affinity of interaction between the β_2AR and IR homo- and heteromers characterized by the signal-to-noise ratio (S/N) at the characteristic frequency (F) in the CIS

Dimer	**S/N ratio**
β_2AR:β_2AR	24.082
β_2AR:IR	15.951
IR:IR	22.407
Trimer	
β_2AR:β_2AR:β_2AR	52.867
β_2AR: $\beta_2$2AR:IR	43.476
β_2AR:IR:IR	25.605
IR:IR:IR	51.146
Tetramer	
β_2AR:β_2AR:β_2AR:β_2AR	81.703
β_2AR:β_2AR:β_2AR:IR	76.505
β_2AR:β_2AR:IR:IR	71.105
β_2AR:IR:IR:IR	29.468
IR:IR:IR:IR	89.617

4.6 INVESTIGATION OF THE β_2AR:IR HETEROMER IN TERMS OF β-ARRESTIN 2 (βARR2) RECRUITMENT

To provide supporting functional evidence for the existence of heteromeric complexes, we used 7TMR:RTK-HIT to monitor ligand-promoted recruitment of βarr2 to the 7TMR:RTK heteromers. The obtained signal generated by HIT is not only indicative of the receptors being in a heteromeric complex, but it also reveals an aspect of the heteromer's pharmacology through generation of ligand-dependent functional responses.

We investigated β_2AR:IR heteromer in HEK-293 cells transiently cotransfected with HA-β_2AR-RLuc8, GFP^2-βarr2 and with or without untagged IR, or in cells transiently cotransfected with IR-RLuc8, GFP^2-βarr2 and with or without untagged HA-β_2AR. In the cells coexpressing either HA-β_2AR-RLuc8 or IR-RLuc8 together with GFP^2-βarr2, we first detected a constitutive BRET^2 signal (BRET$^2_{const}$) indicating constitutive interaction between the HA-β_2AR-RLuc8/IR-RLuc8 and GFP^2-βarr2. Presence of untagged IR significantly increased BRET$^2_{const}$ between the HA-β_2AR-RLuc8 and GFP^2-βarr2 (Table 5) ($p < 0.05$) and, presence of untagged β_2AR also increased BRET$^2_{const}$ between the IR-RLuc8 and GFP^2-βarr2 although not significantly (Table 5)

Table 5: Constitutive BRET^2 signal (BRET$^2_{const}$) generated by non-activated receptor interaction with βarr2 in the absence or presence of untagged receptor

HEK-293 cells were transiently coexpressing indicated RLuc8-tagged receptor constructs and GFP^2-βarr2 in the absence or presence of untagged receptor. BRET$^2_{const}$ was considered specific after the background values obtained with cells transfected only with the individual RLuc8-tagged receptor construct were subtracted. Data are means ± S.E. of two to four independent experiments each performed in triplicate.

Coexpression	**BRET$^2_{const}$ (mBU)**
β_2AR-RLuc8 + GFP^2-βarr2	22.61 ± 0.45
B$_2$AR-RLuc8 + GFP^2-βarr2 + IR	27.83 ± 1.11[a]
IR-RLuc8 + GFP^2-βarr2	21.45 ± 3.99
IR-RLuc8 + GFP^2-βarr2 + β_2AR	26.01 ± 3.43

[a] - $p < 0.05$ as compared with β_2AR-RLuc8 + GFP^2-βarr2 expressing cells

We further generated 7TMR:RTK HIT agonist dose-response curves to pharmacologically characterize the β_2AR:IR heteromerization (Fig. 34, Table 6 and 7). Addition of increasing concentrations of isoproterenol (10^{-12}–10^{-5} M) resulted in a dose-dependent increase in the BRET^2 signal indicative of GFP^2-βarr2 being recruited to agonist-activated HA-β_2AR-RLuc8 (Fig. 34A, blue solid line). Concomitant treatment with

isoproterenol (10^{-12}–10^{-5} M) and insulin (0.1 μM) resulted in a similar response to that observed with isoproterenol alone (Fig. 34B, blue solid line). Cotransfection with untagged IR resulted in a dose-dependent increase in the $BRET^2$ signal (Fig. 34A, blue dashed line) although $BRET^2_{max}$ was significantly smaller ($p < 0.05$) (Table 6). Coexpression of untagged IR produced a similar effect upon treatment with isoproterenol and insulin (Fig. 34B, blue dashed line, Table 6). Isoproterenol potency was slightly lower in those cells compared to cells without untagged IR (Table 7).

Fig. 34C shows antagonist dose-response curve generated in the presence of 1 μM isoproterenol and increasing concentration of β_2AR antagonist pindolol (10^{-13}–10^{-6} M). Increasing concentration of pindolol specifically inhibited agonist-induced GFP^2-βarr2 recruitment to the HA-β_2AR-RLuc8 in the absence (blue solid line) or presence of untagged IR (blue dashed line).

To provide further supporting evidence for the existence of β_2AR:IR heteromer, experiments were also performed with cells expressing IR-RLuc8 and GFP^2-βarr2 and with or without untagged HA-β_2AR (Fig. 34; red lines). In cells coexpressing IR-RLuc8 and GFP^2-βarr2, individual or concomitant treatments with agonists did not induce any significant recruitment of GFP^2-βarr2 to the IR-RLuc8 (Fig. 34A and B; red solid lines, Table 6). In cells coexpressing IR-RLuc8, GFP^2-βarr2 and untagged HA-β_2AR, agonist-promoted $BRET^2$ signal was detected (Fig. 34A and B; red dashed lines). However, $BRET^2_{max}$ was significantly smaller ($p < 0.05$) compared to the $BRET^2_{max}$ generated from agonist-induced interaction between GFP^2-βarr2 and β_2AR-RLuc8 (Table 6). Similarly, the potency of isoproterenol was also significantly decreased (Table 7). β_2AR antagonist pindolol prevented recruitment of GFP^2-βarr2 to the IR-RLuc8:β_2AR heteromer (Fig. 34C; red dashed line).

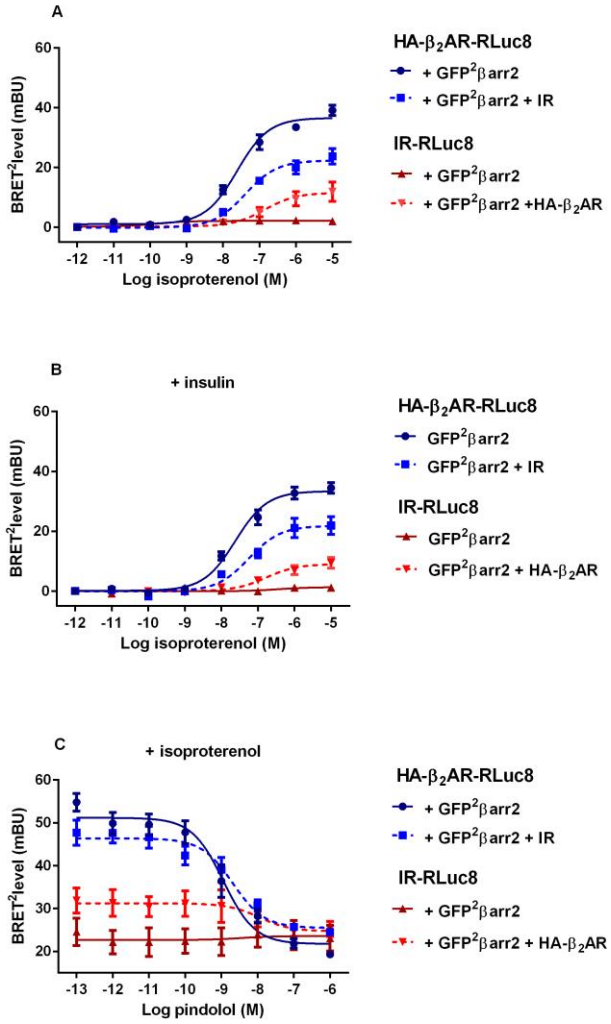

Figure 34: β_2AR:IR-HIT assay with β-arrestin 2

HEK-293 cells coexpressing indicated constructs were treated with A) isoproterenol (10^{-12}–10^{-5} M) B) isoproterenol (10^{-12}–10^{-5} M) and insulin (0.1 µM) C) pindolol (10^{-13}–10^{-6} M) and isoproterenol (10 µM). BRET^2 assays were performed as described in the Material and methods. Dose response curves were generated using a sigmoidal dose-response curve fit (GraphPad Prism 5.0). Data are means ± S.E. of two to four independent experiments each performed in triplicate.

Table 6: Maximal $BRET^2$ signal ($BRET^2_{max}$) generated by agonist-activated receptor interaction with the βarr2 in the absence or presence of untagged receptor

Cells were treated with increasing concentration (10^{-12} to 10^{-5} M) of the relevant agonist (isoproterenol or insulin). When the concomitant effect of isoproterenol and insulin was tested, insulin was added to a 0.1 µM final concentration. $BRET^2_{max}$ is the maximal agonist-induced response that was considered specific after the values obtained with untreated cells were subtracted. Data are means ± S.E. of two to four independent experiments each performed in triplicate.

	$BRET^2_{max}$ (mBU)		
Coexpression	**Isoproterenol**	**insulin**	**isoproterenol + insulin**
β_2AR-RLuc8 + GFP^2-βarr2	36.99 ± 2.49	1.58 ± 0.46	34.17 ± 2.53
β_2AR-RLuc8 + GFP^2-βarr2 + IR	21.37 ± 3.84[a]	-0.16 ± 1.98	19.86 ± 4.58[a]
IR-RLuc8 + GFP^2-βarr2	1.93 ± 0.79	2.95 ± 2.87	0.94 ± 1.64
IR-RLuc8 + GFP^2-βarr2 + β_2AR	10.35 ± 6.06[a,b]	1.95 ± 0.75	8.39 ± 3.24[a,b]

[a] - $p < 0.05$ as compared with β_2AR-RLuc8 + GFP^2-βarr2 -expressing cells

[b] - $p < 0.05$ as compared with β_2AR-RLuc8 + GFP^2-βarr2 + IR -expressing cells.

Table 7: Pharmacological characterization of the receptor interaction with βarr2

EC_{50} values were generated using sigmoidal-dose response curve fit (GraphPad Prism). Data shown are the mean ± S.E. from two to four independent experiments.

	EC_{50} (nM)		
Coexpression	**Isoproterenol**	**insulin**	**isoproterenol + insulin**
β_2AR-RLuc8 + GFP^2-βarr2	28.09 ± 7.10	ND	36.32 ± 20.00
β_2AR-RLuc8 + GFP^2-βarr2 + IR	37.94 ± 14.3	ND	50.04 ± 11.8
IR-RLuc8 + GFP^2-βarr2	ND	ND	ND
IR-RLuc8 + GFP^2-βarr2 + β_2AR	131.8 ± 13.2[a]	ND	166.7 ± 20.66[a]

[a] - $p < 0.05$ as compared with β_2AR-RLuc8 + GFP^2-βarr2 expressing cells

4.6.1 BRET^2 assay with GFP^2-βarr2 1–185 mutant

To investigate the specificity of IR and βarr2 interaction, HEK-293 cells were transiently cotransfected with constructs encoding RLuc8-tagged receptors (IR-RLuc8, HA-β_2AR-RLuc8) together with GFP^2-βarr2 1–185 mutant or GFP^2-βarr2 (Fig. 35). GFP^2-βarr2 1–185 mutant (E186–stop; GAA–TAA) lacks the binding region (amino acids 186–409) for the interaction with the IR [121]. Significantly smaller constitutive BRET^2 signal (BRET$^2_{const}$ = 8.24 ± 0.71 mBU) was detected in cells coexpressing IR-RLuc8 and GFP^2-βarr2 1–185 mutant, compared to constitutive signal obtained with the GFP^2-βarr2 (BRET$^2_{const}$= 22.96 ± 2.18 mBU) ($p < 0.01$) (Fig. 35A). There was no substantial agonist-mediated effect as BRET^2 signal obtained with cells treated with insulin (0.1 μM), isoproterenol (10 μM) or concomitantly with insulin and isoproterenol was comparable with the BRET$^2_{const}$ (Fig. 35B).

Analogously, in cells coexpressing the HA-β_2AR-RLuc8 and GFP^2-βarr2 1–185, significantly smaller BRET^2 signal (BRET$^2_{const}$= 6.36 ± 0.70 mBU) was observed in contrast to constitutive signal obtained with the GFP^2-βarr2 (BRET$^2_{const}$= 20.87 ± 1.48 mBU) ($p < 0.01$) (Fig 35A), indicating that the mutation of βarr2 that limited self-association with the IR, also interfered in the interaction with the β_2AR. We observed agonist-induced increase in the BRET^2 signal in cells coexpressing β_2AR and βarr2 upon treatment with isoproterenol or with insulin and isoproterenol (Fig 35C). Again, in cells coexpressing mutant βarr2 there was no response upon addition of agonists.

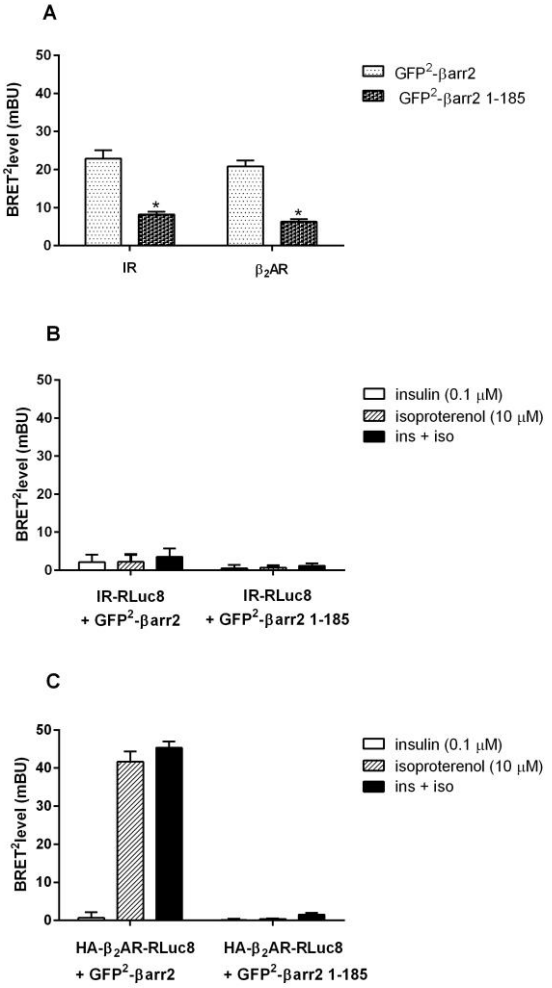

Figure 35: BRET^2 assay with βarr2 1-185 mutant

A) constitutive BRET^2 signal; B) and C) HEK-293 cells coexpressing indicated constructs were treated with insulin (0.1 μM), isoproterenol (1 μM) or concomitantly with insulin and isoproterenol. BRET^2 assays were performed as described in the Material and methods. Data are means ± S.E. of three independent experiments each performed in triplicate.

*, $p < 0.05$ as compared with cells transfected with GFP^2-βarr2

4.7 THE IMPORTANCE OF IR RESIDUES 1269–1314 IN FORMATION OF THE β_2AR:IR HETEROMER

The bioinformatic analysis suggested the end of the 7th TM domain and C-tail of β_2AR and a cytoplasmic part of IR β chain (residues 1269–1314) as possible interacting domains. We used C-terminally tagged RLuc8 IR 1–1271 mutant (IR 1–1271-RLuc8), which lacks IR C-tail region (amino acids from 1272 to 1360), but it has preserved TK catalytic domain [255]. In homologous BRET^2 saturation assays, IR 1–1271–RLuc8 mutant displayed significantly lower BRET$^2_{max}$ value (65 ± 6 *vs.* 143 ± 10 mBU) and slightly reduced affinity (AD_{50} of 1.6 ± 0.6 *vs.* 1.3 ± 0.4) compared to the WT IR (Fig. 36A). For the complex consisting of IR 1-1271-RLuc8:β_2AR-GFP^2 the saturation was not reached; the BRET^2 signal increased linearly, most likely reflecting random collisions between the IR 1-1271-RLuc8 and β_2AR-GFP^2 (Fig. 36B).

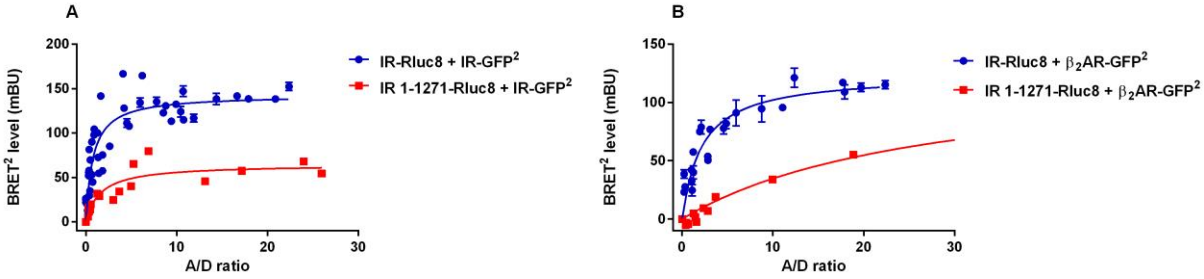

Figure 36: BRET^2 saturation curves of IR 1–1271 mutant homo- and heteromers

HEK-293 cells were transiently cotransfected with constant amounts of RLuc8-tagged and increasing amounts of GFP^2-tagged receptor encoding constructs. BRET^2 values were plotted as a function of the ratio between the acceptor and donor fusion proteins (A/D ratio). Data are means ± S.E. of three independent experiments each performed in triplicate.

Representative BRET^2 saturation curves of WT IR homo-/heteromers from Fig. 25 are shown for comparison.

Further evidence for the role of the proposed IR interaction domain for the interaction with the β_2AR was provided by IR 1–1271:β_2AR HIT assays. As shown in Fig. 37, cotransfection with untagged β_2AR did not result in a substantial agonist-induced increase in BRET signal arguing against IR 1–1271:β_2AR heteromerization.

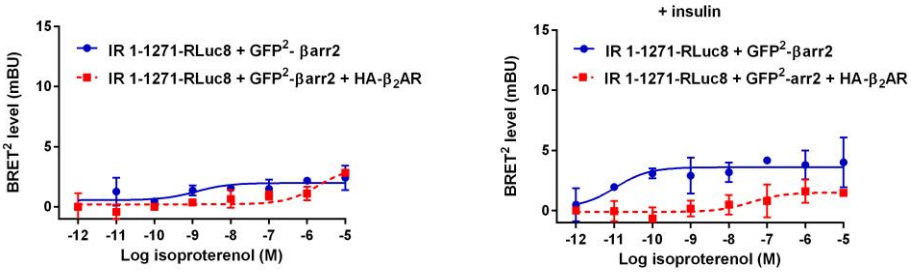

Figure 37: IR 1–1271:β_2AR HIT assay with βarr2

HEK-293 cells coexpressing IR 1–1271-RLuc8, GFP^2-βarr2 with or without untagged HA-β_2AR were treated with isoproterenol (10^{-12}–10^{-5} M) or with isoproterenol (10^{-12}–10^{-5} M) and insulin. BRET^2 assays were performed as described in the Material and methods. Dose response curves were generated using a sigmoidal dose-response curve fit (GraphPad Prism 5.0). Data are means ± S.E. of triplicate observation from a single representative experiment.

4.8 INVESTIGATION OF THE β_2AR:IR HETEROMER IN TERMS OF SHC RECRUIMENT

To investigate the β_2AR:IR heteromer in terms of Shc recruitment and features of those interactions, HEK-293 cells were transiently cotransfected with IR-RLuc8, GFP^2-Shc with or without untagged HA-β_2AR; or with HA-β_2AR-RLuc8, GFP^2-Shc with or without untagged IR.

In cells coexpressing IR-RLuc8 and GFP^2-Shc, constitutive interaction was detected (BRET$^2_{const}$ = 22.29 ± 1.74 mBU). In cells coexpressing untagged HA-β_2AR in addition to IR-RLuc8 and GFP^2-Shc, constitutive BRET^2 signal was slightly higher (BRET$^2_{const}$ = 27 ± 2.05 mBU). Upon addition of increasing concentrations of insulin (10^{-12}–10^{-5}) dose-dependent increase in the BRET^2 signal was observed in cells expressing IR-RLuc8 and GFP^2-Shc (Fig. 38; blue solid line). Cotransfection with untagged HA-β_2AR neither affected insulin-induced BRET$^2_{max}$ (Fig. 38; blue dashed line) nor the potency i.e. EC_{50} of insulin (data not shown). Treatment with isoproterenol did not provoke agonist-induced response (data not shown).

In cells coexpressing HA-β_2AR-RLuc8 and GFP^2-Shc, a constitutive BRET^2 signal was detected (BRET$^2_{const}$ = 22.63 ± 1.00 mBU). Nevertheless, treatment with insulin (0.1 μM) (Fig. 38; red solid line), isoproterenol (10 μM) or concomitantly with isoproterenol (10 μM) and insulin (0.1 μM) did not provoke agonist-induced response (data not shown). In cells coexpressing untagged IR, in addition to HA-β_2AR-RLuc8 and GFP^2-Shc, significantly higher constitutive BRET^2 signal of 26.93 ± 0.74 mBU ($p < 0.05$) was observed. Treatment with insulin resulted in a dose-dependent increase, although BRET$^2_{max}$= 5.63 ± 0.35 mBU was significantly smaller compared to IR-RLuc8 and GFP^2-Shc as well as IR-RLuc8, GFP^2-Shc and HA-β_2AR expressing cells ($p < 0.05$) (Fig. 38; red dashed line).

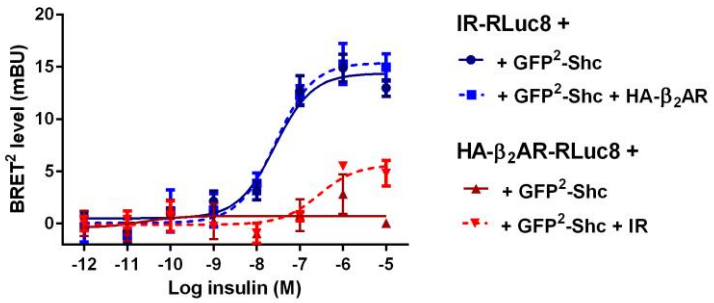

Figure 38: IR-RLuc8:β_2AR-HIT assay using Shc

HEK-293 cells coexpressing indicated constructs were treated with insulin (0.1 μM) and BRET^2 assays performed as described in the Material and methods. Dose response curves were generated using a sigmoidal dose-response curve fit (GraphPad Prism 5.0). Data are means ± S.E. of two independent experiments each performed in triplicate.

4.9 THE EFFECT OF IR COEXPRESSION ON β_2AR cAMP PRODUCTION

The amount of cAMP produced was evaluated in β_2AR-, IR- or β_2AR and IR-expressing cells, to elucidate the role that IR might have on β_2AR in terms of cAMP production. Isoproterenol-activation of β_2AR coupled to the stimulatory Gα_s protein increases the AC activity, which resulted in intracellular cAMP accumulation (Table 8). Basal cAMP value in β_2AR-expressing cells was 2.78 ± 0.29 nM, in IR-expressing cells 0.55 ± 0.11 nM and in β_2AR and

IR-expressing cells 2.68 ± 0.38 nM. Insulin in combination with isoproterenol did not significantly increase the amount of cAMP produced compared to cells treated with isoproterenol only. There was no significant difference between the cells expressing β_2AR or β_2AR and IR in the amount of cAMP produced, indicating that IR does not greatly effect β_2AR production of cAMP. Cells transiently transfected with only IR, demonstrated weak sensitivity to isoproterenol- and isoproterenol and insulin stimulation, which is consistent with IR not triggering the production of cAMP and with the low endogenous expression of the β_2AR in the HEK-293 cells [75].

Table 8: cAMP maximal response in agonist stimulated β_2AR-, IR- or β_2AR and IR-expressing cells

HEK-293 cells expressing β_2AR or IR or β_2AR and IR were treated with isoproterenol (10^{-13} to 10^{-6} M) insulin (10^{-13} to 10^{-6} M) or with isoproterenol (10^{-13} to 10^{-6} M) and insulin (0.1 μM) concomitantly. cAMP assay was performed as described in the Material and methods. cAMP maximal response is cAMP response in stimulated cells with subtracted basal cAMP values. Data are means ± S.E. of four independent experiments each performed in triplicate.

	cAMP max response (nM)		
Receptors	**isoproterenol**	**insulin**	**isoproterenol + insulin**
β_2AR	56.89 ± 19.9	ND	64.2 ± 16.52
IR	5.96 ± 1.84[a]	ND	6.46 ± 1.47[a]
β_2AR + IR	65.72 ± 21.43	ND	76.36 ± 19.6

ND – not detected.

[a] - $p < 0.05$ as compared with β_2AR or β_2AR and IR expressing cells treated with either isoproterenol or isoproterenol and insulin

There was also no statistical difference between EC_{50} values of isoproterenol in β_2AR- or in β_2AR and IR-expressing cells (Table 9). However, upon addition of insulin, isoproterenol potency significantly decreased in the β_2AR and IR expressing cells. EC_{50} values in only IR expressing cells were significantly higher from EC_{50} values in β_2AR and

β_2AR and IR expressing cells treated with either isoproterenol or isoproterenol and insulin ($p < 0.05$) (Table 9)

Table 9: EC_{50} values for agonists in cAMP assay

EC_{50} values were derived from competitive binding curves generated by sigmoidal dose-response curve fit (GraphPad Prism 5.0). Data are means ± S.E. of four independent experiments each performed in triplicate.

	EC_{50} (nM)		
Receptors	**isoproterenol**	**insulin**	**isoproterenol + insulin**
β_2AR	0.13 ± 0.03	ND	0.20 ± 0.08
IR	20.80 ± 9.02[b]	ND	28.57 ± 14.49[b]
β_2AR + IR	0.15 ± 0.02	ND	0.37 ± 0.07[a]

ND – not detected.

[a] - $p < 0.05$ as compared with β_2AR and IR expressing cells treated with isoproterenol only

[b] - $p < 0.05$ as compared with β_2AR and β_2AR and IR expressing cells treated with either isoproterenol or isoproterenol and insulin

5 DISCUSSION

7TMRs form the largest and most important pharmacotherapeutic target in drug discovery. Continual discovery of receptor heteromers expands the repertoire of functional 7TMR units and offers promising new targets for drug development [59]. Increasing evidence for the existence of functional 7TMR:RTK heteromers [80, 142, 151, 171, 256] adds another level of complexity to this system. In the present study, we combined *in vitro* experimental and bioinformatics approaches for the investigation of the β_2AR and IR interaction.

5.1 FUSION CONSTRUCTS CHARACTERIZATION BY RADIOLIGAND BINDING ASSAY AND CONFOCAL MICOSCROPY

The labeling of receptors and interacting proteins with protein tags introduces novel chemical and physical properties, enabling the target proteins to be investigated or manipulated with various techniques. However, fusing such protein tags to the receptors could potentially interfere with their overall functional behavior and it is essential that the receptor is normally processed, trafficked, and retains its functional properties

Cells expressing β_2AR constructs were pharmacologically characterized by radioligand binding assays using ^{125}I-pindolol. Both IC_{50} values for the HA-β_2AR-RLuc8 and β_2AR-GFP^2 were in agreement with the IC_{50} value obtained for the HA-β_2AR, and were in correspondence to those reported for β_2AR fusion constructs [61, 128]. Confocal microscopy images revealed that β_2AR-GFP^2, IR-GFP^2 and HA-β_2AR-RLuc8 had predominant plasma membrane localization in untreated cells, suggesting that attachment of GFP^2 or RLuc8 to the C-terminus of the β_2AR and IR did not affect receptor expression and the transport of the receptor to the plasma membrane. Treatment of cells expressing these constructs with agonists isoproterenol or insulin caused the agonist-induced receptor endocytosis in a similar pattern as previously presented [257, 258], suggesting that protein tags did not alter receptors subcellular localization and their ability to internalize.

Our results are consistent with the findings that GFP and RLuc-tagged receptors retain their biological activity and have comparable trafficking pattern as the wild-type proteins [241, 257, 259-262]. β_2AR-GFP^2 has been shown to be fully-functional biochemically when expressed in HEK-293 cells [263] and C-terminal addition of RLuc did not substantially alter

the levels of expression, the constitutive activity of the β_2AR nor the capacity of isoprenaline to elevate intracellular cyclic AMP levels [264]. IR-RLuc8 and β_2AR-GFP^2 used in our study have been previously characterised [75, 206]. In short, tagged receptors used in our study retained their biological activity having had similar pharmacologic properties and trafficking pattern as the wild-type receptors. It should also be noted that the demonstration of receptor interactions shown in the chapter Results provides evidence for functionality in itself.

5.2 COLOCALIZATION OF β_2AR VISUALIZED BY CONFOCAL MICROSCOPY

Observed constitutive HA-β_2AR-RLuc8 and β_2AR-GFP^2 colocalization is consistent with the probability of β_2AR dimers or oligomers formation [60, 61]. In agonist treated cells, there was a fraction of colocalized β_2ARs as well. In both treated and untreated cells, there was a proportion of receptors that did not colocalize. These findings are in correlation with observations that the association of β_2ARs is not permanent in living cells, and that active and inactive β_2ARs which associate at the cell surface can dissociate during agonist-induced internalization of active protomers [265].

5.3 THE EFFECT OF IR ON β_2AR BINDING PROPERTIES, SURFACE EXPRESSION AND INTERNALIZATION

The IC_{50} values and pharmacological profiles obtained in parallel from the cells expressing β_2AR alone and the cells coexpressing β_2AR and IR, were in agreement, denoting that coexpression of IR did not significantly affect antagonist affinity nor β_2AR binding properties. Similarly, previous reports revealed that β_2AR heteromerization with the β_3AR [65] or DOR [68] did not affect its binding properties.

Functional activities of transmembrane proteins, including the superfamilies of 7TMRs and RTKs can be controlled by intracellular trafficking. Previous studies have suggested that heteromerization could affect agonist-promoted β_2AR endocytosis [64, 68, 72, 171]. Initially, it was observed that IR coexpression reduces β_2AR surface expression and accelerates its internalization. It could be assumed that IR increased constitutive internalization of the β_2AR [56], thereby reducing its surface expression. The extent of isoproterenol-induced β_2AR internalization was comparable to the previously reported internalization rate for β_2AR [266,

267]. The estimated $t_{1/2}$ of ~9 min for isoproterenol-induced β_2AR internalization is also within the range reported for the same receptor using a fluorimetric assay [268]. Augmented agonist-induced β_2AR internalization promoted by IR coexpression is in good agreement with that described in the previous report [166]. The amount of surface-expressed β_2AR lost to internalization in response to insulin in HEK-293, ~15%, correlated well with results obtained in DT_1MF-2 smooth muscle cells and CHO cells [166, 269] but was smaller than the reported value of ~30% in epidermoid carcinoma A431 cells [270]. Furthermore, β_2AR and IR colocalization results in untreated cells correlate well with recent coimmunoprecipitation findings demonstrating that β_2AR and IR form complexes in the mouse heart, in which the stimulation of IR resulted in the reduction of β_2AR:IR complex association [171].

5.4 INTERACTION BETWEEN β_2AR AND IR CHARACTERIZED BY BRET^2 AND INFORMATIONAL SPECTRUM METHOD (ISM)

Advantage of the BRET approach over the coimmunoprecipitation approaches lies in the more quantitative nature of the assay [192]. Conventional BRET assays could be problematic for measuring receptor organization in membranes because, within the crowded two-dimensional plane of the cell membrane, the signal arising from random interactions can reach significant levels [179]. If the receptor expression level is in the physiological range, there is a problem of distinguishing random collisions of donors and acceptors from stable binding. If attention is not paid to the ratio of donor/acceptor molecules used in the assays, the interpretation of the data remains rather qualitative, and controlling this parameter is essential for proper quantitative analysis. Several quantitative assays have been developed to refer these problems [181], and we were able to manage those issues by performing a range of quantitative BRET^2 assays.

BRET^2 saturation assays resulted in hyperbolic curves indicative of a specific constitutive interaction between IR and β_2AR. The BRET$^2_{max}$ obtained for β_2AR homomerization is higher than that described in previous reports [61, 75, 192], whereas the relative affinity of β_2AR for homomerization is within the previously reported range (AD_{50} of 1.7 ± 0.5 *vs.* 1.2 ± 0.33 [192]). The RLuc8/GFP^2 BRET^2 donor/acceptor pair used in our study has the largest Förster distance R_0 (i.e. 8.15 nm), leading to 50% of energy transfer from the donor to acceptor, thereby extending the maximum distance that the BRET^2 system can

accurately measure, compared to previous donor/acceptor pairs [271]. Lower reported $BRET_{max}$ values were obtained with original $BRET^1$ [61] or $BRET^2$ [75, 192] combinations. The $BRET^2_{max}$ values generated in the homologous IR saturation assay were also slightly higher than that previously reported [199]. Single-molecule analysis of fluorescently labeled 7TMRs recently demonstrated that β_2AR had a high tendency of forming dimers, even at low densities comparable to receptor expression in native tissue. However, at higher densities, β_2AR formed a mixture of di-, tri-, and tetramers [253]. Membrane-driven spatial organization of β_2AR also favors its stable/extensive oligomerization [272].

Stimulation with agonist insulin or isoproterenol did not promote any detectable change in the $BRET^2$ signal, indicating that the receptor dimers/oligomers form constitutively and that addition of agonists does not induce a detectable change in the conformational or oligomerization state of the receptor complexes. Previous experiments with the β_2AR in intact cells [61] or with purified receptors [63] indicate that agonists have minor effects that could be either due to small changes in steady-state di-/oligomerization or due to conformational changes in individual protomers. The lack of agonist effect was also reported in FRAP experiments [252]. The inability of agonists to modify the oligomerization status of β_2AR was also reported in studies that utilized other methods [59]. The study by Boute et al. revealed that the substantial insulin-induced effect on the BRET signal could only be detected with partially purified fusion IRs [199].

Both receptors displayed a similar propensity to form homomers as assessed by AD_{50} and S/N values. Affinities for the formation of β_2AR:IR and IR:β_2AR heteromers differed substantially, a finding that could not be explained by a dimer model that assumed a heteromer stoichiometry of 1:1. The lower AD_{50} value observed for the β_2AR-RLuc8:IR-GFP^2 pair could suggest either a higher affinity for heteromer formation or, alternatively, complex oligomer formation. The melatonin MT_2 receptor also displayed a higher propensity for heteromerization with the MT_1 receptor [273], whereas certain receptor pairs (i.e., β_1AR:β_2AR [192], β_2AR:β_3AR [65]), oxytocin and vasopressin receptors [274] showed a similar propensity, and muscarinic acetylcholine receptors [275] showed a slightly lower propensity for heteromerization. However, a simplistic model for interpretation of AD_{50} values and heterologous competition assays data provided evidence for higher-order oligomeric complex formation. A transient increase in the BRET signal suggests that the

energy transfer efficiency E is increased in heterooligomeric complexes due to the smaller distance between the BRET donor/acceptor pair in the complex. A similar effect, i.e. an increased homodimer BRET signal induced by an unrelated, untagged receptor was previously observed with the gastric inhibitory polypeptide receptor [75]. Therefore, both the change in affinities and transient increase in the BRET signal could be a reflection of higher-order oligomeric complexes with affinities for distinct associations such as with trimers and tetramers with 2:1 and 2:2 stoichiometry, respectively, as proposed by Breitwieser et al. [276].

In the view of bioinformatic data at the level of dimer formation, both β_2AR and IR displayed a higher propensity toward homodimerization than heterodimerization, suggesting homodimers as the basic units engaged in heteromerization. Affinity calculation for trimers and tetramers highlighted differences between β_2AR and IR. Apparently, neither IR dimers nor trimers could form high affinity interactions with the β_2AR monomer. However, IR monomers/homodimers can form high affinity heteromers with β_2AR di-/trimers. Considering that both receptors displayed a higher propensity toward homodimerization and that IR is present in the plasma membrane as a disulfide-linked dimer [277], it is plausible to suggest that high-order 7TMR:RTK oligomers most likely comprise heteromers of homodimers (2:2 stoichiometry).

The computer-assisted peptide scanning survey of the primary structure of β_2AR and IR revealed the domain encompassing residues 325–364 and 1269–1314 as prospective interaction domains. The identified region is located at the end of the 7th TM domain and C-terminal tail of β_2AR, and almost completely overlaps with helix 8 (helix adjacent to TM7 running along the internal membrane surface) of β_2AR (residues L324-N357) [254]. A recent study also identified β_2AR helix 8 as an important dimerization surface region [278]. In addition, this region contains major sites (Tyr350/Tyr354 and Tyr364) for IR-mediated phosphorylation of β_2AR [6, 169] and consensus sites of Akt-catalyzed phosphorylation (Ser345/Ser 346) [279]. These results are in accordance with previous findings showing that β_2AR is a substrate for IR and proposing direct interaction between these proteins [6, 169]. The C-terminal cytoplasmic tail, more specifically, the 15-amino acid motif (residues 342–356), was sufficient to confer the β_1AR-β_2AR tail chimera the ability to be regulated by insulin [269].

The prospective interaction domain identified in IR (residues 1269–1314) is positioned in the cytoplasmic part of the IR β chain. This region encompasses the terminal end of the TK catalytic domain and is a part of the C-terminal tail. The C-terminal domain of the IR β subunit has been found to play a key role in the regulation of TK activity [280, 281]. The construct based on proteolytic cleavage used to solve the crystal structure of the IR TK domain of the human IR B-isoform [255] ends at residue 1283, which corresponds to the amino acid at position 1271 in the human IR isoform A used in our study. Therefore, we hypothesized that the terminal end of the IR TK domain and a part of the C-terminal tail are involved in the interaction with β_2AR.

We have employed an IR 1–1271 mutant, which lacks the proposed interaction domain in $BRET^2$ saturation and HIT assays with βarr2 and were able to confirm that the prospective interaction domain is actually requisite for the interaction with the β_2AR. The involvement of intracellular domains (C-terminal tail and ICL3) was found to be fundamental for heterodimerization between the cannabinoid CB_1 receptor, adenosine A_{2A} and dopamine D_2 receptors, thus favoring the idea that electrostatic interactions between intracellular domains are more predominant in receptor heteromers and constitute a general mechanism for receptor heteromerization [282].

Recent data also support the concept of β_2AR:IR heteromerization. Fu et al. [171] described an IR:β_2AR complex in the mouse heart, indicating that crosstalk between these two receptors could provide a molecular basis for the pathophysiology of metabolic and cardiovascular dysfunction under insulin-resistant states. Furthermore, a convincing evidence for a functional link between β_2AR and IR signaling pathways exist in retina, as β_2AR knockout mice exhibited a diabetic retinopathy phenotype [170].

5.5 INVESTIGATION OF THE β_2AR:IR HETEROMER IN TERMS OF βARR2 AND SHC RECRUITMENT

We have employed HIT in studying 7TMR and RTK receptor heteromerization and were able to profile βarr2 recruitment to the β_2AR:IR heteromer in a ligand-dependent manner. The

development of new cell-based assays to study the heteromerization of membrane-bound receptors of different superfamilies, and profile their pharmacology and signaling in real-time and live cells, is of great importance for success in academic/basic research and translation into more effective and safer drugs.

We have clearly demonstrated that isoproterenol induced and pindolol inhibited βarr2 recruitment to the β_2AR:IR heteromer. This is consistent with βarr2 being recruited to the untagged β_2AR in an agonist-dependent manner, and IR-RLuc8 being sufficiently proximal to the β_2AR to allow detectable energy transfer to the GFP^2-βarr2. $BRET^2_{max}$ values generated in the 7TMR:RTK HIT assay were similar to those generated in the $BRET^2$ β_2AR:βarr2 assay and higher than those previously reported [128]. On the contrary IR:βarr2 interaction was only found to be constitutive, no agonist-induced recruitment of the GFP^2-βarr2 to the IR-RLuc8 was observed in the absence of untagged β_2AR.

Expression of an untagged receptor results in a lower $BRET^2_{max}$, so it seems that untagged receptor appears to decrease the proximity between the tagged receptor and βarr2 or to decrease the agonist-promoted recruitment of βarr2. Lower $BRET^2_{max}$ could also be a consequence of changes in receptor:arrestin stoichiometry upon β_2AR:IR heteromerization. In addition, isoproterenol potency was lower in cells expressing untagged receptor. Using an identical assay we have demonstrated insulin induced recruitment of the Shc protein to the β_2AR:IR heteromer and confirmed that β_2AR and IR can form a functional heteromer. In a similar manner, See et al. [212] have profiled the 7TMR:7TMR heteromers i.e. CCR_2-CCR_5 and CCR_2-$CXCR_4$ heteromers, while Ayoub et al. [213] profiled the RTK:RTK heteromers i.e. EGFR and heregulin (HRG) receptor 3 heteromers.

The mechanisms by which arrestins are redistributed from the cytosol to plasma membrane, as well as the mechanisms of the 7TMRs:arrestins interaction have been focus of an intense research for more than twenty years [283]. 7TMR:arrestin binding appears to occur mostly in a 1:1 stoichiometry. In addition, arrestin could also bind two 7TMRs (1:2 stoichiometry). In such case a second 7TMR was proposed to loosely bind to the arrestin C-terminal domain when active receptors are abundant [283]. This transition from 1:1 to 1:2 stoichiometry was proposed for the rhodopsin/opsin:arrestin interaction [284]. Therefore, it is possible that arrestin binds to the β_2AR:IR heteromer.

Alternatively, heteromerization may affect trafficking to or from the plasma membrane. The ligand dependency of the interaction with βarr2 or Shc enabled the assessment that receptors have successfully trafficked to the plasma membrane and are sufficiently functional to bind agonist, in this case becoming phosphorylated and recruiting βarr2 or Shc. This selects against IR and β_2AR being clumped in the ER or degradative compartments due to incorrect or excessive expression, and supports our confocal microscopy results.

Using βarr2 1–185 mutant, we have confirmed that the previously proposed βarr2 interaction domain (amino acids 186–409) [121] with the IR is indeed essential for their interaction. It seems that the same domain is also essential for the constitutive and agonist-promoted βarr2 interaction with the β_2AR. Recent mutagenesis data from Ostermaier et al. [285] support our data; they reveal that in addition to the major interaction sites in the N-domain, mutations of the residues located at the edge and within the C-domain of arr1 strongly reduced binding of the arr1 to the rhodopsin receptor. This is consistent with reports which state that active receptor preferentially engages the arrestin C-domain [286] and that the "lariat loop" (residues 274–300) is implicated in aspects of β-arrestin activation and receptor interaction [287]; including Lys300 as one of the residues responsible for the binding of the phosphorylated receptor C-terminus [285]. In agreement, Hanson et al. [286] found that the interdomain contact surface is important for arrestin interaction with the non-preferred forms of the receptor and that residues in this region play a role in arrestin transition into its high affinity receptor binding state.

5.6 EFFECT OF IR COEXPRESSION ON β_2AR cAMP PRODUCTION

At the molecular level, the ability of insulin to counter regulate β_2ARs can be exerted through insulin-stimulated phosphorylation of β_2AR and its subsequent internalization [165-167]. In our study, coexpression of IR had no significant effect on β_2AR maximal cAMP production. However the potency of isoproterenol was significantly decreased in the β_2AR and IR expressing cells that were concomitantly treated with insulin. Another study demonstrated that insulin promoted phosphorylation of Tyr350/354 and Tyr364 in the C-terminal tail of β_2AR and that phosphorylation of Tyr350/354 attenuates β_2AR activation and cAMP

production in CHO cells [166]. Valiquette et al. [167] also showed that insulin promoted tyrosine phosphorylation of the β_2AR, although their work suggested that the phosphorylation occurred on Tyr141 and resulted in an enhanced ability to activate cAMP production in CHW cells. The reason for the striking differences between the studies is currently unknown, although it may reflect the usage of different cell types.

Receptor heteromers offer a serious of challenges in receptor signaling. For example, the D_1 dopamine receptor subtype is coupled to $G\alpha_s$ proteins, that is, to proteins that mediate increases in cAMP. In contrast, the D_2 subtype is coupled to $G\alpha_i$ proteins, which mediate decreases in cAMP. Interestingly D_1:D_2 receptor heteromers do not couple with $G\alpha_s$ or $G\alpha_i$ but with $G\alpha_q$, which trigger calcium mobilization [288]. In comparison, SSTR5 and β_2AR exert opposing effect in regulation of cAMP, however when coexpressed together and upon combined treatment, β_2AR has a prominent role in regulation of cAMP production [69].

The counter-regulatory effects of insulin and catecholamines on carbohydrate and lipid metabolism are well known, whereas the input of insulin regulation of β_2AR signaling pathway in heart was provided by Fu et al [171]. They have characterized a novel signaling pathway of IR to GRK2 in the heart. In their study, insulin stimulated recruitment of GRK2 to β_2AR, which induced β_2AR phosphorylation at the GRK sites of Ser355/356 and subsequently β_2AR internalization. Insulin thereby suppressed β_2AR-induced cAMP-PKA activities and contractile response in neonatal and adult mouse cardiomyocytes. Another study, demonstrated that β_2AR agonists *in vitro* can restore the downregulation of IR signaling in retinal Müller cells cultured under hyperglycemic conditions. By decreasing the levels of TNF-α and decreasing the phosphorylation of IRS-1Ser307, while increasing tyrosine phosphorylation of IR, their results suggested a possible mechanism by which restoration of β_2AR signaling may protect the retina against diabetes-induced damage [11].

Emerging evidence suggests that inflammation provides a link between obesity and insulin resistance. The noncanonical IκB kinases IKK-ε and TANK-binding kinase 1 are induced in liver and fat by NF-κB activation upon high-fat diet feeding. These kinases attenuate β-adrenergic signaling in white adipose tissue which preserves energy storage [289]. Reilly et al. [290] reported that amlexanox, an approved small-molecule therapeutic presently used in the clinic to treat aphthous ulcers and asthma, is an inhibitor of these kinases.

Treatment of obese mice with amlexanox elevated energy expenditure through increased thermogenesis, producing weight loss, improved insulin sensitivity and decreased steatosis. Because of its record of safety in patients, amlexanox may be an interesting candidate for clinical evaluation in the treatment of obesity and related disorders.

Since the early sixties, work on 7TMRs and on 7TMR-mediated signaling has led to a number of awards, the most recent being the Nobel Prize in Chemistry for 2012. The future of 7TMRs and RTKs research is surely based on their capacity for heteromerization. Recent studies have shown that signal transduction initiated by 7TMRs and RTKs is not organized in distinct signaling cassettes. In fact, signal integration and diversification arises from a complex network involving crosstalk between separate signaling units. A better understanding of the 7TMRs and RTKs crosstalk would reveal new insights into signaling modalities and would potentially open new opportunities for development of more specific therapeutics. In this regard, β_2AR:IR heteromers could potentially generate a basis for the design of new therapeutics that can compete with today's epidemics, such as type-2 diabetes mellitus, obesity and cardiovascular diseases.

6 CONCLUSIONS

1. β_2AR and IR displayed a similar distribution pattern with a high degree of colocalization.

2. IR coexpression had no effect on the ligand binding properties of β_2AR. However, IR reduced β_2AR surface expression, accelerated its internalization and reduced the potency of isoproterenol to activate cAMP production in cells concomitantly treated with insulin

3. BRET^2 data provided evidence for constitutive β_2AR and IR homo- and heteromerization.

4. Receptor affinity for β_2AR:IR heteromer formation is higher compared to receptor affinity for homomer formation in the case of higher-order heteromers, but not in the case of dimers. Therefore, β_2AR:IR oligomers are likely comprising heteromers of homodimers.

5. Bioinformatic data identified prospective interaction domains responsible for β_2AR and IR heteromerization. Importance of the IR β chain cytoplasmic part for the interaction with the β_2AR was experimentally confirmed.

6. βarr2 interacts with IR:β_2AR heteromer in a constitutive and ligand-dependent manner.

7. Interaction between IR and βarr2 is only constitutive and C-domain of the βarr2 is involved in this interaction.

7 SUMMARY

Receptor crosstalk between seven transmembrane receptors (7TMRs) and receptor tyrosine kinases (RTKs) has become an important field in receptor research. The determination of direct interaction and functional interplay between 7TMRs and RTKs is necessary for better understanding of heteromerization in pathological and physiological conditions, and could potentially open new opportunities for development of more specific therapeutics.

Glucose metabolism is under the cooperative regulation of both insulin receptor (IR) and β_2-adrenergic receptor (β_2AR). There are studies demonstrating crosstalk between these two receptors and their endogenous coexpression. Our main focus was to determine direct interaction and functional interplay between IR and β_2AR. Using radioligand binding assay we showed that IR coexpression had no effect on the ligand binding properties of β_2AR. Using confocal microscopy and ELISA assay we showed that i) both receptors displayed a similar distribution pattern in HEK-293 cells with a high degree of colocalization; ii) IR coexpression reduced β_2AR surface expression and accelerated its internalization

To test the possible direct interaction between β_2AR and IR, we employed quantitative bioluminescence resonance energy transfer 2 ($BRET^2$) saturation and competition assays. Saturation assay data suggested constitutive β_2AR and IR homo- and heteromerization. Calculated acceptor/donor (AD_{50}) values as a measure of the relative affinity for homo- and heteromer formation differed among the heteromers that could not be explained by a simple dimer model. In heterologous competition assays, a transient increase in the $BRET^2$ signal with a subsequent hyperbolical decrease was observed, suggesting higher-order heteromer formation.

To complement the $BRET^2$ data, we employed the informational spectrum method (ISM), a virtual spectroscopy method to investigate protein-protein interactions. Computational peptide scanning of β_2AR and IR identified intracellular domains encompassing residues at the end of the 7th TM domain as well as C-terminal tail of β_2AR and a cytoplasmic part of the IR β chain as prospective interaction domains. We have employed an IR mutant missing the proposed interaction domain in $BRET^2$ saturation and heteromer identification technology (HIT) assays with βarr2, and were able to confirm that the prospective interaction domain is actually requisite for the interaction with the β_2AR. ISM

also suggested a high probability of heteromer formation and homodimers as basic units engaged in heteromerization.

Using HIT, we have clearly demonstrated that isoproterenol induced and pindolol inhibited βarr2 recruitment to the β_2AR:IR heteromer. This is consistent with GFP^2-βarr2 being recruited to the untagged β_2AR in an agonist-dependent manner, and IR-RLuc8 being sufficiently proximal to the β_2AR to allow detectable energy transfer to the GFP^2-βarr2. We have also detected a constitutive interaction between IR and βarr2 and demonstrated that βarr2 C-domain is involved in this interaction.

Coexpression of IR had no significant effect on β_2AR maximal Cyclic adenosine monophosphate cAMP production. However, the potency of isoproterenol was significantly decreased in the β_2AR and IR expressing cells concomitantly treated with insulin, which is in consistent with our results that demonstrate that IR reduces β_2AR surface expression and accelerates its internalization.

8 POVZETEK

Proučevanje medsebojnega vpliva oz. sporazumevanja med predstavniki receptorja s sedmimi transmembranskimi območji (7TMR) in receptorja s tirozin-kinazno aktivnostjo (RTK) postaja ena od osrednjih tem na področju receptorske biologije. Ugotavljanje neposredne interakcije in funkcionalne soodvisnosti med različnimi razredi signalnih membranskih receptorjev je nujno za razumevanje pomena heteromerizacije v fizioloških in patoloških stanjih in odpira nove možnosti za razvoj terapevtskih sredstev za heteromerne receptorske tarče.

Pri uravnavanju presnove glukoze sodelujeta β_2-adrenergični (β_2AR) in inzulinski receptorj (IR). Predhodne študije kažejo na medsebojno soodvisnost med IR in β_2AR, njuno endogeno soizražanje v različnih tkivih v organizmu pa je predpogoj za morebitno neposredno interakcijo. V doktorskem delu smo se osredotočili predvsem na proučitev obstoja neposredne interakcije in funkcionalne soodvisnosti med IR in β_2AR in s tem namenom preverjali te hipoteze: i) β_2AR oblikuje konstitutivne heteromere z IR; ii) afiniteta receptorjev za oblikovanje heteromerov β_2AR:IR je višja v primerjavi s homomeri; iii) heteromer β_2AR:IR oblikuje konstitutivne in z agonistom spodbujene interakcije z βarr2; iv) interakcija med IR in βar2 je konstitutivna in v) heteromer β_2AR:IR ima značilen farmakološki fenotip.

S testi vezave radioaktivno označenega liganda smo v prvem delu naloge potrdili funkcionalno neokrnjenost fuzijskih konstruktov β_2AR in proučili vpliv soizražanja IR na vezavne lastnosti β_2AR. Na ravni konfokalne mikroskopije ter s testi ELISA in internalizacije smo spremljali celično lokalizacijo in morebitno kolokalizacijo med β_2AR in IR ter raven površinsko izraženih β_2AR in njihovo hitrost internalizacije. Pokazali smo, da je: i) razporeditev obeh receptorjev v celicah HEK-293 podobna in da imata visoko stopnjo kolokalizacije; ii) da soizražanje IR zmanjša število površinsko izraženih β_2AR in pospeši njihovo hitrost internalizacije in iii) da soizražanje IR nima značilnega vpliva na vezavne lastnosti proučevanih β_2AR za ligande.

Da bi dokazali morebitno neposredno interakcijo med β_2AR in IR, smo uporabili kvantitativne teste $BRET^2$ (resonančni prenos energije z bioluminiscenco), in sicer test zasičenja in kompeticije. S testi zasičenja smo pridobili dokaze za obstoj konstitutivnih homo- in heteromerov. Izračunano razmerje akceptor/donor (A/C_{50}), ki da 50 % maksimalne vrednosti signala $BRET^2$ ter je merilo za relativno afiniteto med akceptorjem in donorjem, je

bilo različno med heteromeri, kar ni mogoče pojasniti s preprostim modelom za dimere. V heterolognem testu kompeticije smo opazili prehodno povišanje signala $BRET^2$, ki mu je sledilo naknadno hiperbolično zmanjšanje signala. Na podlagi teh rezultatov smo predvideli oblikovanje heteromerov višjega reda oz. heterooligomernih kompleksov. Za pridobitev dodatnih dokazov, ki bi potrdili oz. ovrgli oblikovanje heterooligomernih kompleksov, smo uporabili virtualno spektroskopsko metodo informativnega spektra (angl. informational spectrum method (ISM)) za proučevanje proteinsko-proteinskih interakcij. Z računalniško analizo aminokislinskih zaporedij β_2AR in IR smo najprej identificirali znotrajcelični območji na koncu sedmega transmembranskega območja (7TM) in karboksilnega (C)-terminalnega repka β_2AR (aminokislinski ostanki 324–357) in v citoplazemskem delu verige β IR (aminokislinski ostanki 1269–1314) kot morebitni interakcijski domeni ter izračunali afiniteto za interakcije med homo- in heteromeri β_2AR in IR. Slednja predvideva veliko verjetnost nastanka heteromerov iz homodimerov, saj na ravni dimerizacije β_2AR in IR kažeta večjo nagnjenost k homodimerizaciji kot k heterodimerizaciji. Pomen predvidenega interakcijskega območja znotraj IR za heteromerizacijo z β_2AR smo potrdili tudi eksperimentalno. S testoma zasičenja in HIT smo potrdili, da je predvidena domena IR dejansko vključena v heteromerizacijo z β_2AR.

Dodatne dokaze za heteromerizacijo in funkcionalno soodvisnost med β_2AR in IR smo pridobili s testom HIT in testom aktivacije sekundarnega sporočilnega sistema, s katerim smo spremljali znotrajcelično kopičenje cAMP. Tudi rezultati HIT so potrdili heteromerizacijo med β_2AR:IR, saj je agonist β_2AR izoproterenol spodbudil interakcijo med GFP^2-βar2 in heteromerom β_2AR:IR-RLuc8, medtem ko je antagonist β_2AR pindolol preprečil z agonistom spodbujeno interakcijo. To potrjuje, da je z agonistom spodbujena interakcija med βarr2 in IR-RLuc8 pogojena z aktivacijo β_2AR ter da sta neoznačeni β_2AR in IR-RLuc8 v kompleksu na medsebojni razdalji, ki omogoča zaznaven resonančni prenos energije (< 10 nm). Rezultati BRET tudi nedvoumno potrjujejo konstitutivno interakcijo med IR in βar2. Z odstranitvijo C-območja βar2 (mutanta βar2 1–185) smo potrdili, da je to območje nujno za konstitutivno interakcijo med IR in βar2, poleg tega pa je pomembno tudi za konstitutivno ter z agonistom spodbujeno interakcijo med β_2AR in βar2.

S spremljanjem znotrajceličnega kopičenja cikličnega adenozin monofosfata (cAMP) smo ugotovili, da soizražanje IR ni imelo značilnega učinka na maksimalno proizvodnjo

znotrajceličnega cAMP, spodbujeno z aktivacijo β_2AR z izoproterenolom. V celicah, ki so soizražale β_2AR in IR ter so bile sočasno izpostavljene izoproterenolu in inzulinu, smo ugotovili značilno nižjo potenco izoproterenola za kopičenje cAMP.

Če povzamemo, pridobljeni rezultati nudijo dokaze za: i) direktno interakcijo med β_2AR in IR; ii) oblikovanje receptorskih heterooligomerov iz dimernih homodimernih enot; iii) vlogo znotrajceličnih področij v procesu heteromerizacije; iv) zmožnost konstitutivne interakcije med IR in βar2 in v) nakazujejo značilen signalni fenotip heteromera β_2AR:IR.

9 ACKNOWLEDGEMENTS

I would like to thank to:

- Basileus secretariat for awarding me with a PhD grant which started this whole process.
- Mentor prof. dr. Milka Vrecl for scientific contribution, assistance and advice.
- Comentor dr. Jane Nohr for scientific assistance and reviews.
- Luka Drinovec, Sanja Glišić, Nevena Veljković and Christina Pedersen for their scientific contribution.
- Magdalena Dobravec, Marko Cotman, Jasna Špoljar, Neža Gregurević for their professionalism and assistance in the laboratory.
- Asis. dr. Blanka Premov Bajuk and Katarina Babnik for the assistance with laboratory measurements.
- Prof. dr. Robert Frangež for assistance with confocal microscopy.
- Doc. dr.Valentina Kubale Dvojmoč for advice, guidance and being a great friend.
- Former head of the Institute of Anatomy, Hystology and Embriology prof. dr. Azra Pogačnik, prof. dr. Jelka Zabavnik Piano, asis. Jana Branković and all the employers at the Institute of Anatomy, Hystology and Embriology and at the Institute for Physiology, Pharmacology and Toxicology, Veterinary faculty, University of Ljubljana for all of their help.
- Lectors: Jelena Pataki and Nina Novak Kerbler.
- Mateja Stvarnik for administrative assistance, patience and answering all of my questions.
- Brigita Grecs Smole for the review of literature.
- My beloved Klemen Sušec for all of the computer software and assistance with it.

- Members of the commission board for the evaluation of the doctoral dissertation doc. dr. Mojca Benčina, prof. dr. Matjaž Zorko and the president of the commission board prof. dr. Robert Frangež for the review of the doctoral dissertation and a valuable input.

- Slovenian Research Agency (program P4-0053) and European COST Action CM1207 (GLISTEN) for financial support.

I would also want to thank my parents, my grandmother and the rest of my family for their endless love and encouragment. All the support and care they have provided me over the years was the greatest gift. My dear Klemen, Martina and Mateja, thank you for your understanding and love.

10 LITERATURE

1. Kroeze WK, Sheffler DJ and Roth BL. G-protein-coupled receptors at a glance. J Cell Sci 2003; 116(Pt 24): 4867–9.
2. Lattin J et al. G-protein-coupled receptor expression, function, and signaling in macrophages. J Leukoc Biol 2007; 82(1): 16–32.
3. Schlessinger J. Cell signaling by receptor tyrosine kinases. Cell 2000; 103(2): 211–25.
4. Barnes PJ. Receptor heterodimerization: a new level of cross-talk. J Clin Invest 2006; 116(5): 1210–2.
5. Pyne NJ and Pyne S. Receptor tyrosine kinase-G-protein-coupled receptor signalling platforms: out of the shadow? Trends Pharmacol Sci 2011; 32(8): 443–50.
6. Baltensperger K et al. The beta-adrenergic receptor is a substrate for the insulin receptor tyrosine kinase. J Biol Chem 1996; 271(2): 1061–4.
7. Wang H, Doronin S and Malbon CC. Insulin activation of mitogen-activated protein kinases Erk1,2 is amplified via beta-adrenergic receptor expression and requires the integrity of the Tyr350 of the receptor. J Biol Chem 2000; 275(46): 36086–93.
8. Lange LA et al. Association of adipose tissue deposition and beta-2 adrenergic receptor variants: the IRAS family study. Int J Obes (Lond) 2005; 29(5): 449–57.
9. Liggett SB, Shah SD and Cryer PE. Characterization of beta-adrenergic receptors of human skeletal muscle obtained by needle biopsy. Am J Physiol 1988; 254(6 Pt 1): E795–8.
10. Heni M et al. Insulin promotes glycogen storage and cell proliferation in primary human astrocytes. PLoS One 2011; 6(6): e21594 (8 pp.). http://journals.plos.org/plosone/article?id=10.1371/journal.pone.0021594 (July 7, 2014)
11. Walker RJ et al. Role of beta-adrenergic receptor regulation of TNF-alpha and insulin signaling in retinal Muller cells. Invest Ophthalmol Vis Sci 2011; 52(13): 9527–33.
12. Layden BT, Durai, V. & Lowe, Jr., WL. G-Protein-Coupled Receptors, Pancreatic Islets, and Diabetes. Nature Education 2010; 3(9): 13.
13. Kang DS, Tian X and Benovic JL. Role of beta-arrestins and arrestin domain-containing proteins in G protein-coupled receptor trafficking. Curr Opin Cell Biol 2014; 27: 63–71.
14. Ma L and Pei G. Beta-arrestin signaling and regulation of transcription. J Cell Sci 2007; 120(Pt 2): 213–8.
15. Defea K. Beta-arrestins and heterotrimeric G-proteins: collaborators and competitors in signal transduction. Br J Pharmacol 2008; 153 (Suppl 1): S298–309.
16. Luttrell LM et al. Beta-arrestin-dependent formation of beta2 adrenergic receptor-Src protein kinase complexes. Science 1999; 283(5402): 655–61.
17. Luan B et al. Deficiency of a beta-arrestin-2 signal complex contributes to insulin resistance. Nature 2009; 457(7233): 1146–9.
18. Lefkowitz RJ. Historical review: a brief history and personal retrospective of seven-transmembrane receptors. Trends Pharmacol Sci 2004; 25(8): 413–22.
19. Lefkowitz RJ and Shenoy SK. Transduction of receptor signals by beta-arrestins. Science 2005; 308(5721): 512–7.
20. Luttrell LM and Lefkowitz RJ. The role of beta-arrestins in the termination and transduction of G-protein-coupled receptor signals. J Cell Sci 2002; 115(Pt 3): 455–65.

21. Azzi M et al. Beta-arrestin-mediated activation of MAPK by inverse agonists reveals distinct active conformations for G protein-coupled receptors. Proc Natl Acad Sci U S A 2003; 100(20): 11406–11.
22. Kobilka BK. G protein coupled receptor structure and activation. Biochim Biophys Acta 2007; 1768(4): 794–807.
23. Katritch V, Cherezov V and Stevens RC. Structure-function of the G protein-coupled receptor superfamily. Annu Rev Pharmacol Toxicol 2013; 53: 531–56.
24. Joost P and Methner A. Phylogenetic analysis of 277 human G-protein-coupled receptors as a tool for the prediction of orphan receptor ligands. Genome Biol 2002; 3(11): research 0063.1–16. http://www.ncbi.nlm.nih.gov/pmc/articles/PMC133447/ (January 23, 2014)
25. Schioth HB and Fredriksson R. The GRAFS classification system of G-protein coupled receptors in comparative perspective. Gen Comp Endocrinol 2005; 142(1-2): 94–101.
26. Latek D et al. G protein-coupled receptors--recent advances. Acta Biochim Pol 2012; 59(4): 515–29.
27. Venkatakrishnan AJ et al. Molecular signatures of G-protein-coupled receptors. Nature 2013; 494(7436): 185–94.
28. Hollenstein K et al. Insights into the structure of class B GPCRs. Trends Pharmacol Sci 2014; 35(1): 12–22.
29. Tuteja N. Signaling through G protein coupled receptors. Plant Signal Behav 2009; 4(10): 942–7.
30. Gether U. Uncovering molecular mechanisms involved in activation of G protein-coupled receptors. Endocr Rev 2000; 21(1): 90–113.
31. Oldham WM and Hamm HE. Heterotrimeric G protein activation by G-protein-coupled receptors. Nat Rev Mol Cell Biol 2008; 9(1): 60–71.
32. McCudden CR et al. G-protein signaling: back to the future. Cell Mol Life Sci 2005; 62(5): 551–77.
33. Marinissen MJ and Gutkind JS. G-protein-coupled receptors and signaling networks: emerging paradigms. Trends Pharmacol Sci 2001; 22(7): 368–76.
34. DeWire SM et al. Beta-arrestins and cell signaling. Annu Rev Physiol 2007; 69: 483–510.
35. Wei H et al. Independent beta-arrestin 2 and G protein-mediated pathways for angiotensin II activation of extracellular signal-regulated kinases 1 and 2. Proc Natl Acad Sci U S A 2003; 100(19): 10782–7.
36. Violin JD and Lefkowitz RJ. Beta-arrestin-biased ligands at seven-transmembrane receptors. Trends Pharmacol Sci 2007; 28(8): 416–22.
37. Strosberg AD. Structure, function, and regulation of adrenergic receptors. Protein Sci 1993; 2(8): 1198–209.
38. Ahrens RC. Skeletal muscle tremor and the influence of adrenergic drugs. J Asthma 1990; 27(1): 11–20.
39. Dzimiri N. Regulation of beta-adrenoceptor signaling in cardiac function and disease. Pharmacol Rev 1999; 51(3): 465–501.
40. DeWire SM and Violin JD. Biased ligands for better cardiovascular drugs: dissecting G-protein-coupled receptor pharmacology. Circ Res 2011; 109(2): 205–16.
41. Brueckner F et al. Structure of beta-adrenergic receptors. Methods Enzymol 2013; 520: 117–51.
42. Rasmussen SG et al. Crystal structure of the human beta2 adrenergic G-protein-coupled receptor. Nature 2007; 450(7168): 383–7.

43. Cherezov V et al. High-resolution crystal structure of an engineered human beta2-adrenergic G protein-coupled receptor. Science 2007; 318(5854): 1258–65.
44. Rosenbaum DM et al. GPCR engineering yields high-resolution structural insights into beta2-adrenergic receptor function. Science 2007; 318(5854): 1266–73.
45. Ross EM et al. Relationship between the beta-adrenergic receptor and adenylate cyclase. J Biol Chem 1977; 252(16): 5761–75.
46. De Lean A, Stadel JM and Lefkowitz RJ. A ternary complex model explains the agonist-specific binding properties of the adenylate cyclase-coupled beta-adrenergic receptor. J Biol Chem 1980; 255(15): 7108–17.
47. Rasmussen SG et al. Crystal structure of the beta2 adrenergic receptor-Gs protein complex. Nature 2011; 477(7366): 549–55.
48. van der Heyden MA, Wijnhoven TJ and Opthof T. Molecular aspects of adrenergic modulation of cardiac L-type Ca2+ channels. Cardiovasc Res 2005; 65(1): 28–39.
49. Chen-Izu Y et al. G(i)-dependent localization of beta(2)-adrenergic receptor signaling to L-type Ca(2+) channels. Biophys J 2000; 79(5): 2547–56.
50. Jockers R et al. Beta(2)-adrenergic receptor down-regulation. Evidence for a pathway that does not require endocytosis. J Biol Chem 1999; 274(41): 28900–8.
51. Hausdorff WP, Caron MG and Lefkowitz RJ. Turning off the signal: desensitization of beta-adrenergic receptor function. FASEB J 1990; 4(11): 2881–9.
52. Yu SS, Lefkowitz RJ and Hausdorff WP. Beta-adrenergic receptor sequestration. A potential mechanism of receptor resensitization. J Biol Chem 1993; 268(1): 337–41.
53. Drake MT, Shenoy SK and Lefkowitz RJ. Trafficking of G protein-coupled receptors. Circ Res 2006; 99(6): 570–82.
54. Goodman OB, Jr. et al. Beta-arrestin acts as a clathrin adaptor in endocytosis of the beta2-adrenergic receptor. Nature 1996; 383(6599): 447–50.
55. Bohm SK, Grady EF and Bunnett NW. Regulatory mechanisms that modulate signalling by G-protein-coupled receptors. Biochem J 1997; 322 (Pt 1): 1–18.
56. Scarselli M and Donaldson JG. Constitutive internalization of G protein-coupled receptors and G proteins via clathrin-independent endocytosis. J Biol Chem 2009; 284(6): 3577–85.
57. Chini B and Parenti M. G-protein coupled receptors in lipid rafts and caveolae: how, when and why do they go there? J Mol Endocrinol 2004; 32(2): 325–38.
58. Xiang Y et al. Caveolar localization dictates physiologic signaling of beta 2-adrenoceptors in neonatal cardiac myocytes. J Biol Chem 2002; 277(37): 34280–6.
59. Ferre S et al. G protein-coupled receptor oligomerization revisited: functional and pharmacological perspectives. Pharmacol Rev 2014; 66(2): 413–34.
60. Hebert TE et al. A peptide derived from a beta2-adrenergic receptor transmembrane domain inhibits both receptor dimerization and activation. J Biol Chem 1996; 271(27): 16384–92.
61. Angers S et al. Detection of beta 2-adrenergic receptor dimerization in living cells using bioluminescence resonance energy transfer (BRET). Proc Natl Acad Sci U S A 2000; 97(7): 3684–9.
62. Salahpour A et al. Homodimerization of the beta2-adrenergic receptor as a prerequisite for cell surface targeting. J Biol Chem 2004; 279(32): 33390–7.
63. Fung JJ et al. Ligand-regulated oligomerization of beta(2)-adrenoceptors in a model lipid bilayer. EMBO J 2009; 28(21): 3315–28.
64. Lavoie C et al. Beta 1/beta 2-adrenergic receptor heterodimerization regulates beta 2-adrenergic receptor internalization and ERK signaling efficacy. J Biol Chem 2002; 277(38): 35402–10.

65. Breit A, Lagace M and Bouvier M. Hetero-oligomerization between beta2- and beta3-adrenergic receptors generates a beta-adrenergic signaling unit with distinct functional properties. J Biol Chem 2004; 279(27): 28756–65.
66. Uberti MA, Hall RA and Minneman KP. Subtype-specific dimerization of alpha 1-adrenoceptors: effects on receptor expression and pharmacological properties. Mol Pharmacol 2003; 64(6): 1379–90.
67. Uberti MA et al. Heterodimerization with beta2-adrenergic receptors promotes surface expression and functional activity of alpha1D-adrenergic receptors. J Pharmacol Exp Ther 2005; 313(1): 16–23.
68. Jordan BA et al. Oligomerization of opioid receptors with beta 2-adrenergic receptors: a role in trafficking and mitogen-activated protein kinase activation. Proc Natl Acad Sci U S A 2001; 98(1): 343–8.
69. Somvanshi RK et al. Heterodimerization of beta2 adrenergic receptor and somatostatin receptor 5: Implications in modulation of signaling pathway. J Mol Signal 2011; 6: 9.
70. Barki-Harrington L, Luttrell LM and Rockman HA. Dual inhibition of beta-adrenergic and angiotensin II receptors by a single antagonist: a functional role for receptor-receptor interaction in vivo. Circulation 2003; 108(13): 1611–8.
71. Haack KK et al. A novel bioassay for detecting GPCR heterodimerization: transactivation of beta 2 adrenergic receptor by bradykinin receptor. J Biomol Screen 2010; 15(3): 251–60.
72. McGraw DW et al. Airway smooth muscle prostaglandin-EP1 receptors directly modulate beta2-adrenergic receptors within a unique heterodimeric complex. J Clin Invest 2006; 116(5): 1400–9.
73. Hague C et al. Olfactory receptor surface expression is driven by association with the beta2-adrenergic receptor. Proc Natl Acad Sci U S A 2004; 101(37): 13672–6.
74. Berthouze M et al. Constitutive dimerization of human serotonin 5-HT4 receptors in living cells. FEBS Lett 2005; 579(14): 2973–80.
75. Vrecl M et al. Opsin oligomerization in a heterologous cell system. J Recept Signal Transduct Res 2006; 26(5-6): 505–26.
76. LaRocca TJ et al. beta2-Adrenergic receptor signaling in the cardiac myocyte is modulated by interactions with CXCR4. J Cardiovasc Pharmacol 2010; 56(5): 548–59.
77. Hudson BD, Hebert TE and Kelly ME. Ligand- and heterodimer-directed signaling of the CB(1) cannabinoid receptor. Mol Pharmacol 2010; 77(1): 1–9.
78. Kuravi S et al. Third-party bioluminescence resonance energy transfer indicates constitutive association of membrane proteins: application to class a g-protein-coupled receptors and g-proteins. Biophys J 2010; 98(10): 2391–9.
79. Wrzal PK et al. Allosteric interactions between the oxytocin receptor and the beta2-adrenergic receptor in the modulation of ERK1/2 activation are mediated by heterodimerization. Cell Signal 2012; 24(1): 342–50.
80. Maudsley S et al. The beta(2)-adrenergic receptor mediates extracellular signal-regulated kinase activation via assembly of a multi-receptor complex with the epidermal growth factor receptor. J Biol Chem 2000; 275(13): 9572–80.
81. Joiner ML et al. Assembly of a beta2-adrenergic receptor--GluR1 signalling complex for localized cAMP signalling. EMBO J 2010; 29(2): 482–95.
82. Blume-Jensen P and Hunter T. Oncogenic kinase signalling. Nature 2001; 411(6835): 355–65.
83. Ullrich A and Schlessinger J. Signal transduction by receptors with tyrosine kinase activity. Cell 1990; 61(2): 203–12.
84. Cadena DL and Gill GN. Receptor tyrosine kinases. FASEB J 1992; 6(6): 2332-7.

85. Hubbard SR. Structural analysis of receptor tyrosine kinases. Prog Biophys Mol Biol 1999; 71(3-4): 343–58.
86. Hubbard SR and Till JH. Protein tyrosine kinase structure and function. Annu Rev Biochem 2000; 69: 373–98.
87. Lemmon MA and Schlessinger J. Cell signaling by receptor tyrosine kinases. Cell 2010; 141(7): 1117–34.
88. Ward CW and Lawrence MC. Ligand-induced activation of the insulin receptor: a multi-step process involving structural changes in both the ligand and the receptor. Bioessays 2009; 31(4): 422–34.
89. Wilcox G. Insulin and insulin resistance. Clin Biochem Rev 2005; 26(2): 19–39.
90. Seino S et al. Structure of the human insulin receptor gene and characterization of its promoter. Proc Natl Acad Sci U S A 1989; 86(1): 114–8.
91. Belfiore A et al. Insulin receptor isoforms and insulin receptor/insulin-like growth factor receptor hybrids in physiology and disease. Endocr Rev 2009; 30(6): 586–623.
92. Smith BJ et al. Structural resolution of a tandem hormone-binding element in the insulin receptor and its implications for design of peptide agonists. Proc Natl Acad Sci U S A 2010; 107(15): 6771–6.
93. McKern NM et al. Structure of the insulin receptor ectodomain reveals a folded-over conformation. Nature 2006; 443(7108): 218–21.
94. Van Obberghen E et al. Surfing the insulin signaling web. Eur J Clin Invest 2001; 31(11): 966–77.
95. Saltiel AR and Kahn CR. Insulin signalling and the regulation of glucose and lipid metabolism. Nature 2001; 414(6865): 799–806.
96. Lizcano JM and Alessi DR. The insulin signalling pathway. Curr Biol 2002; 12(7): R236–8.
97. Ogawa W, Matozaki T and Kasuga M. Role of binding proteins to IRS-1 in insulin signalling. Mol Cell Biochem 1998; 182(1-2): 13–22.
98. Pearson G et al. Mitogen-activated protein (MAP) kinase pathways: regulation and physiological functions. Endocr Rev 2001; 22(2): 153–83.
99. Wolf G et al. PTB domains of IRS-1 and Shc have distinct but overlapping binding specificities. J Biol Chem 1995; 270(46): 27407–10.
100. Carpentier JL et al. Insulin-induced surface redistribution regulates internalization of the insulin receptor and requires its autophosphorylation. Proc Natl Acad Sci U S A 1992; 89(1): 162–6.
101. Carpentier JL et al. Two steps of insulin receptor internalization depend on different domains of the beta-subunit. J Cell Biol 1993; 122(6): 1243–52.
102. Fan JY et al. Receptor-mediated endocytosis of insulin: role of microvilli, coated pits, and coated vesicles. Proc Natl Acad Sci U S A 1982; 79(24): 7788–91.
103. Paccaud JP, Siddle K and Carpentier JL. Internalization of the human insulin receptor. The insulin-independent pathway. J Biol Chem 1992; 267(18): 13101–6.
104. Smith RM and Jarett L. Differences in adenosine triphosphate dependency of receptor-mediated endocytosis of alpha 2-macroglobulin and insulin correlate with separate routes of ligand-receptor complex internalization. Endocrinology 1990; 126(3): 1551–60.
105. Fagerholm S et al. Rapid insulin-dependent endocytosis of the insulin receptor by caveolae in primary adipocytes. PLoS One 2009; 4(6): e5985 (10 pp.). http://www.ncbi.nlm.nih.gov/pmc/articles/PMC2695004/ (March 24, 2014)
106. McClain DA. Mechanism and role of insulin receptor endocytosis. Am J Med Sci 1992; 304(3): 192–201.

107. Sorkin A and Von Zastrow M. Signal transduction and endocytosis: close encounters of many kinds. Nat Rev Mol Cell Biol 2002; 3(8): 600–14.
108. Bevan AP et al. Selective activation of the rat hepatic endosomal insulin receptor kinase. Role for the endosome in insulin signaling. J Biol Chem 1995; 270(18): 10784–91.
109. Wang B, Balba Y and Knutson VP. Insulin-induced in situ phosphorylation of the insulin receptor located in the plasma membrane versus endosomes. Biochem Biophys Res Commun 1996; 227(1): 27–34.
110. Bevan AP et al. Chloroquine extends the lifetime of the activated insulin receptor complex in endosomes. J Biol Chem 1997; 272(43): 26833–40.
111. Di Guglielmo GM et al. Insulin receptor internalization and signalling. Mol Cell Biochem 1998; 182(1-2): 59–63.
112. Hamer I et al. An arginine to cysteine(252) mutation in insulin receptors from a patient with severe insulin resistance inhibits receptor internalisation but preserves signalling events. Diabetologia 2002; 45(5): 657–67.
113. Ceresa BP et al. Inhibition of clathrin-mediated endocytosis selectively attenuates specific insulin receptor signal transduction pathways. Mol Cell Biol 1998; 18(7): 3862–70.
114. Aubry L, Guetta D and Klein G. The arrestin fold: variations on a theme. Curr Genomics 2009; 10(2): 133–42.
115. Lin CH et al. Arrestin-related ubiquitin-ligase adaptors regulate endocytosis and protein turnover at the cell surface. Cell 2008; 135(4): 714–25.
116. Shi H et al. The retromer subunit Vps26 has an arrestin fold and binds Vps35 through its C-terminal domain. Nat Struct Mol Biol 2006; 13(6): 540–8.
117. Collins BM et al. Structure of Vps26B and mapping of its interaction with the retromer protein complex. Traffic 2008; 9(3): 366–79.
118. Aubry L and Klein G. True arrestins and arrestin-fold proteins: a structure-based appraisal. Prog Mol Biol Transl Sci 2013; 118: 21–56.
119. Gurevich VV and Gurevich EV. The structural basis of arrestin-mediated regulation of G-protein-coupled receptors. Pharmacol Ther 2006; 110(3): 465–502.
120. Kingsmore SF et al. Genetic mapping of the beta-arrestin 1 and 2 genes on mouse chromosomes 7 and 11 respectively. Mamm Genome 1995; 6(4): 306–7.
121. Feng X et al. beta-Arrestins: multifunctional signaling adaptors in type 2 diabetes. Mol Biol Rep 2011; 38(4): 2517–28.
122. Gurevich VV et al. Arrestin interactions with G protein-coupled receptors. Direct binding studies of wild type and mutant arrestins with rhodopsin, beta 2-adrenergic, and m2 muscarinic cholinergic receptors. J Biol Chem 1995; 270(2): 720–31.
123. Oakley RH et al. Differential affinities of visual arrestin, beta arrestin1, and beta arrestin2 for G protein-coupled receptors delineate two major classes of receptors. J Biol Chem 2000; 275(22): 17201–10.
124. Laporte SA et al. The beta2-adrenergic receptor/betaarrestin complex recruits the clathrin adaptor AP-2 during endocytosis. Proc Natl Acad Sci U S A 1999; 96(7): 3712–7.
125. Hausdorff WP et al. A small region of the beta-adrenergic receptor is selectively involved in its rapid regulation. Proc Natl Acad Sci U S A 1991; 88(8): 2979–83.
126. Ferguson SS et al. Role of beta-arrestin in mediating agonist-promoted G protein-coupled receptor internalization. Science 1996; 271(5247): 363–6.

127. Krupnick JG et al. Modulation of the arrestin-clathrin interaction in cells. Characterization of beta-arrestin dominant-negative mutants. J Biol Chem 1997; 272(51): 32507–12.
128. Vrecl M et al. Development of a BRET2 screening assay using beta-arrestin 2 mutants. J Biomol Screen 2004; 9(4): 322–33.
129. Pierce KL and Lefkowitz RJ. Classical and new roles of beta-arrestins in the regulation of G-protein-coupled receptors. Nat Rev Neurosci 2001; 2(10): 727–33.
130. Wisler JW et al. A unique mechanism of beta-blocker action: carvedilol stimulates beta-arrestin signaling. Proc Natl Acad Sci U S A 2007; 104(42): 16657–62.
131. Shenoy SK et al. beta-arrestin-dependent, G protein-independent ERK1/2 activation by the beta2 adrenergic receptor. J Biol Chem 2006; 281(2): 1261–73.
132. Kim IM et al. Beta-blockers alprenolol and carvedilol stimulate beta-arrestin-mediated EGFR transactivation. Proc Natl Acad Sci U S A 2008; 105(38): 14555–60.
133. Zhande R et al. Molecular mechanism of insulin-induced degradation of insulin receptor substrate 1. Mol Cell Biol 2002; 22(4): 1016–26.
134. Ravichandran KS. Signaling via Shc family adapter proteins. Oncogene 2001; 20(44): 6322–30.
135. Pelicci G et al. A novel transforming protein (SHC) with an SH2 domain is implicated in mitogenic signal transduction. Cell 1992; 70(1): 93–104.
136. Sasaoka T and Kobayashi M. The functional significance of Shc in insulin signaling as a substrate of the insulin receptor. Endocr J 2000; 47(4): 373–81.
137. Daaka Y et al. Essential role for G protein-coupled receptor endocytosis in the activation of mitogen-activated protein kinase. J Biol Chem 1998; 273(2): 685–8.
138. Natarajan K and Berk BC. Crosstalk coregulation mechanisms of G protein-coupled receptors and receptor tyrosine kinases. Methods Mol Biol 2006; 332: 51–77.
139. Marty C and Ye RD. Heterotrimeric G protein signaling outside the realm of seven transmembrane domain receptors. Mol Pharmacol 2010; 78(1): 12–8.
140. Daub H et al. Role of transactivation of the EGF receptor in signalling by G-protein-coupled receptors. Nature 1996; 379(6565): 557–60.
141. Prenzel N et al. EGF receptor transactivation by G-protein-coupled receptors requires metalloproteinase cleavage of proHB-EGF. Nature 1999; 402(6764): 884–8.
142. Wang C et al. Dopamine D2 receptor stimulation of mitogen-activated protein kinases mediated by cell type-dependent transactivation of receptor tyrosine kinases. J Neurochem 2005; 93(4): 899–909.
143. Flajolet M et al. FGF acts as a co-transmitter through adenosine A(2A) receptor to regulate synaptic plasticity. Nat Neurosci 2008; 11(12): 1402–9.
144. Heyworth CM et al. The action of islet activating protein (pertussis toxin) on insulin's ability to inhibit adenylate cyclase and activate cyclic AMP phosphodiesterases in hepatocytes. Biochem J 1986; 235(1): 145–9.
145. Rothenberg PL and Kahn CR. Insulin inhibits pertussis toxin-catalyzed ADP-ribosylation of G-proteins. Evidence for a novel interaction between insulin receptors and G-proteins. J Biol Chem 1988; 263(30): 15546–52.
146. Luttrell L et al. A pertussis toxin-sensitive G-protein mediates some aspects of insulin action in BC3H-1 murine myocytes. J Biol Chem 1990; 265(28): 16873–9.
147. Luttrell LM et al. G beta gamma subunits mediate mitogen-activated protein kinase activation by the tyrosine kinase insulin-like growth factor 1 receptor. J Biol Chem 1995; 270(28): 16495–8.

148. Waters C et al. Sphingosine 1-phosphate and platelet-derived growth factor (PDGF) act via PDGF beta receptor-sphingosine 1-phosphate receptor complexes in airway smooth muscle cells. J Biol Chem 2003; 278(8): 6282–90.
149. Long JS et al. The functional PDGFbeta receptor-S1P1 receptor signaling complex is involved in regulating migration of mouse embryonic fibroblasts in response to platelet derived growth factor. Prostaglandins Other Lipid Mediat 2006; 80(1-2): 74–80.
150. Alderton F et al. Tethering of the platelet-derived growth factor beta receptor to G-protein-coupled receptors. A novel platform for integrative signaling by these receptor classes in mammalian cells. J Biol Chem 2001; 276(30): 28578–85.
151. Waters CM et al. c-Src is involved in regulating signal transmission from PDGFbeta receptor-GPCR(s) complexes in mammalian cells. Cell Signal 2005; 17(2): 263–77.
152. Waters CM et al. Cell migration activated by platelet-derived growth factor receptor is blocked by an inverse agonist of the sphingosine 1-phosphate receptor-1. FASEB J 2006; 20(3): 509–11.
153. Parrill AL et al. Identification of Edg1 receptor residues that recognize sphingosine 1-phosphate. J Biol Chem 2000; 275(50): 39379–84.
154. Akekawatchai C et al. Transactivation of CXCR4 by the insulin-like growth factor-1 receptor (IGF-1R) in human MDA-MB-231 breast cancer epithelial cells. J Biol Chem 2005; 280(48): 39701–8.
155. Delcourt N et al. PACAP type I receptor transactivation is essential for IGF-1 receptor signalling and antiapoptotic activity in neurons. EMBO J 2007; 26(6): 1542–51.
156. Bergelin N et al. S1P1 and VEGFR-2 form a signaling complex with extracellularly regulated kinase 1/2 and protein kinase C-alpha regulating ML-1 thyroid carcinoma cell migration. Endocrinology 2010; 151(7): 2994–3005.
157. Moughal NA et al. Nerve growth factor signaling involves interaction between the Trk A receptor and lysophosphatidate receptor 1 systems: nuclear translocation of the lysophosphatidate receptor 1 and Trk A receptors in pheochromocytoma 12 cells. Cell Signal 2004; 16(1): 127–36.
158. Moughal NA et al. Protean agonism of the lysophosphatidic acid receptor-1 with Ki16425 reduces nerve growth factor-induced neurite outgrowth in pheochromocytoma 12 cells. J Neurochem 2006; 98(6): 1920–9.
159. Pierce KL, Luttrell LM and Lefkowitz RJ. New mechanisms in heptahelical receptor signaling to mitogen activated protein kinase cascades. Oncogene 2001; 20(13): 1532–9.
160. Lowes VL, Ip NY and Wong YH. Integration of signals from receptor tyrosine kinases and g protein-coupled receptors. Neurosignals 2002; 11(1): 5–19.
161. van Biesen T et al. Receptor-tyrosine-kinase- and G beta gamma-mediated MAP kinase activation by a common signalling pathway. Nature 1995; 376(6543): 781–4.
162. Borroto-Escuela DO et al. Bioluminescence resonance energy transfer methods to study G protein-coupled receptor-receptor tyrosine kinase heteroreceptor complexes. Methods Cell Biol 2013; 117: 141–64.
163. White MF and Kahn CR. The insulin signaling system. J Biol Chem 1994; 269(1): 1–4.
164. Sprague JE and Arbelaez AM. Glucose counterregulatory responses to hypoglycemia. Pediatr Endocrinol Rev 2011; 9(1): 463–73.
165. Hadcock JR et al. Cross-talk between tyrosine kinase and G-protein-linked receptors. Phosphorylation of beta 2-adrenergic receptors in response to insulin. J Biol Chem 1992; 267(36): 26017–22.

166. Karoor V et al. Insulin stimulates sequestration of beta-adrenergic receptors and enhanced association of beta-adrenergic receptors with Grb2 via tyrosine 350. J Biol Chem 1998; 273(49): 33035–41.
167. Valiquette M et al. Mutation of tyrosine-141 inhibits insulin-promoted tyrosine phosphorylation and increased responsiveness of the human beta 2-adrenergic receptor. EMBO J 1995; 14(22): 5542–9.
168. Fan G et al. c-Src tyrosine kinase binds the beta 2-adrenergic receptor via phospho-Tyr-350, phosphorylates G-protein-linked receptor kinase 2, and mediates agonist-induced receptor desensitization. J Biol Chem 2001; 276(16): 13240–7.
169. Doronin S, Wang Hy HY and Malbon CC. Insulin stimulates phosphorylation of the beta 2-adrenergic receptor by the insulin receptor, creating a potent feedback inhibitor of its tyrosine kinase. J Biol Chem 2002; 277(12): 10698–703.
170. Jiang Y et al. beta2-adrenergic receptor knockout mice exhibit A diabetic retinopathy phenotype. PLoS One 2013; 8(7): e70555 (8 pp.). http://journals.plos.org/plosone/article?id=10.1371/journal.pone.0070555 (August 5, 2014)
171. Fu Q et al. Insulin inhibits cardiac contractility by inducing a Gi-biased beta2 adrenergic signaling in hearts. Diabetes 2014; 63 (8): 2676–89.
172. Szidonya L, Cserzo M and Hunyady L. Dimerization and oligomerization of G-protein-coupled receptors: debated structures with established and emerging functions. J Endocrinol 2008; 196(3): 435–53.
173. Pyne NJ et al. Experimental systems for studying the role of G-protein-coupled receptors in receptor tyrosine kinase signal transduction. Methods Enzymol 2004; 390: 451–75.
174. Cox G and Sheppard CJ. Practical limits of resolution in confocal and non-linear microscopy. Microsc Res Tech 2004; 63(1): 18–22.
175. Pfleger KD and Eidne KA. Monitoring the formation of dynamic G-protein-coupled receptor-protein complexes in living cells. Biochem J 2005; 385(Pt 3): 625–37.
176. Hart RC et al. Mechanism of the enzyme-catalyzed bioluminescent oxidation of coelenterate-type luciferin. Biochem Biophys Res Commun 1978; 81(3): 980–6.
177. Pfleger KD and Eidne KA. New technologies: bioluminescence resonance energy transfer (BRET) for the detection of real time interactions involving G-protein coupled receptors. Pituitary 2003; 6(3): 141–51.
178. Xie Q et al. Bioluminescence resonance energy transfer (BRET) imaging in plant seedlings and mammalian cells. Methods Mol Biol 2011; 680: 3–28.
179. Felce JH and Davis SJ. Unraveling receptor stoichiometry using bret. Front Endocrinol 2012; 3: e86 (4 pp.). http://www.ncbi.nlm.nih.gov/pmc/articles/PMC3394964/ (March 25, 2014)
180. Lohse MJ, Nuber S and Hoffmann C. Fluorescence/bioluminescence resonance energy transfer techniques to study G-protein-coupled receptor activation and signaling. Pharmacol Rev 2012; 64(2): 299–336.
181. Drinovec L et al. Mathematical models for quantitative assessment of bioluminescence resonance energy transfer: application to seven transmembrane receptors oligomerization. Front Endocrinol 2012; 3: e104 (10 pp.). http://www.ncbi.nlm.nih.gov/pmc/articles/PMC3428587/ (December 10, 2013)
182. Kroeger KM et al. Constitutive and agonist-dependent homo-oligomerization of the thyrotropin-releasing hormone receptor. Detection in living cells using bioluminescence resonance energy transfer. J Biol Chem 2001; 276(16): 12736–43.

183. Hanyaloglu AC et al. Homo- and hetero-oligomerization of thyrotropin-releasing hormone (TRH) receptor subtypes. Differential regulation of beta-arrestins 1 and 2. J Biol Chem 2002; 277(52): 50422–30.
184. Watts AO et al. beta-Arrestin recruitment and G protein signaling by the atypical human chemokine decoy receptor CCX-CKR. J Biol Chem 2013; 288(10): 7169–81.
185. Groer CE et al. Agonist-directed interactions with specific beta-arrestins determine mu-opioid receptor trafficking, ubiquitination, and dephosphorylation. J Biol Chem 2011; 286(36): 31731–41.
186. Klewe IV et al. Recruitment of beta-arrestin2 to the dopamine D2 receptor: insights into anti-psychotic and anti-parkinsonian drug receptor signaling. Neuropharmacology 2008; 54(8): 1215–22.
187. Leduc M et al. Functional selectivity of natural and synthetic prostaglandin EP4 receptor ligands. J Pharmacol Exp Ther 2009; 331(1): 297–307.
188. Coulon V et al. Subcellular imaging of dynamic protein interactions by bioluminescence resonance energy transfer. Biophys J 2008; 94(3): 1001–9.
189. Ayoub MA et al. Monitoring of ligand-independent dimerization and ligand-induced conformational changes of melatonin receptors in living cells by bioluminescence resonance energy transfer. J Biol Chem 2002; 277(24): 21522–8.
190. Milligan G, Wilson S and Lopez-Gimenez JF. The specificity and molecular basis of alpha1-adrenoceptor and CXCR chemokine receptor dimerization. J Mol Neurosci 2005; 26(2-3): 161–8.
191. Small KM et al. Alpha2A- and alpha2C-adrenergic receptors form homo- and heterodimers: the heterodimeric state impairs agonist-promoted GRK phosphorylation and beta-arrestin recruitment. Biochemistry 2006; 45(15): 4760–7.
192. Mercier JF et al. Quantitative assessment of beta 1- and beta 2-adrenergic receptor homo- and heterodimerization by bioluminescence resonance energy transfer. J Biol Chem 2002; 277(47): 44925–31.
193. Harikumar KG et al. Transmembrane segment peptides can disrupt cholecystokinin receptor oligomerization without affecting receptor function. Biochemistry 2006; 45(49): 14706–16.
194. Gehret AU et al. Oligomerization of the yeast alpha-factor receptor: implications for dominant negative effects of mutant receptors. J Biol Chem 2006; 281(30): 20698–714.
195. Ayoub MA, Al-Senaidy A and Pin JP. Receptor-G protein interaction studied by bioluminescence resonance energy transfer: lessons from protease-activated receptor 1. Front Endocrinol 2012; 3: e82 (13 pp.). http://www.ncbi.nlm.nih.gov/pmc/articles/PMC3381121/ (April 4, 2014)
196. Lisenbee CS and Miller LJ. Secretin receptor oligomers form intracellularly during maturation through receptor core domains. Biochemistry 2006; 45(27): 8216–26.
197. Borroto-Escuela DO et al. The M(5) muscarinic acetylcholine receptor third intracellular loop regulates receptor function and oligomerization. Biochim Biophys Acta 2010; 1803(7): 813–25.
198. Tan PK et al. Monitoring interactions between receptor tyrosine kinases and their downstream effector proteins in living cells using bioluminescence resonance energy transfer. Mol Pharmacol 2007; 72(6): 1440–6.
199. Boute N, Pernet K and Issad T. Monitoring the activation state of the insulin receptor using bioluminescence resonance energy transfer. Mol Pharmacol 2001; 60(4): 640–5.
200. Issad T, Boute N and Pernet K. The activity of the insulin receptor assessed by bioluminescence resonance energy transfer. Ann N Y Acad Sci 2002; 973: 120–3.

201. Issad T, Boute N and Pernet K. A homogenous assay to monitor the activity of the insulin receptor using Bioluminescence Resonance Energy Transfer. Biochem Pharmacol 2002; 64(5-6): 813–7.
202. Blanquart C, Achi J and Issad T. Characterization of IRA/IRB hybrid insulin receptors using bioluminescence resonance energy transfer. Biochem Pharmacol 2008; 76(7): 873–83.
203. Boute N et al. Dynamics of the interaction between the insulin receptor and protein tyrosine-phosphatase 1B in living cells. EMBO Rep 2003; 4(3): 313–9.
204. Nouaille S et al. Interaction between the insulin receptor and Grb14: a dynamic study in living cells using BRET. Biochem Pharmacol 2006; 72(11): 1355–66.
205. Nouaille S et al. Interaction with Grb14 results in site-specific regulation of tyrosine phosphorylation of the insulin receptor. EMBO Rep 2006; 7(5): 512–8.
206. Kulahin N et al. A BRET assay for monitoring insulin receptor interactions and ligand pharmacology. J Recept Signal Transduct Res 2012; 32(2): 57–64.
207. Siddiqui S et al. BRET Biosensor Analysis of Receptor Tyrosine Kinase Functionality. Front Endocrinol 2013; 4: e46 (11 pp.). http://www.ncbi.nlm.nih.gov/pmc/articles/PMC3620488/ (March 7, 2014)
208. Borroto-Escuela DO et al. Fibroblast growth factor receptor 1- 5-hydroxytryptamine 1A heteroreceptor complexes and their enhancement of hippocampal plasticity. Biol Psychiatry 2012; 71(1): 84–91.
209. Borroto-Escuela DO et al. Dynamic modulation of FGFR1-5-HT1A heteroreceptor complexes. Agonist treatment enhances participation of FGFR1 and 5-HT1A homodimers and recruitment of beta-arrestin2. Biochem Biophys Res Commun 2013; 441(2): 387–92.
210. Milligan G and Smith NJ. Allosteric modulation of heterodimeric G-protein-coupled receptors. Trends Pharmacol Sci 2007; 28(12): 615–20.
211. Ferre S et al. Building a new conceptual framework for receptor heteromers. Nat Chem Biol 2009; 5(3): 131–4.
212. See HB et al. Application of G protein-coupled receptor-heteromer identification technology to monitor beta-arrestin recruitment to G protein-coupled receptor heteromers. Assay Drug Dev Technol 2011; 9(1): 21–30.
213. Ayoub MA et al. Profiling epidermal growth factor receptor and heregulin receptor 3 heteromerization using receptor tyrosine kinase heteromer investigation technology. PLoS One 2013; 8(5): p. e64672 (10 pp.). http://www.ncbi.nlm.nih.gov/pmc/articles/PMC3659105/ (April 9, 2014)
214. Veljkovic V et al. Is it possible to analyze DNA and protein sequences by the methods of digital signal processing? IEEE Trans Biomed Eng 1985; 32(5): 337–41.
215. Veljkovic V et al. Identification of hemagglutinin structural domain and polymorphisms which may modulate swine H1N1 interactions with human receptor. BMC Struct Biol 2009; 9: e62 (11 pp.). http://www.biomedcentral.com/1472-6807/9/62 (March 1, 2014)
216. Veljkovic V et al. Characterization of conserved properties of hemagglutinin of H5N1 and human influenza viruses: possible consequences for therapy and infection control. BMC Struct Biol 2009; 9: e21 (10 pp.). http://www.biomedcentral.com/1472-6807/9/21 (February 12, 2014)
217. Veljkovic N et al. Discovery of new therapeutic targets by the informational spectrum method. Curr Protein Pept Sci 2008; 9(5): 493–506.
218. Doliana R et al. EMILINs interact with anthrax protective antigen and inhibit toxin action in vitro. Matrix Biol 2008; 27(2): 96–106.

219. Kim TK and Eberwine JH. Mammalian cell transfection: the present and the future. Anal Bioanal Chem 2010; 397(8): 3173–8.
220. Svendsen AM et al. Cooperative binding of insulin-like Peptide 3 to a dimeric relaxin family peptide receptor 2. Endocrinology 2008; 149(3): 1113–20.
221. Yoshida N and Sato M. Plasmid uptake by bacteria: a comparison of methods and efficiencies. Appl Microbiol Biotechnol 2009; 83(5): 791–8.
222. Bergmans HE, van Die IM and Hoekstra WP. Transformation in *Escherichia coli*: stages in the process. J Bacteriol 1981; 146(2): 564–70.
223. Mandel M and Higa A. Calcium-dependent bacteriophage DNA infection. 1970. Biotechnology 1992; 24: 198–201.
224. Dower WJ. Electroporation of bacteria: a general approach to genetic transformation. Genet Eng (N Y) 1990; 12: 275–95.
225. Drury L. Transformation of bacteria by electroporation. Methods Mol Biol 1994; 31: 1–8.
226. Smith FD, Harpending PR and Sanford JC. Biolistic transformation of prokaryotes: factors that affect biolistic transformation of very small cells. J Gen Microbiol 1992; 138(1): 239–48.
227. Kurien BT and Scofield RH. Polyethylene glycol-mediated bacterial colony transformation. Biotechniques 1995; 18(6): 1023–6.
228. Song Y et al. Ultrasound-mediated DNA transfer for bacteria. Nucleic Acids Res 2007; 35(19): e129 (9 pp.). http://www.ncbi.nlm.nih.gov/pmc/articles/PMC2095817/ (April 2, 2014)
229. Mandel M and Higa A. Calcium-dependent bacteriophage DNA infection. J Mol Biol 1970; 53(1): 159–62.
230. Dagert M and Ehrlich SD. Prolonged incubation in calcium chloride improves the competence of *Escherichia coli* cells. Gene 1979; 6(1): 23–8.
231. Huff JP et al. Optimization of routine transformation of *Escherichia coli* with plasmid DNA. Biotechniques 1990; 9(5): 570–2, 74, 76–7.
232. Nakata Y, Tang X and Yokoyama KK. Preparation of competent cells for high-efficiency plasmid transformation of *Escherichia coli*. Methods Mol Biol 1997; 69: 129–37.
233. Birnboim HC and Doly J. A rapid alkaline extraction procedure for screening recombinant plasmid DNA. Nucleic Acids Res 1979; 7(6): 1513–23.
234. Tan SC and Yiap BC. DNA, RNA, and protein extraction: the past and the present. J Biomed Biotechnol 2009; 2009: e574398 (10 pp.). http://www.hindawi.com/journals/bmri/2009/574398/ (March 29, 2015)
235. Pingoud A, Alves J and Geiger R. Restriction enzymes. Methods Mol Biol 1993; 16: 107–200.
236. Kessler C and Manta V. Specificity of restriction endonucleases and DNA modification methyltransferases a review (Edition 3). Gene 1990; 92(1-2): 1–248.
237. Vrecl M et al. Agonist-induced endocytosis and recycling of the gonadotropin-releasing hormone receptor: effect of beta-arrestin on internalization kinetics. Mol Endocrinol 1998; 12(12): 1818–29.
238. Holst B et al. Common structural basis for constitutive activity of the ghrelin receptor family. J Biol Chem 2004; 279(51): 53806–17.
239. Kubale V et al. Evidence for a role of caveolin-1 in neurokinin-1 receptor plasma-membrane localization, efficient signaling, and interaction with beta-arrestin 2. Cell Tissue Res 2007; 330(2): 231–45.

240. Maguire JJ, Kuc RE and Davenport AP. Radioligand binding assays and their analysis. Methods Mol Biol 2012; 897: 31–77.
241. Ramsay D et al. Homo- and hetero-oligomeric interactions between G-protein-coupled receptors in living cells monitored by two variants of bioluminescence resonance energy transfer (BRET): hetero-oligomers between receptor subtypes form more efficiently than between less closely related sequences. Biochem J 2002; 365(Pt 2): 429–40.
242. Verschure PJ et al. The contribution of quantitative confocal laser scanning microscopy in cartilage research: chondrocyte insulin-like growth factor-1 receptors in health and pathology. Microsc Res Tech 1997; 37(4): 285–98.
243. Angers S, Salahpour A and Bouvier M. Dimerization: an emerging concept for G protein-coupled receptor ontogeny and function. Annu Rev Pharmacol Toxicol 2002; 42: 409–35.
244. Xu Y, Piston DW and Johnson CH. A bioluminescence resonance energy transfer (BRET) system: application to interacting circadian clock proteins. Proc Natl Acad Sci U S A 1999; 96(1): 151–6.
245. Heding A. Use of the BRET 7TM receptor/beta-arrestin assay in drug discovery and screening. Expert Rev Mol Diagn 2004; 4(3): 403–11.
246. De A, Loening AM and Gambhir SS. An improved bioluminescence resonance energy transfer strategy for imaging intracellular events in single cells and living subjects. Cancer Res 2007; 67(15): 7175-83.
247. Loening AM et al. Consensus guided mutagenesis of *Renilla luciferase* yields enhanced stability and light output. Protein Eng Des Sel 2006; 19(9): 391–400.
248. Kubale V and Vrecl M. Novi postopki za ugotavljanje proteinsko-proteinskih interakcij v živih celicah = Novel tools to identify protein-protein interactions in living cells. Vet nov 2004; 30(9, 10): 71-8, 360–1.
249. Veatch W and Stryer L. The dimeric nature of the gramicidin A transmembrane channel: conductance and fluorescence energy transfer studies of hybrid channels. Journal of molecular biology 1977; 113(1): 89–102.
250. Ayoub MA and Pfleger KD. Recent advances in bioluminescence resonance energy transfer technologies to study GPCR heteromerization. Curr Opin Pharmacol 2010; 10(1): 44–52.
251. Mustafa S and Pfleger KD. G protein-coupled receptor heteromer identification technology: identification and profiling of GPCR heteromers. J Lab Autom 2011; 16(4): 285–91.
252. Dorsch S et al. Analysis of receptor oligomerization by FRAP microscopy. Nat Methods 2009; 6(3): 225–30.
253. Calebiro D et al. Single-molecule analysis of fluorescently labeled G-protein-coupled receptors reveals complexes with distinct dynamics and organization. Proc Natl Acad Sci U S A 2013; 110(2): 743–8.
254. Katragadda M, Maciejewski MW and Yeagle PL. Structural studies of the putative helix 8 in the human beta(2) adrenergic receptor: an NMR study. Biochim Biophys Acta 2004; 1663(1-2): 74-81.
255. Hubbard SR et al. Crystal structure of the tyrosine kinase domain of the human insulin receptor. Nature 1994; 372(6508): 746–54.
256. Flajolet M et al. FGF acts as a co-transmitter through adenosine A(2A) receptor to regulate synaptic plasticity. Nature neuroscience 2008; 11(12): 1402–9.
257. Giudice J et al. Differential endocytosis and signaling dynamics of insulin receptor variants IR-A and IR-B. J Cell Sci 2011; 124(Pt 5): 801–11.

258. Pierce KL et al. Role of endocytosis in the activation of the extracellular signal-regulated kinase cascade by sequestering and nonsequestering G protein-coupled receptors. Proc Natl Acad Sci U S A 2000; 97(4): 1489–94.
259. Ogawa H et al. Localization, trafficking, and temperature-dependence of the *Aequorea* green fluorescent protein in cultured vertebrate cells. Proc Natl Acad Sci U S A 1995; 92(25): 11899–903.
260. Wang D et al. Opioid receptor homo- and heterodimerization in living cells by quantitative bioluminescence resonance energy transfer. Mol Pharmacol 2005; 67(6): 2173–84.
261. Kocan M et al. Demonstration of improvements to the bioluminescence resonance energy transfer (BRET) technology for the monitoring of G protein-coupled receptors in live cells. J Biomol Screen 2008; 13(9): 888–98.
262. Kocan M et al. Enhanced BRET Technology for the Monitoring of Agonist-Induced and Agonist-Independent Interactions between GPCRs and beta-Arrestins. Front Endocrinol 2010; 1: e. 12 (9 pp.). http://www.ncbi.nlm.nih.gov/pubmed/22654789 (February 9, 2014)
263. Barak LS et al. Internal trafficking and surface mobility of a functionally intact beta2-adrenergic receptor-green fluorescent protein conjugate. Mol Pharmacol 1997; 51(2): 177–84.
264. Ramsay D et al. Detection of receptor ligands by monitoring selective stabilization of a *Renilla luciferase*-tagged, constitutively active mutant, G-protein-coupled receptor. Br J Pharmacol 2001; 133(2): 315–23.
265. Lan TH, Kuravi S and Lambert NA. Internalization dissociates beta2-adrenergic receptors. PLoS One 2011; 6(2): e17361 (7 pp.). http://journals.plos.org/plosone/article?id=10.1371/journal.pone.0017361 (March 9, 2014)
266. Oakley RH et al. Association of beta-arrestin with G protein-coupled receptors during clathrin-mediated endocytosis dictates the profile of receptor resensitization. J Biol Chem 1999; 274(45): 32248–57.
267. Seachrist JL, Anborgh PH and Ferguson SS. beta 2-adrenergic receptor internalization, endosomal sorting, and plasma membrane recycling are regulated by rab GTPases. J Biol Chem 2000; 275(35): 27221–8.
268. Di Certo MG et al. Delayed internalization and lack of recycling in a beta2-adrenergic receptor fused to the G protein alpha-subunit. BMC cell biology 2008; 9: e56 (12 pp.). http://www.ncbi.nlm.nih.gov/pmc/articles/PMC2569931/ (May 2, 2014)
269. Gavi S et al. The 15-amino acid motif of the C terminus of the beta2-adrenergic receptor is sufficient to confer insulin-stimulated counterregulation to the beta1-adrenergic receptor. Endocrinology 2005; 146(1): 450–7.
270. Shumay E et al. Trafficking of beta2-adrenergic receptors: insulin and beta-agonists regulate internalization by distinct cytoskeletal pathways. J Cell Sci 2004; 117(Pt 4): 593–600.
271. Dacres H et al. Effect of enhanced *Renilla luciferase* and fluorescent protein variants on the Forster distance of Bioluminescence resonance energy transfer (BRET). Biochem Biophys Res Commun 2012; 425(3): 625–9.
272. Mondal S et al. Membrane driven spatial organization of GPCRs. Sci Rep 2013; 3: e2909 (9 pp.). http://www.ncbi.nlm.nih.gov/pmc/articles/PMC3793225/ (May 4, 2014)

273. Ayoub MA et al. Preferential formation of MT1/MT2 melatonin receptor heterodimers with distinct ligand interaction properties compared with MT2 homodimers. Mol Pharmacol 2004; 66(2): 312–21.
274. Terrillon S et al. Oxytocin and vasopressin V1a and V2 receptors form constitutive homo- and heterodimers during biosynthesis. Mol Endocrinol 2003; 17(4): 677–91.
275. Goin JC and Nathanson NM. Quantitative analysis of muscarinic acetylcholine receptor homo- and heterodimerization in live cells: regulation of receptor down-regulation by heterodimerization. J Biol Chem 2006; 281(9): 5416–25.
276. Breitwieser GE. G protein-coupled receptor oligomerization: implications for G protein activation and cell signaling. Circ Res 2004; 94(1): 17–27.
277. De Meyts P. The insulin receptor: a prototype for dimeric, allosteric membrane receptors? Trends in biochemical sciences 2008; 33(8): 376–84.
278. Ghosh A, Sonavane U and Joshi R. Multiscale modelling to understand the self-assembly mechanism of human beta2-adrenergic receptor in lipid bilayer. Computational biology and chemistry 2014; 48: 29–39.
279. Doronin S et al. Akt mediates sequestration of the beta(2)-adrenergic receptor in response to insulin. J Biol Chem 2002; 277(17): 15124–31.
280. Mothe I et al. Tyrosine kinase activity of a chimeric insulin-like-growth-factor-1 receptor containing the insulin receptor C-terminal domain. Comparison with the tyrosine kinase activities of the insulin and insulin-like-growth-factor-1 receptors using a cell-free system. Eur J Biochem 1995; 228(3): 842–8.
281. Soni P et al. The differential effects of pp120 (Ceacam 1) on the mitogenic action of insulin and insulin-like growth factor 1 are regulated by the nonconserved tyrosine 1316 in the insulin receptor. Mol Cell Biol 2000; 20(11): 3896–905.
282. Navarro G et al. Interactions between intracellular domains as key determinants of the quaternary structure and function of receptor heteromers. J Biol Chem 2010; 285(35): 27346–59.
283. Lohse MJ and Hoffmann C. Arrestin interactions with G protein-coupled receptors. Handb Exp Pharmacol 2014; 219: 15–56.
284. Sommer ME, Hofmann KP and Heck M. Distinct loops in arrestin differentially regulate ligand binding within the GPCR opsin. Nat Commun 2012; 3: 995.
285. Ostermaier MK et al. Functional map of arrestin-1 at single amino acid resolution. Proc Natl Acad Sci U S A 2014; 111(5): 1825–30.
286. Hanson SM and Gurevich VV. The differential engagement of arrestin surface charges by the various functional forms of the receptor. J Biol Chem 2006; 281(6): 3458–62.
287. Han M et al. Crystal structure of beta-arrestin at 1.9 A: possible mechanism of receptor binding and membrane Translocation. Structure 2001; 9(9): 869–80.
288. Hasbi A, O'Dowd BF and George SR. Dopamine D1-D2 receptor heteromer signaling pathway in the brain: emerging physiological relevance. Mol Brain 2011; 4: e26 (6 pp.).
http://www.molecularbrain.com/content/4/1/26 (May 7, 2014)
289. Mowers J et al. Inflammation produces catecholamine resistance in obesity via activation of PDE3B by the protein kinases IKK{varepsilon} and TBK1. Elife 2013; 2: e01119 (12 pp.).
http://www.ncbi.nlm.nih.gov/pmc/articles/PMC3869376/ (January 9, 2014)
290. Reilly SM et al. An inhibitor of the protein kinases TBK1 and IKK-varepsilon improves obesity-related metabolic dysfunctions in mice. Nat Med 2013; 19(3): 313–21.

11 APPENDIX

Original scientific article:

Mandic M et al. Demonstration of a direct interaction between beta2-adrenergic receptor and insulin receptor by BRET and bioinformatics. PLoS One 2014; 9(11): e112664 (15 pp.).

http://www.ncbi.nlm.nih.gov/pmc/articles/PMC4234468/ (January 6, 2015)